ARL

The University of Texas at Austin

TECHNICAL REPORT

13 March 2000
ARL-TR-00-01

Copy Number _____

ADS MNT and FET: Array Element Localization Analysis and Results

Technical Report under Contract N00039-96-D-0051, TO No. 0236,
TD No. 1406046, ADS Acoustic Test and Evaluation and System Engineering III

Peter E. McCarty, Marton I. Garay, Mary R. Parse, and Russell E. Henrichs

Prepared for: Space and Naval Warfare Systems Command Headquarters
4301 Pacific Coast Highway (OT-1) • San Diego, CA 92110-3127

Monitored by: Naval Sea Systems Command
Department of the Navy • Washington, DC 20362-5101

Acknowledgment of Support and Disclaimer (DFARS 252.235-7010):
This material is based upon work supported by the Naval Sea Systems Command
under Contract No. N00039-96-D-0051, Task Order No. 0236.
Any opinions, findings and conclusions, or recommendations expressed in this material are those of the author(s)
and do not necessarily reflect the views of the Naval Sea Systems Command.

Approved for public release; distribution is unlimited.

Applied Research Laboratories•The University of Texas at Austin•Post Office Box 8029•Austin, Texas 78713-8029

REPORT DOCUMENTATION PAGE

Form Approved
OMB No. 0704-0188

1. AGENCY USE ONLY (Leave blank)	2. REPORT DATE	3. REPORT TYPE AND DATES COVERED
	13-03-2000	technical

4. TITLE AND SUBTITLE

ADS MNT and FET: Array Element Localization Analysis and Results
Technical Report under Contract N00039-96-D-0051, TO No. 0236, TD No. 1406046,
ADS Acoustic Test and Evaluation and System Engineering III

5. FUNDING NUMBERS

N00039-96-D-0051
TO No. 0236
TD No. 1406046

6. AUTHOR(S)

McCarty, Peter E. Garay, Marton I. Parse, Mary R. Henrichs, Russell E.

7. PERFORMING ORGANIZATION NAMES(S) AND ADDRESS(ES)

Applied Research Laboratories
The University of Texas at Austin
P.O. Box 8029
Austin, Texas 78713-8029

8. PERFORMING ORGANIZATION REPORT NUMBER

ARL-TR-00-01

9. SPONSORING/MONITORING AGENCY NAME(S) AND ADDRESS(ES)

Space and Naval Warfare Systems Command
Headquarters
4301 Pacific Coast Highway (OT-1)
San Diego, CA 92110-3127

Naval Sea Systems Command
Department of the Navy
Washington, DC 20362-5101

10. SPONSORING/MONITORING AGENCY REPORT NUMBER

11. SUPPLEMENTARY NOTES

(See reverse side for "Acknowledgment of Support . . . (DFARS 252.235-7010)" and for ARL:UT copyright statement.)

12a. DISTRIBUTION/AVAILABILITY STATEMENT

Approved for public release; distribution is unlimited.

12b. DISTRIBUTION CODE

13. ABSTRACT (Maximum 200 words)

Accurate array element localization (AEL) is an important component of optimizing the detection performance of bottom-mounted acoustic arrays. Use of the nominal element positions can lead to significant degradations in beamforming performance when the array has been subject to real-world deployment methods. Methods of accurately estimating array element positions using both overt and covert methods have been developed by the Advanced Deployable System (ADS) program, and were used during the ADS Fleet Evaluation Test (FET) and Multi-Node Test (MNT). "FET" henceforth is used to denote both the FET and the MNT. During FET, data were collected for AEL analysis. This report first explains the AEL algorithms used, and then presents AEL results for the 18 arrays deployed during FET. The algorithm generally achieves an accuracy on the order of 0.5 meters when using acoustic data with a bandwidth of 150 Hz.

14. SUBJECT TERMS

ADS / Advanced Deployable System
FET / Fleet Evaluation Test
AEL / array element localization
MNT / Multi-Node Test

15. NUMBER OF PAGES

91

16. PRICE CODE

17. SECURITY CLASSIFICATION OF REPORT	18. SECURITY CLASSIFICATION OF THIS PAGE	19. SECURITY CLASSIFICATION OF ABSTRACT	20. LIMITATION OF ABSTRACT
UNCLASSIFIED	UNCLASSIFIED	UNCLASSIFIED	SAR

NSN 7540-01-280-5500

Standard Form 298 (Rev. 2-89)
Prescribed by ANSI Std. 239-18
298-102

11. SUPPLEMENTARY NOTES (cont'd)

Contract No. N00039-96-D-0051
Acknowledgment of Support
This material is based upon work supported by the Naval Sea Systems Command under Contract No. N00039-96-D-0051, Task Order No. 0236.

Contract No. N00039-96-D-0051
Disclaimer
Any opinions, findings and conclusions, or recommendations expressed in this material are those of the author(s) and do not necessarily reflect the views of the Naval Sea Systems Command.

TABLE OF CONTENTS

		Page
LIST OF FIGURES		v
PUBLICATION NOTES		ix
1.	INTRODUCTION	1
2.	CORRELATION APPROACH TO AEL	3
	2.1 TIME DELAY MEASUREMENTS FROM OMNI×OMNI CORRELAGRAMS	3
	2.2 MODELING OF TIME DELAYS, AND ADJUSTMENT OF ELEMENT POSITIONS	5
	2.3 ADS AEL ALGORITHM VARIANTS	8
	2.4 QUALITY ASSESSMENT OF ALGORITHM RESULTS	14
	2.5 ARRAY APERTURE ESTIMATION USING SOURCES OF OPPORTUNITY	17
3.	IMPLEMENTATION IN PAS	21
4.	AEL RESULTS FOR FET AND MNT	23
5.	DISCUSSION OF AEL RESULTS	33
	5.1 COMPARISON OF RESULTS AND ACCURACY ESTIMATES	33
	5.2 AUTOMATION OF THE AEL PROCESS	35
	5.3 THREE-DIMENSIONAL AEL	37
APPENDIX A		39
APPENDIX B		59

This page intentionally left blank.

LIST OF FIGURES

Figure		Page
2.1	Correlation-based AEL algorithmic flowchart	4
2.2	Sample omni×omni correlagram with track indicated by red outline	6
2.3	AEL algorithm variants	9
2.4	Effects of applying far-field AEL algorithm to a mid-field source of opportunity	12
2.5	Source-receiver geometry upon successful algorithm convergence	15
2.6	Source-receiver geometry upon unsuccessful algorithm convergence	16
2.7	Aperture estimation for node 11, using sources of opportunity	18
3.1	AEL data flow in the analysis processor	22
4.1	AEL results for MNT-only nodes	24
4.2	AEL results for string 1	25
4.3	AEL results for string 2	26
4.4	AEL results for string 3	27
4.5	AEL results for string 4	28
4.6	Array aperture, LOB, and curvature summary	30
5.1	Omni×omni correlagrams for far-field and mid-field contacts	34
B.1	Node 11. Omni×omni correlagram for near-field contact during AEL event, with processed track highlighted	61
B.2	Node 11. Navigation geometry during AEL event, and source track upon convergence	62
B.3	Node 12. Omni×omni correlagram for near-field contact during AEL event, with processed track highlighted	63
B.4	Node 12. Geometry during AEL event (top) and source track upon convergence (bottom)	64
B.5	Node 21. Omni×omni correlagram for near-field contact during AEL event, with processed track highlighted	65
B.6	Node 21. Geometry during AEL event (top) and source track upon convergence (bottom)	66
B.7	Node 22. Omni×omni correlagram for near-field contact during AEL event, with processed track highlighted	67

Figure		Page
B.8	Node 22. Geometry during AEL event (top) and source track upon convergence (bottom)	68
B.9	Node 23. Omni×omni correlagram for near-field contact during AEL event, with processed track highlighted	69
B.10	Node 23. Geometry during AEL event (top) and source track upon convergence (bottom)	70
B.11	Node 24. Omni×omni correlagram for near-field contact during AEL event, with processed track highlighted	71
B.12	Node 24. Geometry during AEL event (top) and source track upon convergence (bottom)	72
B.13	Node 31. Omni×omni correlagram for near-field contact during AEL event, with processed track highlighted	73
B.14	Node 31. Geometry during AEL event (top) and source track upon convergence (bottom)	74
B.15	Node 32. Omni×omni correlagram for near-field contact during AEL event, with processed track highlighted	75
B.16	Node 32. Geometry during AEL event (top) and source track upon convergence (bottom)	76
B.17	Node 33. Omni×omni correlagram for near-field contact during AEL event, with processed track highlighted	77
B.18	Node 33. Geometry during AEL event (top) and source track upon convergence (bottom)	78
B.19	Node 34. Omni correlagram during AEL event, with processed track highlighted	79
B.20	Node 34. Geometry during AEL event (top) and source track upon convergence (bottom)	80
B.21	Node 41. Omni×omni correlagram for near-field contact during AEL event, with processed track highlighted	81
B.22	Node 41. Geometry during AEL event (top) and source track upon convergence (bottom)	82
B.23	Node 42. Omni×omni correlagram for near-field contact during AEL event, with processed track highlighted	83
B.24	Node 42. Navigation geometry during AEL event, where a green "+" indicates time processed, a black "+" indicates time not processed, and a red "o" indicates receiver location	84
B.25	Node 43. Omni×omni correlagram for near-field contact during AEL event, with processed track highlighted	85

Figure		Page
B.26	Node 43. Geometry during AEL event (top) and source track upon convergence (bottom)	86
B.27	Node 44. Omni×omni correlagram during AEL event, with processed track highlighted.....	87
B.28	Node 44. Geometry during AEL event (top) and source track upon convergence (bottom)	88

This page intentionally left blank.

PUBLICATION NOTES

Acknowledgment of Support and Disclaimer (DFARS 252.235.7010)

Contract No. N00039-96-D-0051
Acknowledgment of Support

This material is based upon work supported by the Naval Sea Systems Command under Contract No. N00039-96-D-0051, Task Order No. 0236.

Contract No. N00039-96-D-0051
Disclaimer

Any opinions, findings and conclusions, or recommendations expressed in this material are those of the author(s) and do not necessarily reflect the views of the Naval Sea Systems Command.

This page intentionally left blank.

1. INTRODUCTION

Between February and May of 1999, the Advanced Deployable System (ADS) program deployed a total of 18 arrays off the southern California coast as part of the U.S. Navy's Multi-Node Test (MNT) and Fleet Evaluation Test (FET) exercises. Data from these arrays arrived via underwater cable at a shore processing site, where the data were beamformed and displayed for detection analysis.

Such analysis requires that the beamformer and postbeamforming processors be provided with array configuration information, including the relative positions of each receiver element within the array and the overall orientation of the array. Historical evidence indicates that deployment of a linear array, fully elongated and properly positioned, is the exception rather than the norm in array deployment. Accurate estimation of array configuration and orientation is necessary to ensure optimal performance of both the individual nodes and the field as a whole.

To ensure this level of performance, methods and tools have been developed by the ADS program to perform array element localization (AEL). The correlation-based AEL algorithm implemented at FET/MNT evolved from methods developed over several years at ARL:UT, where they were used for analysis of many diverse data sets collected by several different programs. These methods were implemented and refined within the ADS processing and automation system (PAS), primarily within the analysis processor (AP).

During FET (henceforth used to include both the FET and MNT exercises), data were collected for AEL analysis. This included data collected during events involving USN ships RV7 and RV1 in motion near each node (overt method) and data collected during events of opportunity (covert method). These data were analyzed, primarily on-site in quasi-real time, but also post-test. This report summarizes the results of these analyses.

In Section 2, an overview of the AEL process is presented, with implementation details discussed in Section 3. Results from all events are then shown in Section 4, with observations, accuracy estimates, lessons learned, and conclusions covered in Section 5. Appendices list the best available element positions for each array, as well as showing the omnidirectional (omni×omni) correlagrams and geometries used during analysis.

2. CORRELATION APPROACH TO AEL

The basis of the correlation approach to array element localization is the measurement of the timings of a set of signals at the different receiver elements. These timings are modeled using assumed positions for the receiver elements. The assumed element positions are iteratively adjusted to minimize the mean square error between the measured and modeled timings, using a Hessian-based nonlinear optimization routine. Detailed discussion of this process follows.

2.1 TIME DELAY MEASUREMENTS FROM OMNI×OMNI CORRELAGRAMS

Traditionally, timing measurements used for AEL analysis were obtained from impulsive events (explosive charges or lightbulb implosions), or from matched filtering of modulated waveforms such as hyperbolic frequency modulations (HFMs). Because of the necessity for covert operation of the ADS system, as well as for the ease of conducting exercises without any need for source employment, an approach was developed to obtain the necessary timing measurements directly from the radiated noise of surface ships.

In this approach, illustrated in Fig. 2.1, an omni×omni correlagram is formed between a particular pair of receiver elements. During the transit of an acoustic source, a trace will be observed on the correlagram. The trace is caused by the broadband energy naturally radiated by the ship, and will change in bearing as the source transits. The time delay measured from the correlagram represents the difference in travel time from the source to each receiver of the pair. The absolute travel time is not required in AEL analysis.

- Measure time delay vs time along a CPA event from an omnidirectional (omnixomni) correlogram (2.1a)
  - Sample 10-20 points along the track
  - Use a set of omnixomni correlation pairs spanning the array

Iterate

- Compute ranges between each receiver and source combination
  - Based on current or initial estimate of source and receiver positions (2.1b)
- Using ray trace results, compute travel times
- Compute a time difference (τ_{estim}) corresponding to each time difference (τ_{meas}) measured from the data correlagram
- Compute mean squared error function

$$E = \sum_{\substack{\text{source} \\ \text{positions}}} \sum_{\substack{\text{hydrophone} \\ \text{pairs}}} \left| \tau_{meas} - \tau_{estim} \right|^2$$

- Use nonlinear optimization algorithm to find receiver (and source) positions that minimize the total error (E)
- Q/A and reporting of results
  - How do interelement separations compare to nominal?
  - Is source track distorted from initial track?
  - Is high time delay error associated with particular omnixomni pairs or sources?

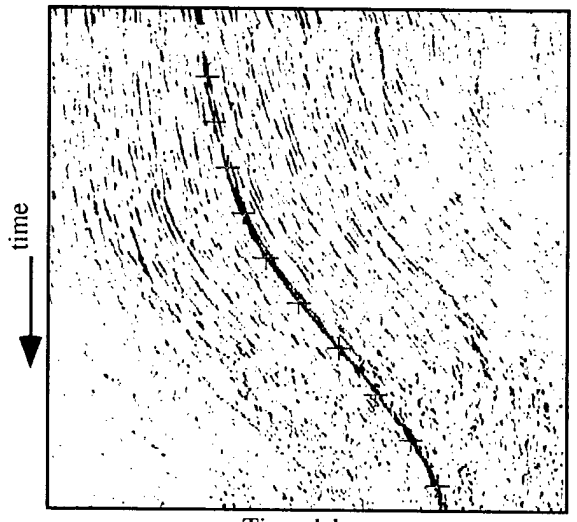

(a) Ch5xch13 correlagram

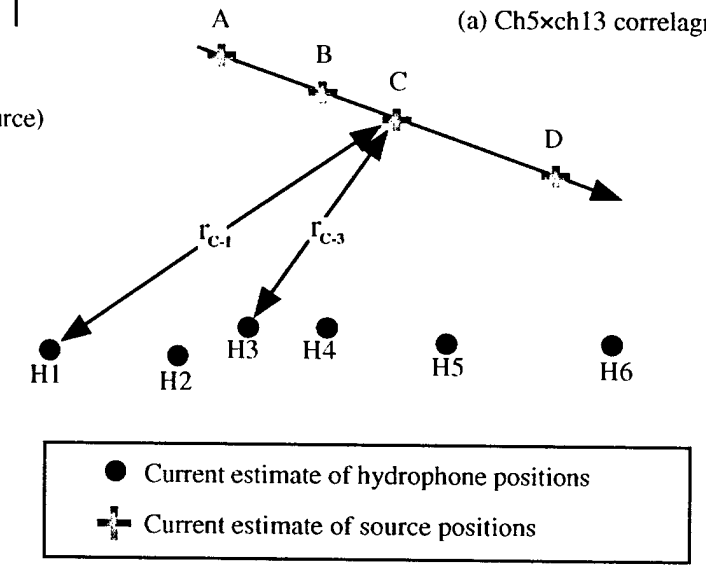

(b) Source and receiver estimation

AS-00-01

Figure 2.1: Correlation-based AEL algorithmic flowchart.

Between 10 and 30 specific times are selected during the transit of the source; at these points travel time difference is measured. In addition, measurements are obtained for up to 3N omni×omni correlagrams, where N is the number of receivers in the array. In this manner, a highly redundant set of time delay measurements is obtained, saved in an array of dimension [(number of source points) by (number of omnidirectional pairs)].

Obtaining this set of measured time delays is one of the more difficult steps in the AEL process, both in terms of expenditure of analyst time and in terms of complexity of automation. A partially automated program has been developed to obtain time delay measurements from a series of correlagrams, but the program currently requires analyst supervision, both to correctly identify the trace of interest, and to ensure that the tracker does not jump to an adjacent trace. Figure 2.2 shows an example omni×omni correlagram from FET, with the desired trace outlined in red. Other traces, some very close in bearing, offer ample opportunities for introduction of errors by an unsupervised tracking program.

2.2 MODELING OF TIME DELAYS AND ADJUSTMENT OF ELEMENT POSITIONS

The next step in the array element localization process is to model the array of time delays based on assumed positions for the source and receivers. Using methods discussed in Section 2.3, these source and receiver positions are initialized, and then travel time differences are computed, based on this model.

Next comes computation of the RMS error between these modeled travel time differences and those measured from the omni×omni correlagrams. An iterative

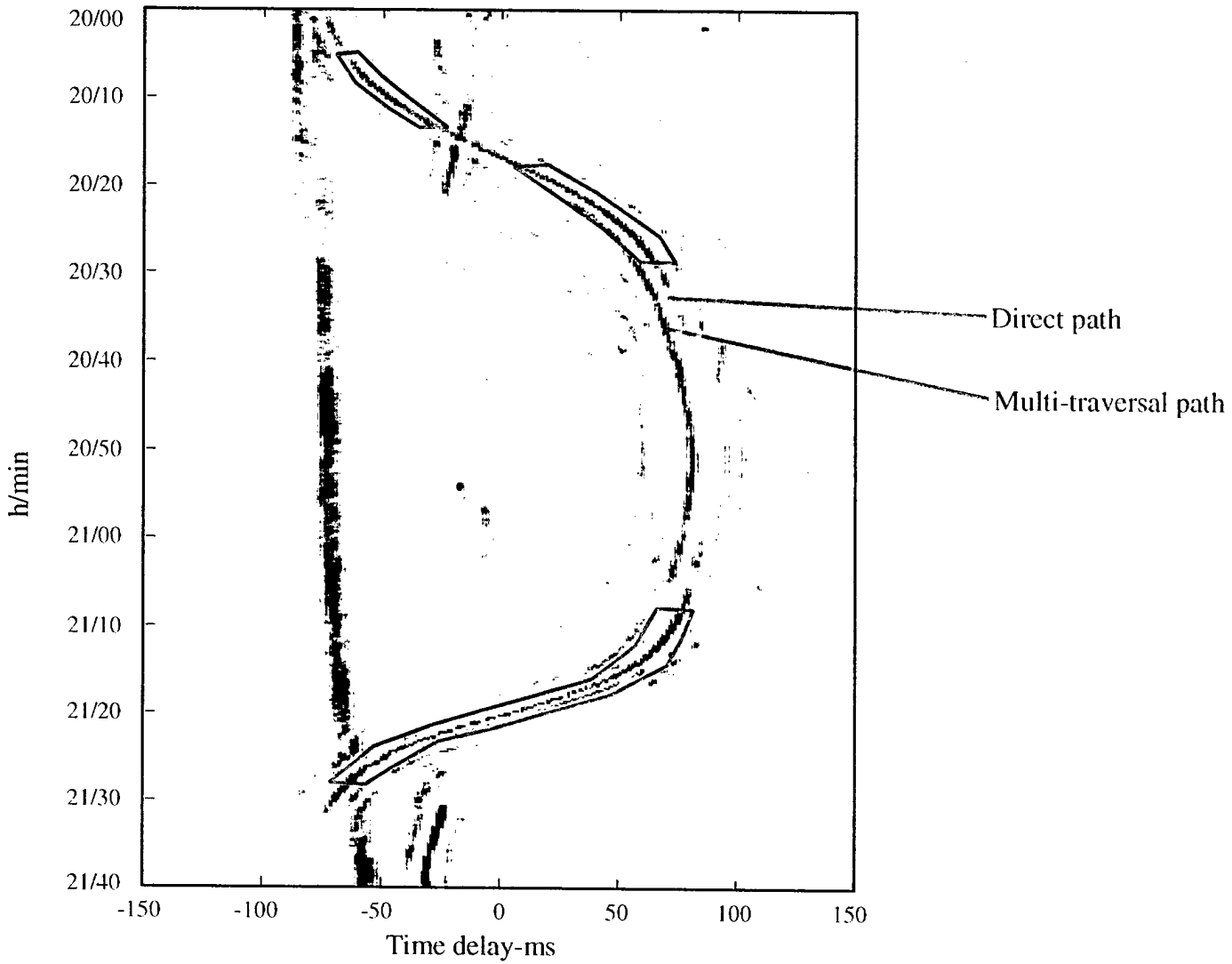

Figure 2.2: Example omni×omni correlagram with track indicated by red outline. Hydrophones 1 and 13, Node 11 (084/20/00 to 084/24/40)

nonlinear optimization algorithm is employed to adjust unknown parameters until the root mean square (RMS) error is minimized. In this case, the unknown parameters are the x-y positions of each receiver element (assumed to have constant depth), and parameters describing the source positions or track. This algorithm iterates until the RMS error decreases to less than a preset tolerance, at which point the algorithm is considered to have converged.

Two nonlinear optimization methods have been employed. The first is the inverse Hessian method, in which it is assumed that the error surface is quadratic with respect to the unknown parameters, and the update to the unknown parameters is based on a local estimate to this quadratic surface. This assumption is generally good when unknown parameters are close to their optimal values. In terms of the AEL problem, this assumption is good when the error has a simple dependence on the unknown parameters, and when the initialized system (sources and receivers) is reasonably near the solution. This is the case when the source positions are described in terms of x-y locations or bearings, and when these x-y positions are accurately initialized using GPS measurements.

For a more complicated source track description, such as the 4-parameter approach discussed in Section 2.3, the error surface is no longer quadratic with respect to the source parameters, and so the Hessian-based method cannot be reliably used. In such a case, a steepest descent algorithm is employed, the update to the unknown parameters being based on the local gradient of the RMS error. This algorithm can navigate through a more complex error surface in search of the optimal solution.

Although the steepest descent algorithm is more robust against complexities in the error surface and against poor initialization, the inverse Hessian method is much faster, and so is used where possible. The inverse Hessian method generally requires 10–25 iterations to converge, while the steepest descent method requires at least 50.

2.3 ADS AEL ALGORITHM VARIANTS

This section describes details of the source track description, the relationship between the source/receiver positions and the time delays, and the means of initializing the unknown parameters. The algorithms presented here can be organized as shown in Fig. 2.3, according to the availability of accurate initialization and the distance from the receivers to the source.

The availability of accurate initialization of unknown parameters depends on whether dedicated assets that can provide accurate navigational information are available for AEL runs, or whether analysis will be based on sources of opportunity, such as passing merchant shipping. When navigational information is available, source positions can be accurately initialized directly from the GPS data. In these cases, GPS data are also generally available for the deployment platform, allowing for an accurate estimate of the receiver array's absolute position and line of bearing.

When accurate navigational information is not available, parameters describing the source track must be initialized via grid search methods, obtaining an initialization that minimizes the RMS difference between the measured and the predicted time delays.

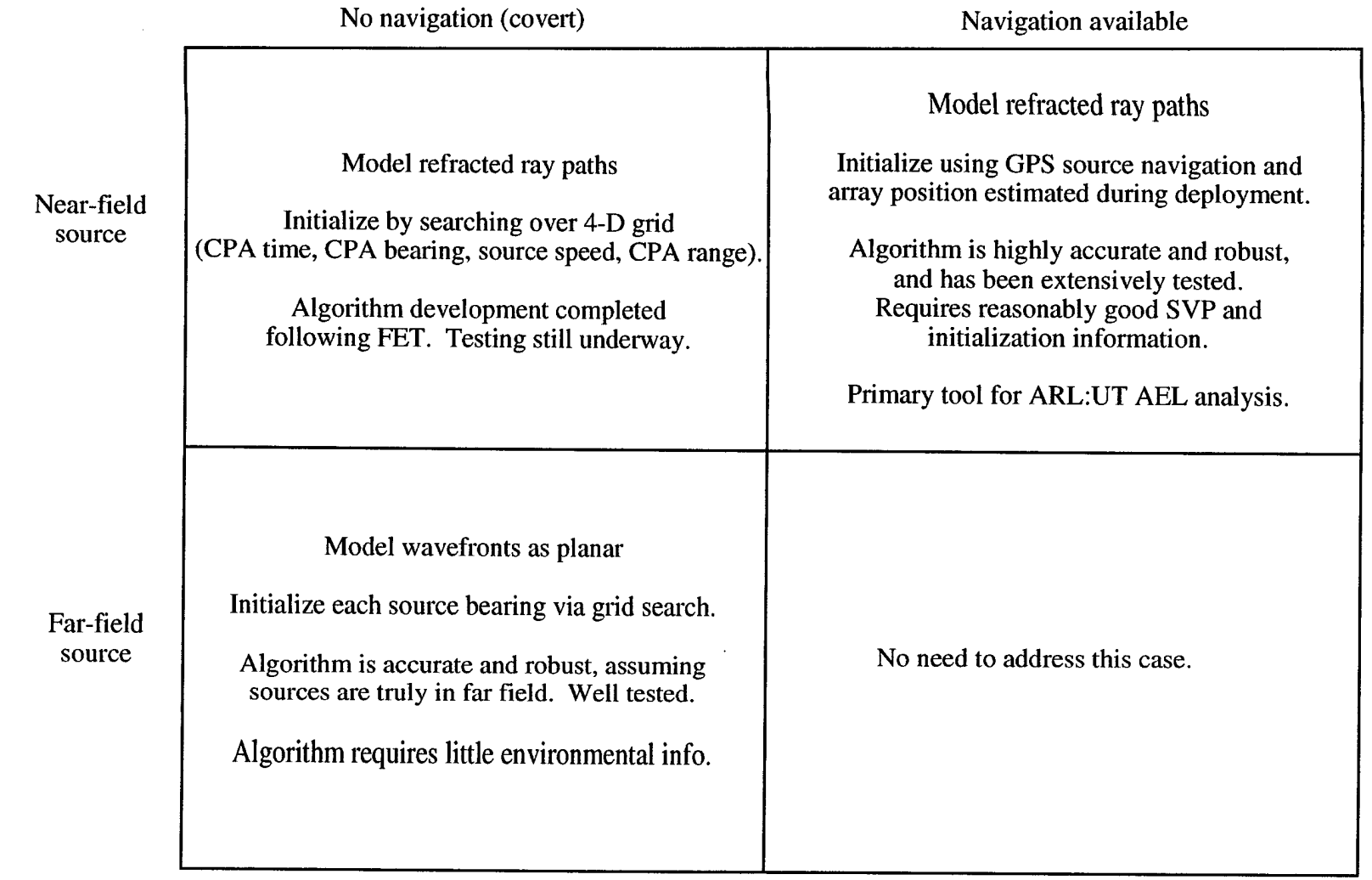

Figure 2.3: AEL algorithm variants.

AS-00-03

The second trait distinguishing AEL algorithm variants from one another is the distance from the receiver array to the acoustic source being used for AEL. One option is to have sources in the near field, meaning that propagation from source to receiver is via direct path. This lack of bottom interactions means that the refracted ray paths can be accurately modeled even when no information regarding bottom structure is available.

Generally, detailed bottom information is not available in the early phases of a deployment, which is when AEL must be performed. For sources in direct path range, propagation path information (including travel time) can be obtained using only the sound speed or velocity profile (SVP) in the water, which is generally available. In this case, a ray trace program is used to obtain the relationship between source-receiver separation and travel time, and this information can then be used to compute modeled travel time differences based on the current estimates of the source and receiver positions.

AEL analysis can also be based on far-field sources. There is no clear boundary between far-field and mid-field sources, only a gradually diminishing error resulting from substituting one for the other. Simply, a far-field source is one for which the wavefront of the arriving signal can be treated as a plane wave. For a source that is 15 km distant, the actual wavefront will deviate from planar by about 2 m across a 500-m aperture. A deviation of 1 m would require a contact about 30 km away. The far-field AEL algorithm would represent this wavefront as planar, and so induce a comparable bow in the receiver shape, as illustrated in Fig. 2.4. Treating a wavefront as planar greatly simplifies the algorithm, resulting in improved robustness and speed, but it remains important to estimate the range to the source and, if necessary, correct the overall array curvature.

As shown in Fig. 2.3, these two sets of options allow for four algorithm choices, one of which (far field with navigation) has been left unimplemented because of irrelevance. The other three options have been implemented within the ADS AEL software suite.

The first AEL variant is a near-field source with known navigation. This is a variant that traditionally has shown excellent robustness and accuracy, having been used successfully on dozens of data sets, both by ADS and other programs. This algorithm requires a reasonably accurate estimate of the sound speed profile and the water depth. Like all variants discussed here, it is currently implemented to treat all receiver elements as being in the same horizontal plane, although this variant can be expanded to treat the receiver element depths as unknowns.

The second AEL variant is a far-field source with unknown navigation. This algorithm was developed specifically for the ADS program in response to the need for covert AEL. Each source position is fully defined by its bearing, which is initialized by a simple grid search. This algorithm has proven robust, accurate, and fast, with the primary source of error being the incorrect identification of a mid-field source as being in the far field. The most effective way to rectify incorrect mid-field identification appears to be by using a field processor, which would make use of multi-node holding of contacts to identify the sources of opportunity and to estimate their ranges.

The third AEL variant is a near-field source with unknown navigation. Development of this algorithm was motivated not only by the need for covert AEL but

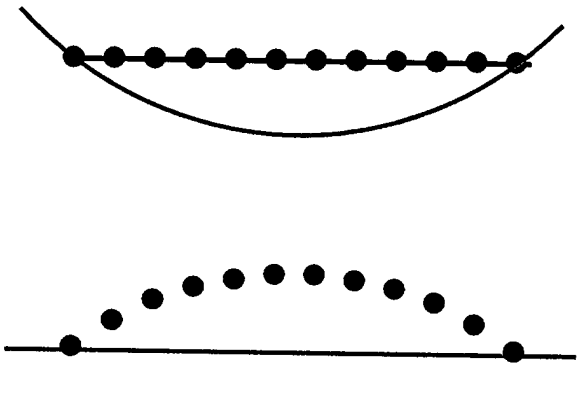

Actual array shape (linear)
Actual wavefront shape (curved)

Assumed wavefront shape (linear)
Found array shape (bowed)

For an acoustic source in the near field (broadside), wavefront arrives later at the ends of a straight array than at the center.

If wavefront is assumed to be linear, then to get the same wavefront timings, the array must be bowed towards the source.

To avoid this bias in the found solutions:
- Use the near-field algorithm for these nearby sources
- Find some far-field sources
- Estimate the range to the source and correct

(a) Actual and assumed wavefront shapes

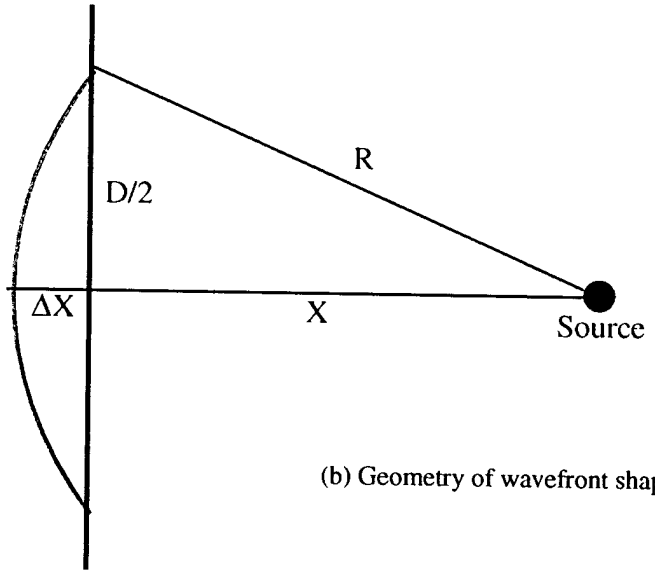

D = Array aperture
X = Distance from array center to source
R = Distance from array end point to source
ΔX = Error at array center between assumed (straight) and actual (curved) wavefront shapes

$$X = \sqrt{(R^2 - (D/2)^2)} = R \cdot \sqrt{(1 - (D/(2 \cdot R)))^2}$$

$$\Delta X = R - X = R \cdot (1 - (1 - D^2/(8 \cdot R^2))) = D^2/(8 \cdot R)$$

For D = 500, R = 2500, ΔX = 12 m
For D = 500, R = 15,000, ΔX = 2 m

(b) Geometry of wavefront shape mismatches

Figure 2.4: Effects of applying far-field AEL algorithm to a mid-field source of opportunity.

AS-00-04

also by the difficulty of identifying true far-field contacts, as well as the possible lack of high signal-to-noise ratio (SNR) far-field contacts in highly cluttered environments. Near-field sources of opportunity are available in abundance in most environments; therefore SNR is not an issue. The difficulty of this method is that too little information is available to guarantee algorithm convergence in a general case. To limit the degrees of freedom of the system, it is assumed that the source of opportunity has passed the array on a constant-speed straight-line course. Thus, the source track can be defined by four parameters, in this case being the time of closest point of approach (CPA), the bearing to the CPA point, the CPA range, and the speed. With these four parameters as unknowns, along with the *x*-*y* location of each receiver element, a solution can usually be obtained. This algorithm has not proven to be as robust and reliable as the other two, mainly due to the difficulty of obtaining an accurate enough initialization of the source track, and so it should still be considered to be in a developmental stage.

The distinction between having navigation available and not available can generally be compared to the difference between overt and covert AEL. Overt AEL is done in a way that could compromise the location of the nodes, such as driving a back-and-forth pattern around each node with a surface ship, as was done in FET. Covert AEL indicates the intent to derive array configurations without doing anything that would give away the locations of the nodes, as was demonstrated at FET using the far-field no-navigation algorithm. There are exceptions to this, such as using radar to obtain navigational information on near-field sources of opportunity, or having a dedicated surface asset transit through the field in a fairly linear manner but along a path that brings it past some or all of the nodes in the field.

2.4 QUALITY ASSESSMENT OF ALGORITHM RESULTS

As the AEL process proceeds, various diagnostic displays are provided to allow for an assessment of the validity of the solution obtained. Some of these are listed below.

- As the linetracker runs, it displays a sequence of omni×omni correlagrams, with the derived time-τ relationship superimposed. This relationship shows if the linetracker has skipped traces, or if the trace of interest has faded out.
- Scoring of the time-τ points is shown, which allows thresholding to be applied to remove low quality data.
- As AEL iterates, the current estimates of the source and receiver positions are displayed. For the near-field navigation method, the distortion of the source track should be minimal, as shown in Fig. 2.5. Significant distortion of the source track, as for example in Fig. 2.6, indicates systematic errors such as depth variation of the receiver array or poor initialization of sources or receivers. Appendix B contains displays for all events of the source track upon convergence.
- Upon algorithm convergence, the distances between adjacent receiver elements are compared to the planned separations. Since the length of cable between elements limits their true separation, significant over-nominal separation is generally an indication of problems such as incorrect linetracking, or an incorrect environmental description.

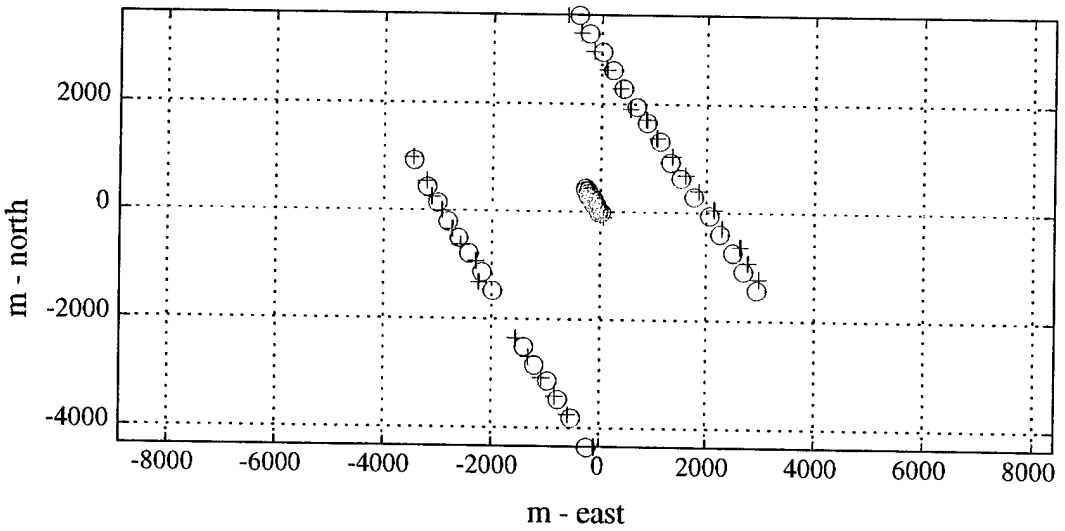

Source positions: original (o) and current (+)
Receiver Positions: original (o) and current (+)

Figure 2.5: Source-receiver geometry upon successful algorithm convergence. Node 11, event 084/20/00

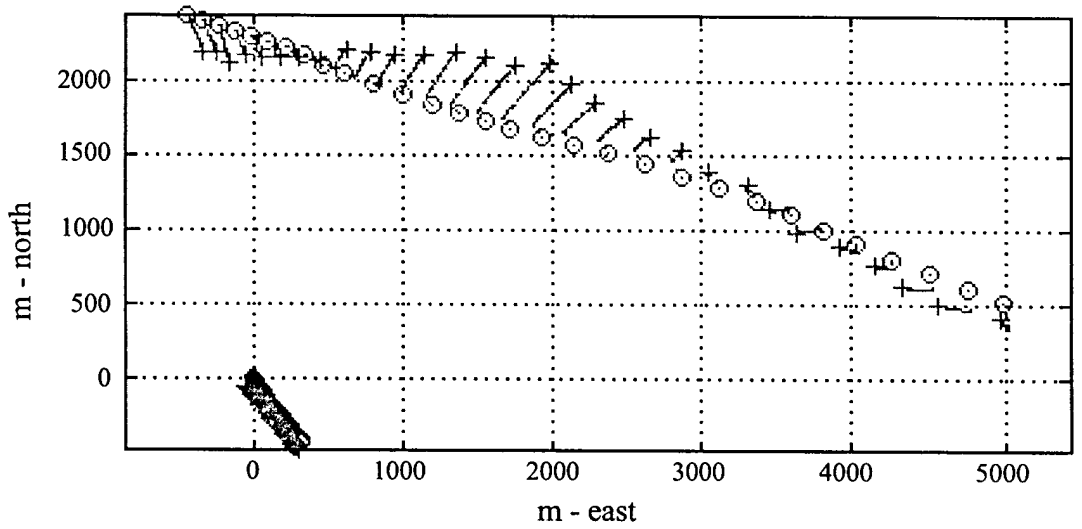

Source positions: original (o) and current (+)
Receiver positions: original (o) and current (+)

Figure 2.6: Source-receiver geometry upon unsuccessful algorithm convergence.
In this example, systematic errors resulting from an offset in assumed receiver position cause a distorted source track upon convergence, suggesting that the solution obtained is not trustworthy.
Node 33, event 087/09/00

AS-00-06

- Upon algorithm convergence, the RMS error between the modeled and the measured time delays is computed. A high RMS error indicates either premature convergence of the algorithm or noisy but otherwise correct data.

2.5 ARRAY APERTURE ESTIMATION USING SOURCES OF OPPORTUNITY

The low tension deployment of the FET arrays often resulted in arrays being relatively straight but with their apertures compressed. When these arrays were beamformed with a nominal (full aperture) array description, the apparent "endfire" beams were actually oversteered, resulting in reduced sensitivity of those beams. This caused white space to appear at the edges of the correlagrams, and similarly degraded the narrowband "endfire" beams.

Because full AEL solutions for all nodes were weeks away (due mainly to RV7's busy schedule), a means was needed to quickly obtain accurate estimates of the array aperture. To meet this need, the following tool was developed on-site. A series of omni×omni correlagrams was collected (see Fig. 2.7). These correlagrams were already being computed for use by AEL. Specific omnidirectional pairs were chosen in such a way that, using four correlagrams, the arrival time at hydrophone 1 could be related to that at hydrophone 40 (of the 40 LF hydrophones) for use in estimating the entire aperture. In the example in Fig. 2.7, the omnidirectional pairs are 1×13, 13×21, 21×31, and 31×40.

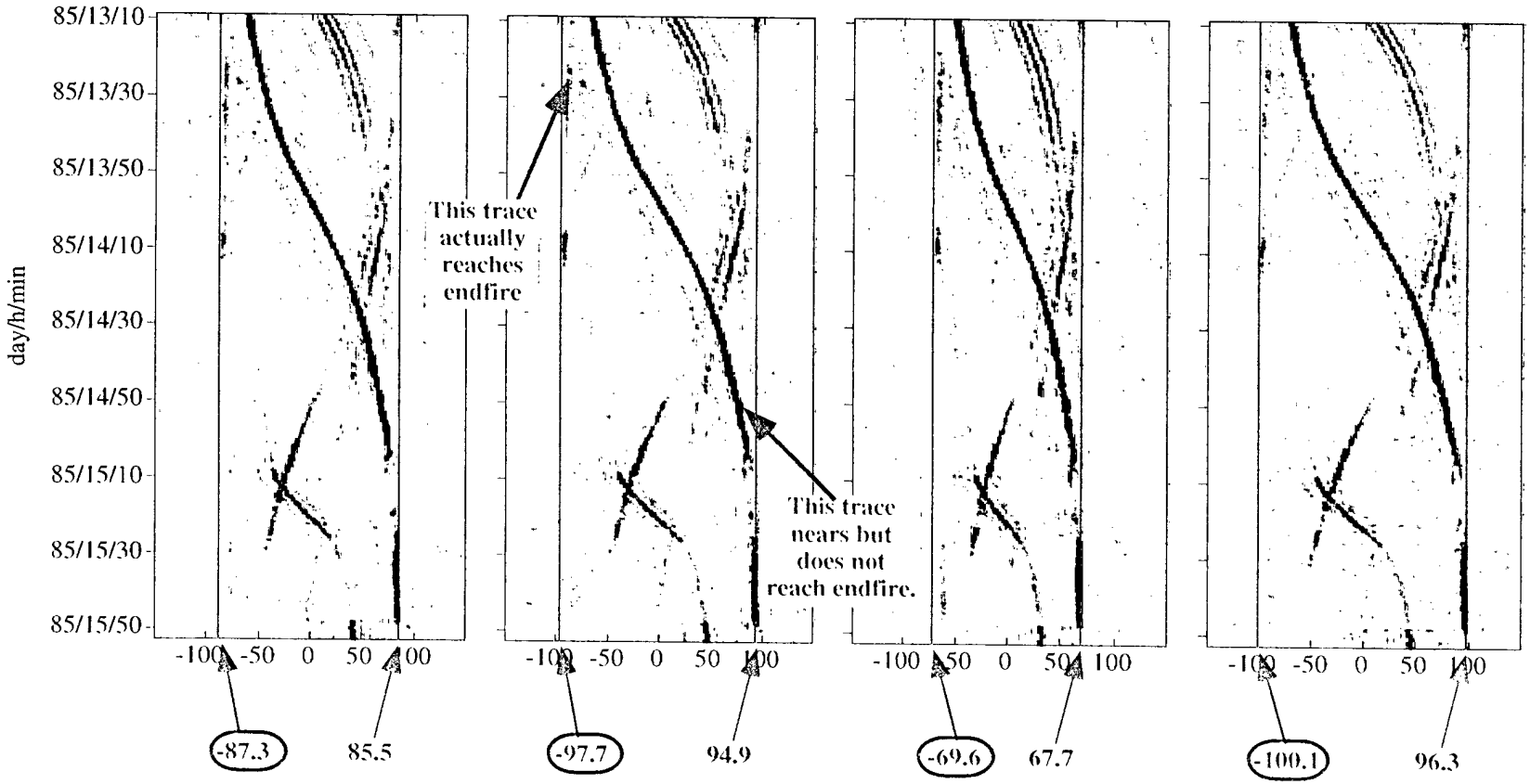

Total time delay = 87.3 + 97.7 + 69.6 + 100.1 = 354.7 ms

Estimated aperture = 354.7 ms * 1.481 m/ms = 525.3 m

Compression = 525.3m / 534m = 98.4%

Figure 2.7: Aperture estimation for node 11, using sources of opportunity.

AS-00-07

The maximum time delay (maximum in absolute value) of acoustic sources was measured on each correlagram. It was assumed that some source of opportunity would cross endfire in the 3 h of data buffered on disk at any one time. The total travel time from hydrophone 1 to hydrophone 40 could then be obtained as the sum of the four travel times extracted from these omnixomni correlagrams. The sound speed could then be used to convert this travel time to an aperture estimate.

This process could then be repeated, in case no source of opportunity had actually reached endfire during the 3-h period. In fact, because the entire procedure was so fast and easy, it was repeated several times during the test, generally returning very consistent results.

This method proved to be very accurate, providing an even better estimate of the array aperture than the overt AEL method. It was also fast, calculating aperture estimates for all 16 nodes in a few hours.

This page intentionally left blank.

3. IMPLEMENTATION IN PAS

The AEL algorithms and related software were implemented in MATLAB and C, primarily on the analysis processor (AP). MATLAB proved a very useful environment because it allowed for easy code modifications, provided convenient graphics tools, and offered easy adaptation to new analysis tasks. The general AP configuration and data flow are summarized in Fig. 3.1.

The generic multiprocessor (GMP) beamformer produced omni×omni correlagrams, over the band from 10 to 150 Hz, for a set of omnidirectional pairs selected at the site (to account for dead hydrophones, etc.). These omni×omni correlagrams were made available in shared memory, and were collected by a disk buffer manager resident on the AP, and stored in a 3-h buffer on disk.

A MATLAB program, with a display similar to that in Fig. 2.7, imaged the data in the buffer. When data useful for AEL were observed on a particular node, the buffered data for that node were "grabbed" into a permanent disk file for later analysis.

The remaining steps in the AEL process, including the linetracker, were implemented in MATLAB and C, and resided exclusively on the AP. When the AEL algorithm converged to a solution, and that solution was judged acceptable for use in the remainder of PAS (processing automation system), a configuration file was generated and copied to the appropriate beamformer.

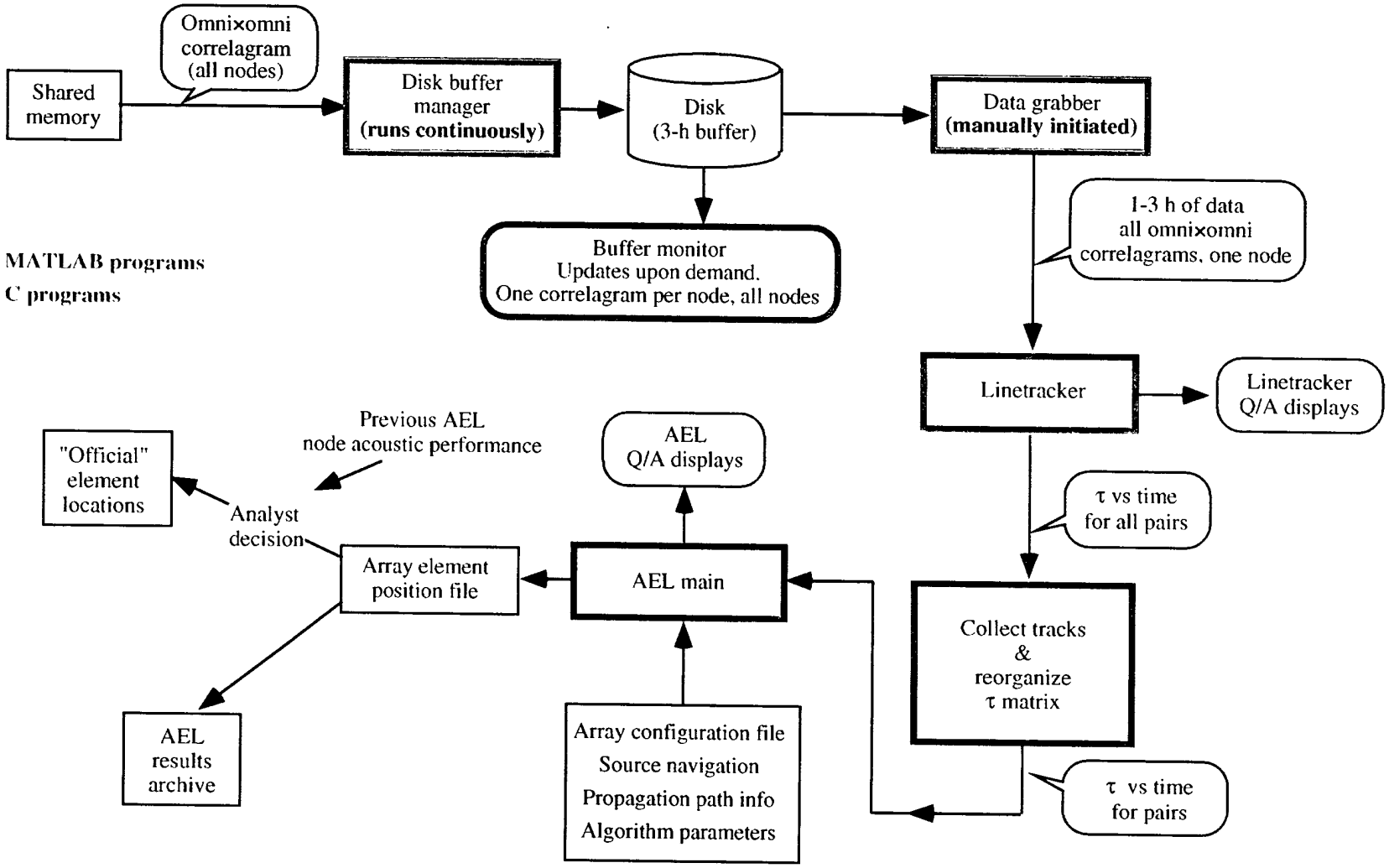

Figure 3.1: AEL data flow in the analysis processor.

AS-00-08

4. AEL RESULTS FOR FET AND MNT

The AEL results for all FET and MNT nodes are summarized in Figs. 4.1 to 4.5. In these figures, the dark blue and cyan (light blue) symbols indicate solutions obtained with the overt near-field AEL method, using RV7 or RV1. The red symbols show results from the far-field AEL algorithm, which used distant sources of opportunity. Green symbols show results from the element calibration (ELCAL) analysis, which was a completely independent array shape analysis conducted for a few FET/MNT arrays by George Shepard at BBN Systems and Technologies. Brown symbols designate results from the near-field covert method, which is still under development.

For all methods, the following convention is used to report element positions. The x and y axes are in the horizontal plane, with the origin of coordinates at either hydrophone 1 or at the lowest numbered normally functioning LF hydrophone. The x-axis passes through either hydrophone 40 or the highest numbered normally functioning LF hydrophone. The x-y-z axes form a right-hand coordinate system, with the z-axis pointing into the ocean floor. So that this document may be unclassified, the x and y receiver coordinates are normalized by the constant factor fmin. The value of fmin (or equivalently, the planned array aperture) may be requested from PMS 407, SPAWAR.

All AEL results make use of the aperture estimates collected from sources of opportunity, as discussed in Section 2.5. As mentioned there, this method provided the most reliable method of estimating the array aperture, and all results obtained from other methods were scaled accordingly.

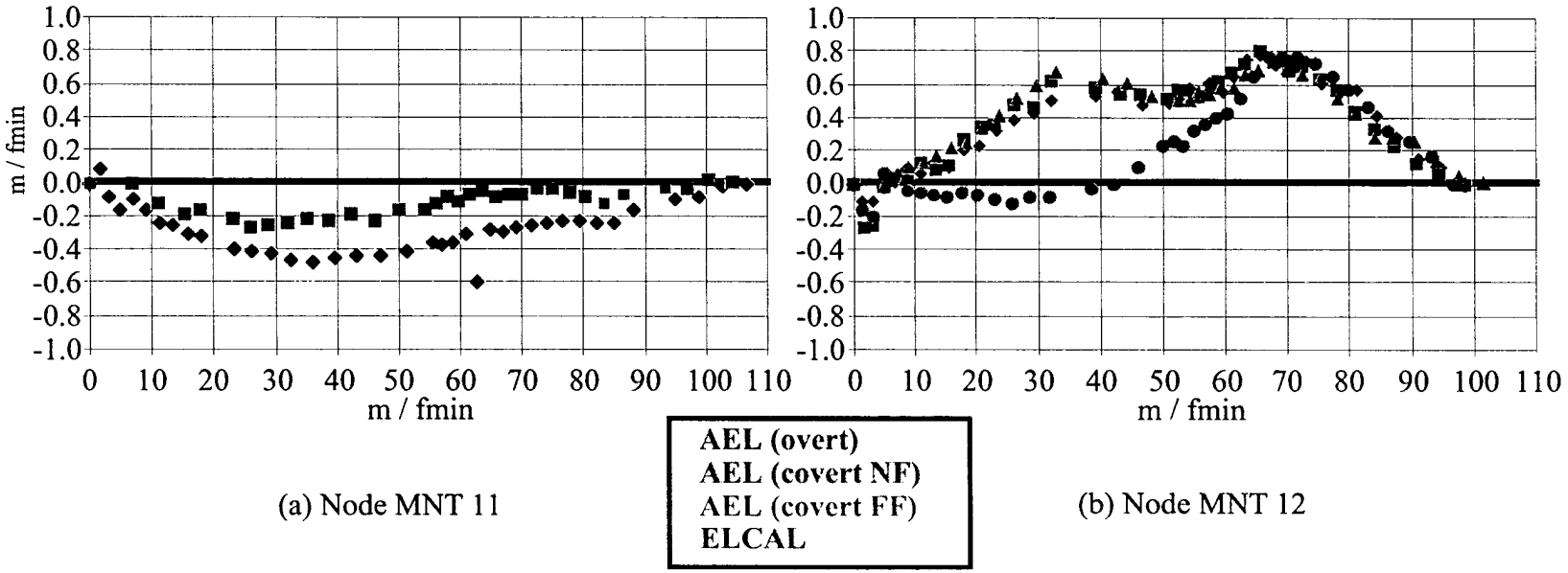

Figure 4.1: AEL results for MNT-only nodes.

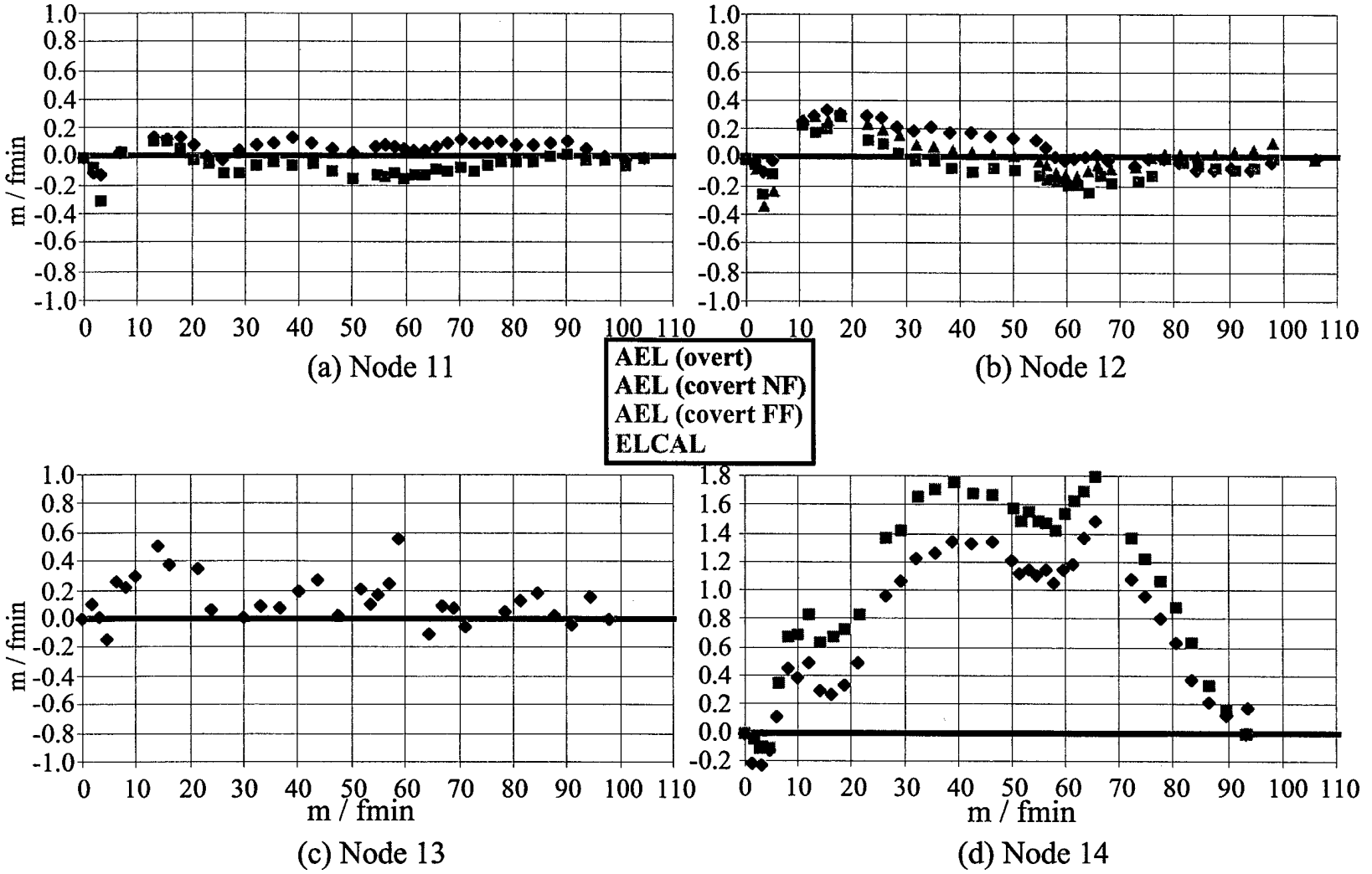

Figure 4.2: AEL results for string 1.

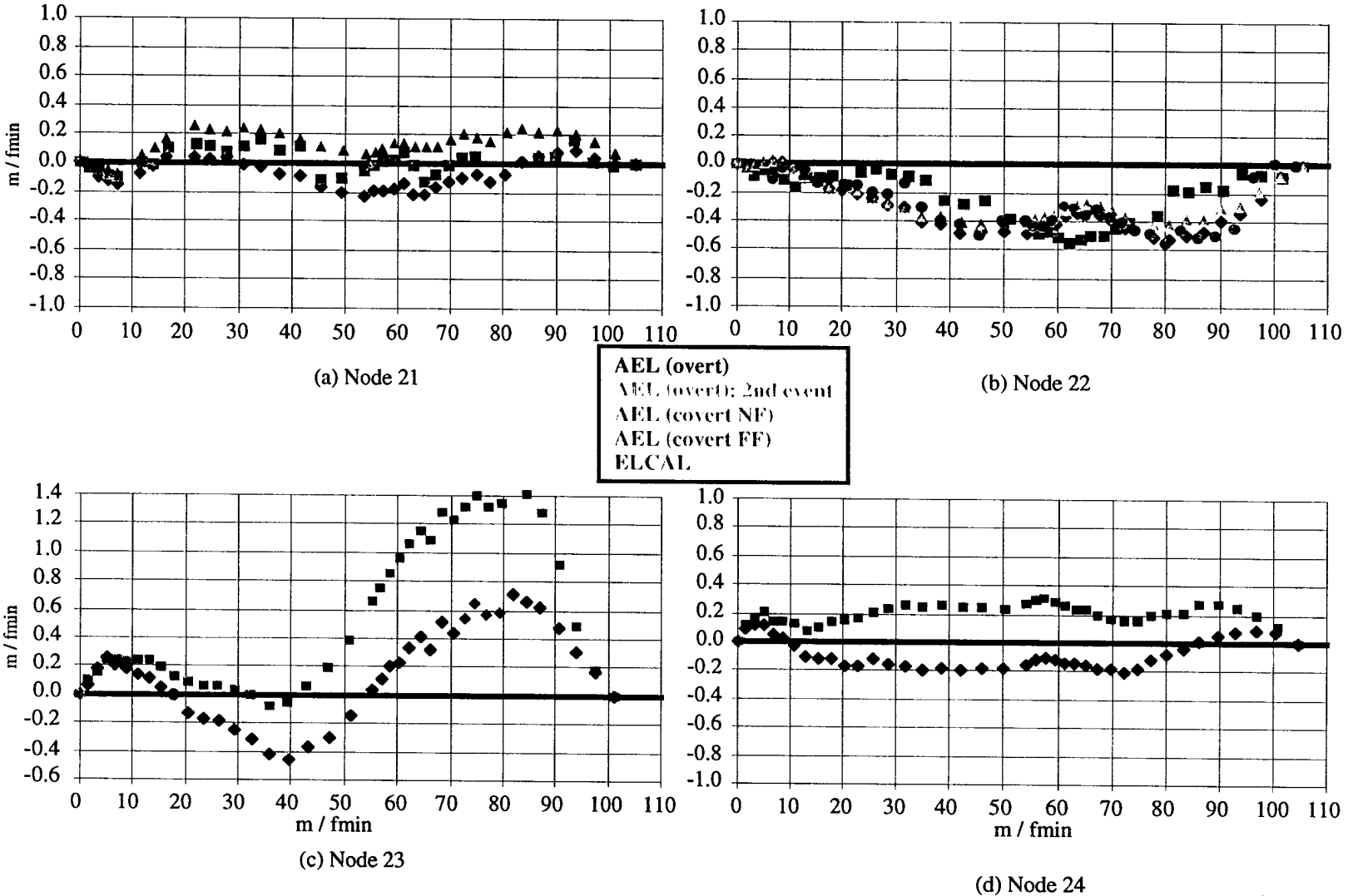

(a) Node 21

(b) Node 22

(c) Node 23

(d) Node 24

Figure 4.3: AEL results for string 2.

AS-00-11

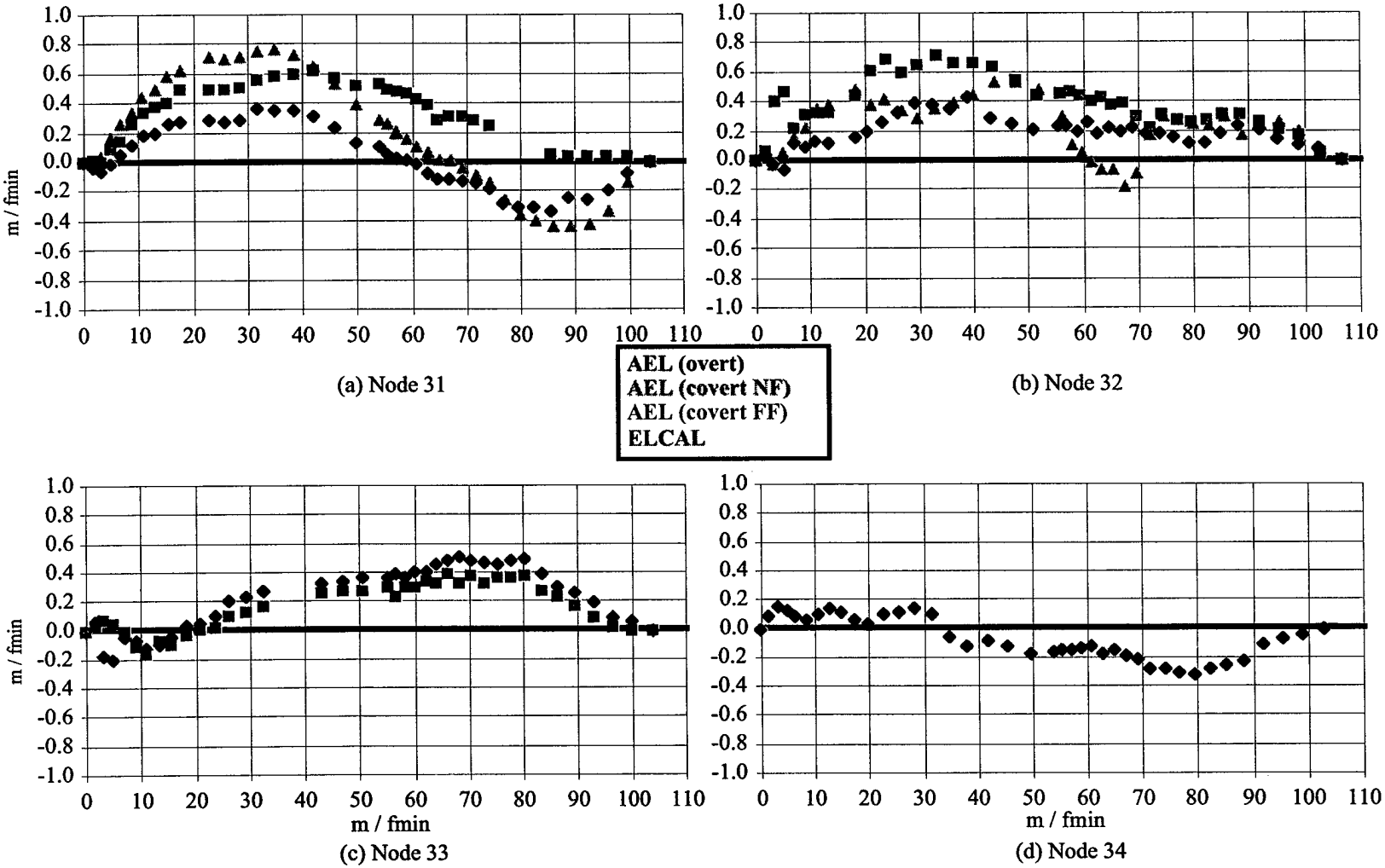

Figure 4.4: AEL results for string 3.

AS-00-12

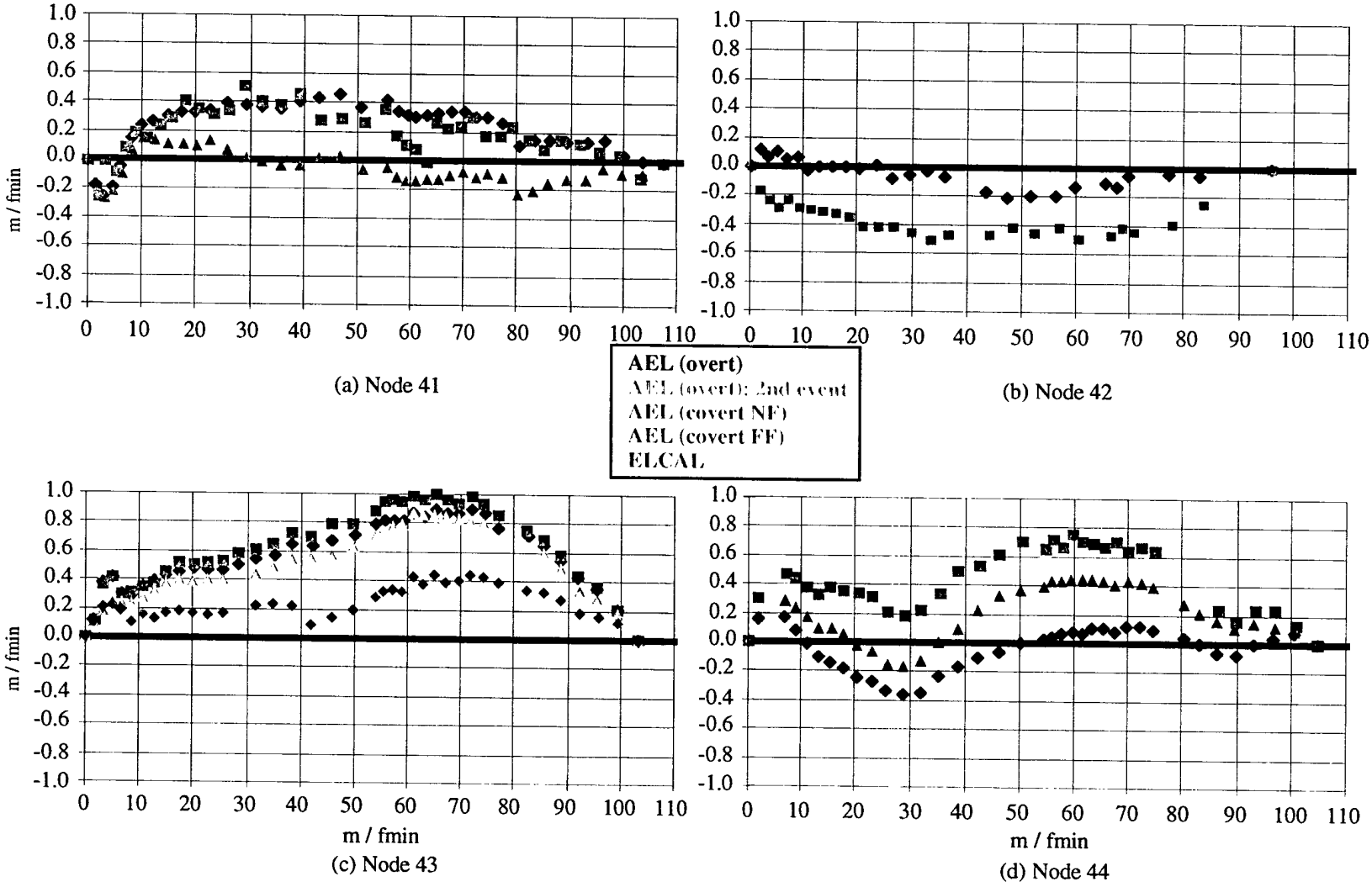

Figure 4.5: AEL results for string 4.

AS-00-13

In general, the agreement between the different AEL methods is quite close. In particular, where ELCAL results are available, they generally agreed very well with the corresponding AEL results. There was sometimes disagreement between the far-field (covert) and the near-field (overt) AEL results, generally as a result of mistaking a mid-field source of opportunity for one in the far field. Performance for the near-field covert algorithm was less satisfactory, indicating the need for further developmental work.

Figure 4.6 represents tabulated array apertures and deviation from linear for all nodes, along with a note indicating what array configuration was used in the PAS beamformer. In all but three cases the array was sufficiently straight, taking into account such factors as the angle between the two subarrays, to use a linear array description in PAS, thereby eliminating the problem of dealing with front and back beam sets. In the three cases where the arrays were not straight enough, the full AEL solution was used in the beamforming.

The lines of bearing (LOBs) collected in Fig. 4.6 note the position of hydrophone 40 relative to hydrophone 1. This number is referred to as the direction of lay (DOL) in the GMP beamformer. DOL is measured in units of degrees east of north. For the most part, the absolute position (latitude-longitude) of hydrophone 1 was not obtained from AEL, but was rather an input to the AEL process.

In Appendix A, the best estimate of *x-y* hydrophone positions is tabulated for each array, using the convention discussed in Section 2.5.

Node	% full aperture	Array LOB
11	98.1	325°
12	99.2	0°
13	91.9	326°
14	87.4	18°
21	100	330°
22	98.7	31°
23	100	20°
24	97.9	78°
31	97.3	327°
32	100	357°
33	97.5	330°
34	96.4	105°
41	100	122°
42	100	99°
43	96.7	199°
44	97.9	120°

Node	Max y-deviation (m/fmin)	Shape used in PAS beamformer
MNT 11	0.5	linear
MNT 12	0.8	full AEL
11	< 0.2	linear
12	0.3	linear
13	0.3	linear
14	1.5	full AEL
21	< 0.2	linear
22	0.5	linear
23	0.7	linear
24	< 0.2	linear
31	0.6	linear
32	0.4	linear
33	0.5	linear
34	0.3	linear
41	0.5	linear
42	< 0.2	linear
43	0.9	full AEL
44	0.5	linear

Figure 4.6: Array aperture, LOB, and curvature summary.

In Appendix B, various displays are shown for each of the overt near-field AEL events. These displays are useful for determining the trustworthiness of the results for each case. Examples of the omni×omni correlagrams are shown, which demonstrate the bearing extent achieved by the source (more is better) and the SNR (more is better). It appeared that RV1 was a much quieter ship than RV7, to the extent that RV1 was nearly too quiet for use as an AEL source. RV1 was used for the AEL runs at nodes 23, 41, and 42.

Other displays in Appendix B include run geometry, both from the navigation (top) and upon algorithm convergence (bottom). Results suggest that good agreement between the initial and the converged geometry is the strongest indicator of a correct solution.

This page intentionally left blank.

5. DISCUSSION OF AEL RESULTS

5.1 COMPARISON OF RESULTS AND ACCURACY ESTIMATES

Excluding the results from the near-field covert method, the different AEL algorithms generally provided comparable results. One exception to this occurred during use of the far-field covert method, when a midrange source of opportunity was mistaken for a far-field contact. It was often difficult to distinguish between these two cases based solely on the omni×omni correlagram, as the example in Fig. 5.1 illustrates. This source of error came in to play for the far-field solutions for nodes 31, 32, 44, and perhaps for MNT 11 as well.

As discussed earlier, the field processor can provide the means to determine the range to a source of opportunity being considered for far-field AEL. If the source is not sufficiently distant, it should not be selected for use in AEL. As an alternative to discarding such a source of opportunity, the data from that source could be processed and then a correction to the overall array curvature could be applied to the result, based on the range to the source as obtained from the field processor.

For cases where ELCAL and overt AEL results were both available (nodes 22 and MNT 12), the agreement was excellent. Both the overall shape and the detailed variations matched well. Since agreement between such qualitatively different methods cannot be coincidental, these two cases provide the best opportunity for estimating the accuracy of the overt AEL results in general.

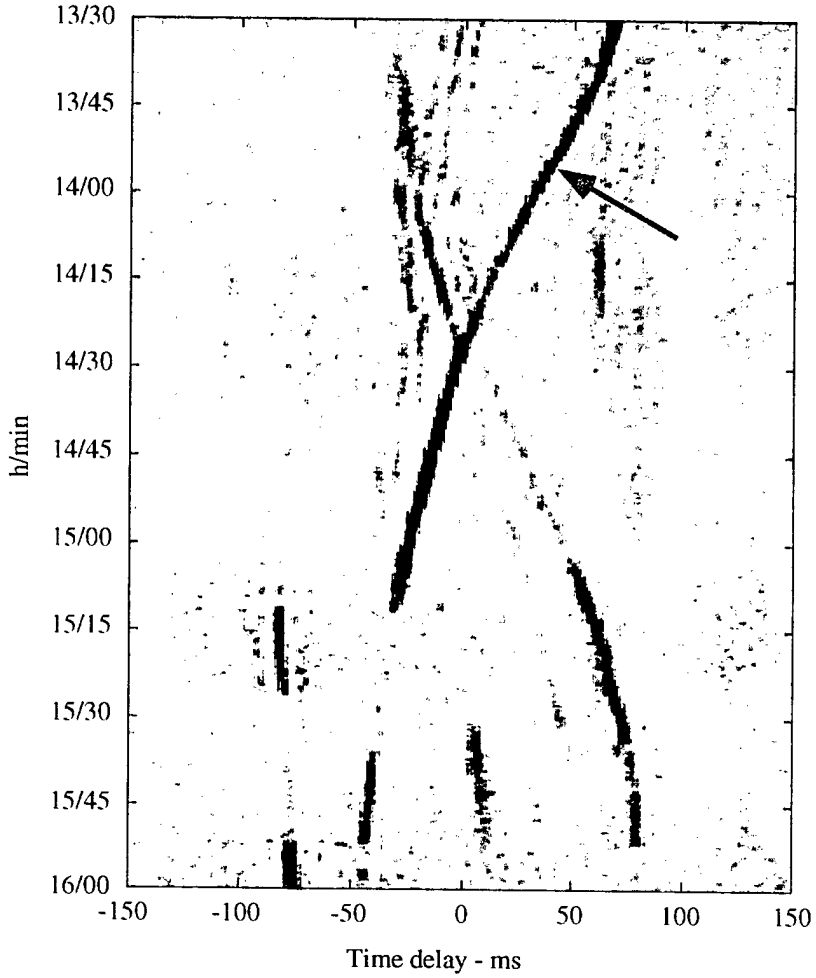

(a) True far-field contact
Node 43, 085/13/30 to 085/16/00

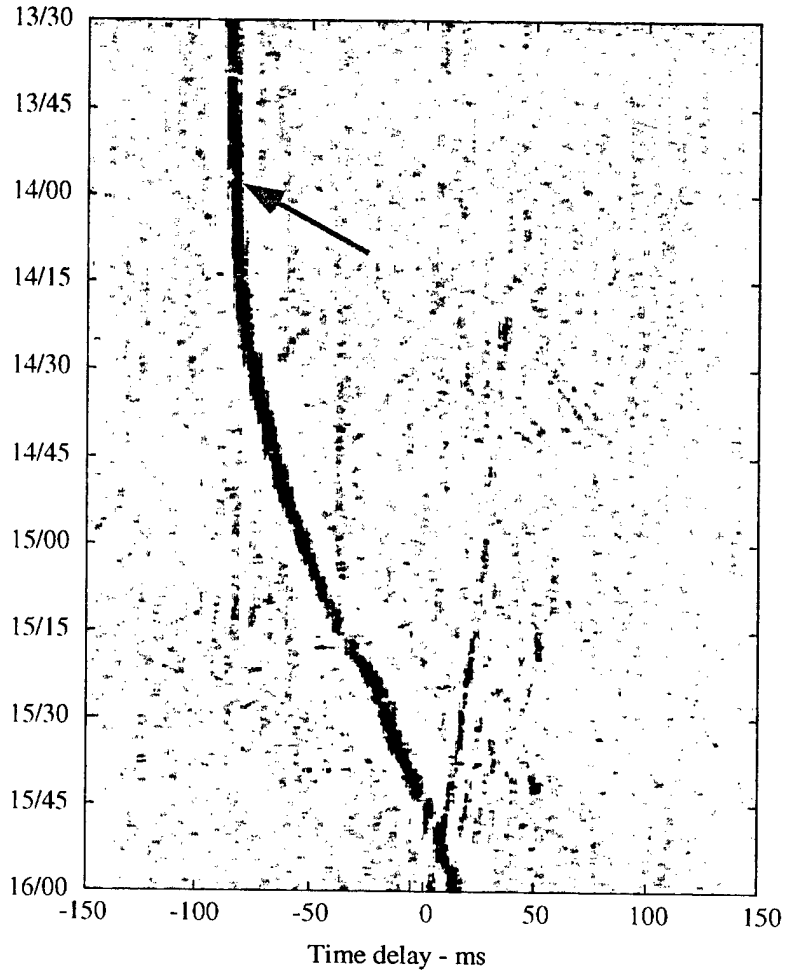

(b) Apparent far-field contact, actually in mid-field
Node 44, 105/13/30 to 105/16/00

AS-00-15

Figure 5.1: Omnixomni correlagrams for far-field and mid-field contacts.

In both of these cases, the maximum deviation between element positions found by the two methods is about 0.5 m, with a mean deviation of about 0.3 m. This degree of error corresponds to 10% of a wavelength at 300 to 500 Hz, offering precision adequate for the ADS application.

These two nodes (22 and MNT 12) represent optimal cases for the AEL algorithm, where there were no complicating issues (such as bottom slopes), and where no red flags were present in the operation of the AEL algorithm (such as source track distortion). Some arrays, such as nodes 23, 31, 33, and 44, showed indications of such difficulties, and so should be assigned a somewhat higher uncertainty (perhaps 1.0 m).

5.2 AUTOMATION OF THE AEL PROCESS

In general, during FET the performance reliability and accuracy of the AEL array shape estimation algorithm were excellent. The major obstacle remaining before it is considered "fleet ready" is its degree of automation. That is, the AEL algorithm implemented in a production ADS system must be capable of returning array shape estimates without the focused attention of a scientist. Based on FET experience, the algorithm is definitely not at that point yet.

One option is to integrate additional automation into the correlation-based process that was used at FET. The process was hands-on by intent during FET to allow a careful evaluation of its performance and accuracy. Certainly, additional automation could be added to the code. For instance, a more automated linetracking algorithm under

development at ARL:UT has shown reasonable reliability when tested on FET data. Also, algorithms could be developed to recognize the occurrence of a usable CPA event, based on bearing rate and SNR. Such an algorithm is in the developmental stage at ARL:UT.

Already, in addition to operating reliably and accurately, the entire AEL algorithm iterates to completion without requiring analyst interaction. The role of the analyst is to examine the algorithm output and assess its quality. However, the primary quality assessment clues (distortion of source track during iteration, over-nominal element separations, and RMS error upon convergence) could be quantitatively measured and acceptability thresholds defined for each.

In this scenario—using these acceptability thresholds as screening criteria—AEL would be running out-of-sight of the operator, and when a reasonable solution had been obtained for a particular node, an alert would be logged. It would still be necessary for a somewhat knowledgeable human operator to inspect the results, which in this case would be a sample omni×omni correlagram with the trace selected, the quantitative Q/A clues with thresholds noted, and a before-and-after beam correlagram. Previous solutions obtained for this node would also be provided for comparison. The operator would then decide whether to update the beamformer.

In addition to correlation-based AEL, alternative algorithms are also being considered. Attention has been focused on the correlation-based algorithm described here because of its accuracy and reliability. However, other array shape estimation

algorithms have also shown promise, and offer better prospects for automation. For example, a signal-gain-based algorithm has been examined at ARL:UT, and has shown good performance on simulated data. Additional research on this and other alternative approaches may produce an algorithm that offers acceptable accuracy with a higher degree of automation than correlation-based AEL can provide.

Finally, the array aperture estimation method that uses sources of opportunity could probably be automated fairly easily to quickly provide good aperture estimates with minimal operator interaction. This algorithm can be viewed as the first step in the overall AEL process, and could possibly be expanded to compute all of the receiver x-positions (positions parallel to the array axis). Knowing the x-positions would make it easier to obtain the y-positions (perpendicular to array axis) using other methods.

5.3 THREE-DIMENSIONAL AEL

It became apparent during FET that mission planning and deployment considerations prevent placement of all arrays in areas where the bottom is flat. This is a significant factor in the evaluation of the AEL algorithm, since for a few arrays, the known depth variation over the aperture of the array accounted for some discrepancies observed in the AEL results.

This finding has motivated discussion of restructuring AEL to solve for the depth of each receiver, rather than assuming that all array elements are at the same depth. Earlier versions of the correlation-based AEL algorithm have solved for the depth of each

receiver, but for reasons of speed and robustness, a two-dimensional approach was implemented in PAS during FET. Certainly, it is possible to implement a full three-dimensional algorithm for ADS, but at the cost of some complexity and computational load, as well as possible reductions in the robustness of the solution.

A simpler alternative would be to add an AEL input for the depth profile collected from the towed deployment vehicle (TDV). Comparison of the depth profile obtained from the ELCAL analysis to that from the TDV showed good agreement, indicating that the TDV depth information provided a reasonably accurate estimate. With this as an input to AEL, a solution for the x and y components of the receiver positions would be straightforward, and the errors associated with ignoring the depth variations would be avoided.

APPENDIX A

Results — Best Estimates of *x-y* Hydrophone Positions

This page intentionally left blank.

BEST ESTIMATES OF *x-y* HYDROPHONE POSITIONS

Element positions will be tabulated for each array deployed during FET. These results are the "best" approximation, generally based on the near-field overt AEL analysis using RV1 and RV7, although the ELCAL results are used for node MNT 11, and the near-field covert results are used for node 23.

The following convention is used to report element positions. The x and y axes are in the horizontal plane, with the origin of coordinates at either hydrophone 1 or at the lowest numbered non-dead LF hydrophone. The x-axis passes through either hydrophone 40 or the highest numbered non-dead LF hydrophone. The x-y-z axes form a right-hand coordinate system, with the z-axis pointing into the ocean floor.

This page intentionally left blank.

Node MNT 11

Hydrophone Number			Planned Positions	Best Solution (ELCAL)	
1-40	1-48	1-52	x(m/fmin)	x(m/fmin)	y(m/fmin)
1	1	1	0.00	x(m)	y(m)
2	2	2	1.67	0.00	0.00
3	7	7	3.40	--NOT LOCALIZED--	
4	11	15	5.28	--NOT LOCALIZED--	
5	13	17	7.19	--NOT LOCALIZED--	
6	14	18	9.22	6.80	-0.01
7	15	19	11.36	8.75	-0.06
8	16	20	13.60	10.88	-0.13
9	17	21	15.96	13.02	-0.17
10	18	22	18.44	15.35	-0.19
11	19	23	21.04	17.82	-0.17
12	20	24	23.77	--DEAD--	
13	21	25	26.65	22.89	-0.22
14	22	26	29.67	25.76	-0.27
15	23	27	32.84	28.73	-0.25
16	24	28	36.17	31.87	-0.25
17	25	29	39.67	35.15	-0.21
18	26	30	43.35	38.63	-0.23
19	27	31	47.22	42.25	-0.19
20	28	32	51.29	46.09	-0.23
21	29	33	55.56	50.16	-0.16
22	30	34	57.22	54.37	-0.17
23	31	35	58.97	56.03	-0.13
24	32	36	60.81	57.74	-0.08
25	33	37	62.75	59.57	-0.11
26	34	38	64.78	61.49	-0.07
27	35	39	66.91	63.47	-0.05
28	36	40	69.16	65.56	-0.08
29	37	41	71.52	67.76	-0.08
30	38	42	73.99	70.07	-0.08
31	39	43	76.59	72.42	-0.03
32	40	44	79.33	74.93	-0.04
33	41	45	82.20	77.57	-0.06
34	42	46	85.22	80.36	-0.08
35	43	47	88.39	83.29	-0.12
36	44	48	91.73	86.43	-0.07
37	45	49	95.23	--DEAD--	
38	46	50	98.91	93.16	-0.03
39	47	51	102.78	96.75	-0.04
40	48	52	106.84	100.49	0.01

Node MNT 12

Hydrophone Number			Planned Positions	Best Solution	
1-40	1-48	1-52	x(m/fmin)	x(m/fmin)	y(m/fmin)
1	1	1	0.00	--DEAD--	
2	2	2	1.67	0.00	0.00
3	7	7	3.40	1.59	-0.11
4	11	15	5.28	3.27	-0.10
5	13	17	7.19	5.01	-0.02
6	14	18	9.22	6.90	0.01
7	15	19	11.36	8.88	0.09
8	16	20	13.60	11.07	0.06
9	17	21	15.96	13.26	0.12
10	18	22	18.44	15.63	0.10
11	19	23	21.04	18.08	0.20
12	20	24	23.77	20.72	0.23
13	21	25	26.65	23.39	0.32
14	22	26	29.67	26.26	0.39
15	23	27	32.84	29.29	0.42
16	24	28	36.17	32.46	0.51
17	25	29	39.67	--DEAD--	
18	26	30	43.35	39.30	0.53
19	27	31	47.22	43.01	0.56
20	28	32	51.29	46.83	0.48
21	29	33	55.56	50.95	0.48
22	30	34	57.22	52.50	0.51
23	31	35	58.97	54.14	0.56
24	32	36	60.81	55.86	0.53
25	33	37	62.75	57.63	0.60
26	34	38	64.78	59.47	0.56
27	35	39	66.91	61.49	0.65
28	36	40	69.16	63.58	0.75
29	37	41	71.52	65.80	0.78
30	38	42	73.99	68.07	0.73
31	39	43	76.59	70.42	0.74
32	40	44	79.33	72.95	0.73
33	41	45	82.20	75.64	0.61
34	42	46	85.22	78.39	0.56
35	43	47	88.39	81.20	0.57
36	44	48	91.73	84.36	0.42
37	45	49	95.23	87.56	0.28
38	46	50	98.91	91.03	0.15
39	47	51	102.78	94.68	0.10
40	48	52	106.84	98.53	0.00

Node 11

Hydrophone Number			Planned Positions	Best Solution	
1-40	1-48	1-52	x(m/fmin)	x(m/fmin)	y(m/fmin)
1	1	1	0.00	0.00	0.00
2	2	2	1.67	1.61	-0.12
3	7	7	3.40	3.25	-0.12
4	11	15	5.28	--DEAD--	
5	13	17	7.19	6.81	0.04
6	14	18	9.22	--DEAD--	
7	15	19	11.36	--DEAD--	
8	16	20	13.60	13.11	0.14
9	17	21	15.96	15.44	0.12
10	18	22	18.44	17.88	0.13
11	19	23	21.04	20.37	0.08
12	20	24	23.77	23.09	0.00
13	21	25	26.65	25.94	-0.01
14	22	26	29.67	28.86	0.04
15	23	27	32.84	32.03	0.09
16	24	28	36.17	35.32	0.10
17	25	29	39.67	38.79	0.13
18	26	30	43.35	42.44	0.10
19	27	31	47.22	46.27	0.06
20	28	32	51.29	50.29	0.03
21	29	33	55.56	54.54	0.07
22	30	34	57.22	56.15	0.09
23	31	35	58.97	57.91	0.07
24	32	36	60.81	59.75	0.05
25	33	37	62.75	61.67	0.04
26	34	38	64.78	63.64	0.05
27	35	39	66.91	65.74	0.08
28	36	40	69.16	67.91	0.10
29	37	41	71.52	70.24	0.12
30	38	42	73.99	72.69	0.09
31	39	43	76.59	75.21	0.09
32	40	44	79.33	77.88	0.11
33	41	45	82.20	80.76	0.09
34	42	46	85.22	83.74	0.08
35	43	47	88.39	86.85	0.10
36	44	48	91.73	90.20	0.10
37	45	49	95.23	93.73	0.06
38	46	50	98.91	97.33	0.00
39	47	51	102.78	101.14	-0.02
40	48	52	106.84	104.77	0.00

Node 12

Hydrophone Number			Planned Positions	Best Solution	
1-40	1-48	1-52	x(m/fmin)	x(m/fmin)	y(m/fmin)
1	1	1	0.00	0.00	0.00
2	2	2	1.67	1.60	-0.06
3	7	7	3.40	3.18	-0.10
4	11	15	5.28	4.82	-0.02
5	13	17	7.19	--DEAD--	
6	14	18	9.22	--DEAD--	
7	15	19	11.36	10.58	0.25
8	16	20	13.60	12.74	0.29
9	17	21	15.96	15.11	0.33
10	18	22	18.44	17.61	0.31
11	19	23	21.04	--DEAD--	
12	20	24	23.77	22.66	0.30
13	21	25	26.65	25.47	0.29
14	22	26	29.67	28.51	0.22
15	23	27	32.84	31.61	0.19
16	24	28	36.17	34.87	0.21
17	25	29	39.67	38.37	0.17
18	26	30	43.35	42.06	0.17
19	27	31	47.22	45.92	0.15
20	28	32	51.29	50.00	0.13
21	29	33	55.56	54.31	0.12
22	30	34	57.22	55.91	0.07
23	31	35	58.97	57.71	0.00
24	32	36	60.81	59.54	-0.02
25	33	37	62.75	61.46	-0.01
26	34	38	64.78	63.51	0.00
27	35	39	66.91	65.63	0.02
28	36	40	69.16	67.85	-0.02
29	37	41	71.52	--DEAD--	
30	38	42	73.99	72.60	-0.05
31	39	43	76.59	75.29	0.00
32	40	44	79.33	77.96	-0.01
33	41	45	82.20	80.91	-0.03
34	42	46	85.22	83.95	-0.09
35	43	47	88.39	87.27	-0.09
36	44	48	91.73	90.58	-0.07
37	45	49	95.23	94.10	-0.08
38	46	50	98.91	97.91	-0.03
39	47	51	102.78	--DEAD--	
40	48	52	106.84	105.95	0.00

Node 13

Hydrophone Number			Planned Positions	Best Solution	
1-40	1-48	1-52	x(m/fmin)	x(m/fmin)	y(m/fmin)
1	1	1	0.00	0.00	0.00
2	2	2	1.67	1.61	0.10
3	7	7	3.40	3.12	0.01
4	11	15	5.28	4.72	-0.15
5	13	17	7.19	6.31	0.25
6	14	18	9.22	8.12	0.21
7	15	19	11.36	9.97	0.30
8	16	20	13.60	--DEAD--	
9	17	21	15.96	14.13	0.51
10	18	22	18.44	16.39	0.38
11	19	23	21.04	--DEAD--	
12	20	24	23.77	21.41	0.35
13	21	25	26.65	24.00	0.07
14	22	26	29.67	--DEAD--	
15	23	27	32.84	29.91	0.02
16	24	28	36.17	33.09	0.09
17	25	29	39.67	36.51	0.08
18	26	30	43.35	40.03	0.19
19	27	31	47.22	43.74	0.28
20	28	32	51.29	47.60	0.02
21	29	33	55.56	51.80	0.21
22	30	34	57.22	53.42	0.10
23	31	35	58.97	55.15	0.17
24	32	36	60.81	56.98	0.24
25	33	37	62.75	59.04	0.55
26	34	38	64.78	--DEAD--	
27	35	39	66.91	--DEAD--	
28	36	40	69.16	64.65	-0.11
29	37	41	71.52	66.82	0.10
30	38	42	73.99	69.03	0.08
31	39	43	76.59	71.29	-0.05
32	40	44	79.33	--NOT LOCALIZED--	
33	41	45	82.20	--NOT LOCALIZED--	
34	42	46	85.22	78.80	0.05
35	43	47	88.39	81.43	0.13
36	44	48	91.73	84.46	0.18
37	45	49	95.23	87.72	0.02
38	46	50	98.91	91.04	-0.04
39	47	51	102.78	94.49	0.16
40	48	52	106.84	98.15	0.00

Node 14

Hydrophone Number			Planned Positions	Best Solution	
1-40	1-48	1-52	x(m/fmin)	x(m/fmin)	y(m/fmin)
1	1	1	0.00	0.00	0.00
2	2	2	1.67	1.56	-0.21
3	7	7	3.40	3.09	-0.23
4	11	15	5.28	4.61	-0.13
5	13	17	7.19	6.19	0.12
6	14	18	9.22	7.99	0.46
7	15	19	11.36	9.86	0.39
8	16	20	13.60	11.92	0.49
9	17	21	15.96	14.08	0.30
10	18	22	18.44	16.35	0.27
11	19	23	21.04	18.68	0.33
12	20	24	23.77	21.26	0.49
13	21	25	26.65	--DEAD--	
14	22	26	29.67	26.50	0.97
15	23	27	32.84	29.37	1.07
16	24	28	36.17	32.38	1.22
17	25	29	39.67	35.68	1.26
18	26	30	43.35	39.04	1.34
19	27	31	47.22	42.62	1.32
20	28	32	51.29	46.36	1.34
21	29	33	55.56	50.15	1.21
22	30	34	57.22	51.52	1.11
23	31	35	58.97	53.11	1.14
24	32	36	60.81	54.66	1.11
25	33	37	62.75	56.24	1.15
26	34	38	64.78	57.97	1.05
27	35	39	66.91	59.68	1.15
28	36	40	69.16	61.53	1.19
29	37	41	71.52	63.46	1.37
30	38	42	73.99	65.52	1.49
31	39	43	76.59	--DEAD--	
32	40	44	79.33	--DEAD--	
33	41	45	82.20	72.35	1.08
34	42	46	85.22	74.96	0.97
35	43	47	88.39	77.61	0.81
36	44	48	91.73	80.47	0.64
37	45	49	95.23	83.47	0.38
38	46	50	98.91	86.58	0.21
39	47	51	102.78	89.89	0.13
40	48	52	106.84	93.34	0.00

Node 21

Hydrophone Number			Planned Positions	Best Solution	
1-40	1-48	1-52	x(m/fmin)	x(m/fmin)	y(m/fmin)
1	1	1	0.00	--DEAD--	
2	2	2	1.67	0.00	0.00
3	7	7	3.40	1.56	-0.03
4	11	15	5.28	3.39	-0.10
5	13	17	7.19	5.22	-0.13
6	14	18	9.22	7.12	-0.15
7	15	19	11.36	--DEAD--	
8	16	20	13.60	11.52	-0.07
9	17	21	15.96	13.83	-0.02
10	18	22	18.44	16.47	0.04
11	19	23	21.04	--DEAD--	
12	20	24	23.77	21.72	0.04
13	21	25	26.65	24.50	0.03
14	22	26	29.67	27.58	0.04
15	23	27	32.84	30.70	-0.01
16	24	28	36.17	34.10	-0.03
17	25	29	39.67	37.56	-0.07
18	26	30	43.35	41.34	-0.08
19	27	31	47.22	45.31	-0.17
20	28	32	51.29	49.38	-0.21
21	29	33	55.56	53.71	-0.23
22	30	34	57.22	55.38	-0.19
23	31	35	58.97	57.20	-0.19
24	32	36	60.81	59.17	-0.17
25	33	37	62.75	61.03	-0.14
26	34	38	64.78	62.84	-0.22
27	35	39	66.91	65.08	-0.22
28	36	40	69.16	67.17	-0.17
29	37	41	71.52	69.60	-0.12
30	38	42	73.99	72.06	-0.11
31	39	43	76.59	74.70	-0.08
32	40	44	79.33	77.45	-0.13
33	41	45	82.20	80.37	-0.08
34	42	46	85.22	83.39	0.01
35	43	47	88.39	86.63	0.05
36	44	48	91.73	89.98	0.07
37	45	49	95.23	93.52	0.09
38	46	50	98.91	97.19	0.03
39	47	51	102.78	101.09	0.00
40	48	52	106.84	105.17	0.00

Node 22

Hydrophone Number			Planned Positions	Best Solution	
1-40	1-48	1-52	x(m/fmin)	x(m/fmin)	y(m/fmin)
1	1	1	0.00	0.00	0.00
2	2	2	1.67	--NOT LOCALIZED--	
3	7	7	3.40	--NOT LOCALIZED--	
4	11	15	5.28	--NOT LOCALIZE-D-	
5	13	17	7.19	6.67	0.00
6	14	18	9.22	8.63	0.00
7	15	19	11.36	10.68	-0.03
8	16	20	13.60	12.83	-0.10
9	17	21	15.96	15.13	-0.11
10	18	22	18.44	17.52	-0.18
11	19	23	21.04	20.02	-0.18
12	20	24	23.77	22.72	-0.21
13	21	25	26.65	25.56	-0.24
14	22	26	29.67	28.51	-0.29
15	23	27	32.84	31.61	-0.31
16	24	28	36.17	34.88	-0.41
17	25	29	39.67	38.38	-0.43
18	26	30	43.35	42.03	-0.49
19	27	31	47.22	45.86	-0.48
20	28	32	51.29	49.94	-0.48
21	29	33	55.56	54.21	-0.49
22	30	34	57.22	55.83	-0.48
23	31	35	58.97	57.63	-0.45
24	32	36	60.81	59.45	-0.42
25	33	37	62.75	61.40	-0.37
26	34	38	64.78	63.44	-0.34
27	35	39	66.91	65.48	-0.32
28	36	40	69.16	67.76	-0.36
29	37	41	71.52	70.07	-0.40
30	38	42	73.99	72.48	-0.45
31	39	43	76.59	--DEAD--	
32	40	44	79.33	77.79	-0.51
33	41	45	82.20	80.62	-0.53
34	42	46	85.22	83.62	-0.50
35	43	47	88.39	86.88	-0.48
36	44	48	91.73	90.22	-0.40
37	45	49	95.23	93.72	-0.35
38	46	50	98.91	97.45	-0.24
39	47	51	102.78	101.32	-0.09
40	48	52	106.84	105.41	0.00

Node 23

Hydrophone Number			Planned Positions	Best Solution (NF Nonav)	
1-40	1-48	1-52	x(m/fmin)	x(m/fmin)	y(m/fmin)
1	1	1	0.00	0.00	0.00
2	2	2	1.67	1.62	0.10
3	7	7	3.40	3.22	0.16
4	11	15	5.28	5.00	0.24
5	13	17	7.19	6.80	0.24
6	14	18	9.22	8.74	0.23
7	15	19	11.36	10.82	0.24
8	16	20	13.60	13.05	0.25
9	17	21	15.96	15.40	0.19
10	18	22	18.44	17.84	0.13
11	19	23	21.04	20.41	0.09
12	20	24	23.77	23.23	0.06
13	21	25	26.65	26.10	0.07
14	22	26	29.67	29.11	0.04
15	23	27	32.84	32.32	0.00
16	24	28	36.17	35.64	-0.08
17	25	29	39.67	39.16	-0.05
18	26	30	43.35	42.84	0.06
19	27	31	47.22	46.69	0.19
20	28	32	51.29	50.74	0.39
21	29	33	55.56	55.05	0.66
22	30	34	57.22	56.73	0.76
23	31	35	58.97	58.49	0.86
24	32	36	60.81	60.38	0.96
25	33	37	62.75	62.23	1.07
26	34	38	64.78	64.24	1.16
27	35	39	66.91	66.29	1.09
28	36	40	69.16	68.20	1.28
29	37	41	71.52	70.38	1.23
30	38	42	73.99	72.63	1.32
31	39	43	76.59	74.92	1.40
32	40	44	79.33	77.20	1.32
33	41	45	82.20	79.61	1.35
34	42	46	85.22	81.97	1.52
35	43	47	88.39	84.37	1.42
36	44	48	91.73	87.30	1.28
37	45	49	95.23	90.71	0.92
38	46	50	98.91	94.05	0.49
39	47	51	102.78	97.41	0.18
40	48	52	106.84	101.20	0.00

Node 24

Hydrophone Number			Planned Positions	Best Solution	
1-40	1-48	1-52	x(m/fmin)	x(m/fmin)	y(m/fmin)
1	1	1	0.00	0.00	0.00
2	2	2	1.67	1.59	0.09
3	7	7	3.40	3.17	0.11
4	11	15	5.28	4.92	0.12
5	13	17	7.19	6.73	0.05
6	14	18	9.22	8.65	0.03
7	15	19	11.36	10.71	-0.03
8	16	20	13.60	12.89	-0.10
9	17	21	15.96	15.22	-0.12
10	18	22	18.44	17.70	-0.11
11	19	23	21.04	20.12	-0.16
12	20	24	23.77	22.84	-0.17
13	21	25	26.65	25.61	-0.12
14	22	26	29.67	28.58	-0.15
15	23	27	32.84	31.69	-0.17
16	24	28	36.17	35.01	-0.20
17	25	29	39.67	38.48	-0.18
18	26	30	43.35	42.11	-0.20
19	27	31	47.22	46.05	-0.18
20	28	32	51.29	49.90	-0.18
21	29	33	55.56	54.13	-0.15
22	30	34	57.22	55.78	-0.12
23	31	35	58.97	57.52	-0.10
24	32	36	60.81	59.32	-0.12
25	33	37	62.75	61.24	-0.14
26	34	38	64.78	63.05	-0.15
27	35	39	66.91	65.14	-0.16
28	36	40	69.16	67.35	-0.18
29	37	41	71.52	69.68	-0.18
30	38	42	73.99	72.13	-0.20
31	39	43	76.59	74.67	-0.18
32	40	44	79.33	77.26	-0.12
33	41	45	82.20	80.11	-0.08
34	42	46	85.22	83.13	-0.04
35	43	47	88.39	86.29	0.02
36	44	48	91.73	89.61	0.06
37	45	49	95.23	93.07	0.08
38	46	50	98.91	96.70	0.09
39	47	51	102.78	100.53	0.08
40	48	52	106.84	104.56	0.00

Node 31

Hydrophone Number			Planned Positions	Best Solution	
1-40	1-48	1-52	x(m/fmin)	x(m/fmin)	y(m/fmin)
1	1	1	0.00	0.00	0.00
2	2	2	1.67	1.61	-0.04
3	7	7	3.40	3.22	-0.07
4	11	15	5.28	4.97	-0.01
5	13	17	7.19	6.78	0.06
6	14	18	9.22	8.82	0.12
7	15	19	11.36	10.88	0.18
8	16	20	13.60	13.12	0.20
9	17	21	15.96	15.45	0.26
10	18	22	18.44	17.77	0.27
11	19	23	21.04	--DEAD--	
12	20	24	23.77	22.93	0.29
13	21	25	26.65	25.75	0.27
14	22	26	29.67	28.67	0.28
15	23	27	32.84	31.75	0.36
16	24	28	36.17	35.05	0.35
17	25	29	39.67	38.49	0.35
18	26	30	43.35	42.15	0.31
19	27	31	47.22	45.97	0.24
20	28	32	51.29	49.96	0.13
21	29	33	55.56	54.08	0.10
22	30	34	57.22	55.64	0.06
23	31	35	58.97	57.34	0.03
24	32	36	60.81	59.11	0.01
25	33	37	62.75	60.99	-0.02
26	34	38	64.78	62.89	-0.08
27	35	39	66.91	64.90	-0.12
28	36	40	69.16	66.99	-0.12
29	37	41	71.52	69.32	-0.13
30	38	42	73.99	71.67	-0.14
31	39	43	76.59	74.16	-0.18
32	40	44	79.33	76.76	-0.29
33	41	45	82.20	79.60	-0.32
34	42	46	85.22	82.58	-0.32
35	43	47	88.39	85.67	-0.34
36	44	48	91.73	88.87	-0.24
37	45	49	95.23	92.43	-0.26
38	46	50	98.91	96.06	-0.20
39	47	51	102.78	99.87	-0.08
40	48	52	106.84	103.92	0.00

Node 32

Hydrophone Number			Planned Positions	Best Solution	
1-40	1-48	1-52	x(m/fmin)	x(m/fmin)	y(m/fmin)
1	1	1	0.00	0.00	0.00
2	2	2	1.67	1.67	0.04
3	7	7	3.40	3.29	-0.03
4	11	15	5.28	5.15	-0.07
5	13	17	7.19	7.02	0.11
6	14	18	9.22	9.07	0.09
7	15	19	11.36	10.94	0.13
8	16	20	13.60	13.39	0.11
9	17	21	15.96	--DEAD--	
10	18	22	18.44	18.22	0.15
11	19	23	21.04	20.69	0.20
12	20	24	23.77	23.34	0.26
13	21	25	26.65	26.31	0.33
14	22	26	29.67	29.27	0.38
15	23	27	32.84	32.46	0.37
16	24	28	36.17	35.80	0.35
17	25	29	39.67	39.08	0.43
18	26	30	43.35	43.09	0.29
19	27	31	47.22	46.95	0.25
20	28	32	51.29	51.06	0.21
21	29	33	55.56	55.37	0.24
22	30	34	57.22	57.07	0.23
23	31	35	58.97	58.90	0.20
24	32	36	60.81	60.72	0.26
25	33	37	62.75	62.75	0.19
26	34	38	64.78	64.64	0.22
27	35	39	66.91	66.82	0.19
28	36	40	69.16	69.01	0.22
29	37	41	71.52	71.47	0.18
30	38	42	73.99	73.88	0.18
31	39	43	76.59	76.50	0.16
32	40	44	79.33	79.35	0.11
33	41	45	82.20	82.05	0.12
34	42	46	85.22	84.94	0.19
35	43	47	88.39	88.06	0.23
36	44	48	91.73	91.79	0.20
37	45	49	95.23	95.04	0.14
38	46	50	98.91	98.90	0.10
39	47	51	102.78	102.65	0.08
40	48	52	106.84	106.80	0.00

Node 41

Hydrophone Number			Planned Positions	Best Solution	
1-40	1-48	1-52	x(m/fmin)	x(m/fmin)	y(m/fmin)
1	1	1	0.00	0.00	0.00
2	2	2	1.67	1.95	-0.26
3	7	7	3.40	3.25	0.00
4	11	15	5.28	5.17	-0.09
5	13	17	7.19	6.88	0.09
6	14	18	9.22	8.87	0.19
7	15	19	11.36	11.03	0.16
8	16	20	13.60	13.28	0.24
9	17	21	15.96	15.67	0.30
10	18	22	18.44	17.85	0.41
11	19	23	21.04	20.42	0.35
12	20	24	23.77	23.28	0.31
13	21	25	26.65	26.17	0.34
14	22	26	29.67	28.91	0.52
15	23	27	32.84	32.21	0.41
16	24	28	36.17	35.66	0.39
17	25	29	39.67	39.16	0.46
18	26	30	43.35	42.99	0.28
19	27	31	47.22	46.91	0.30
20	28	32	51.29	50.99	0.27
21	29	33	55.56	55.15	0.36
22	30	34	57.22	57.01	0.17
23	31	35	58.97	58.81	0.11
24	32	36	60.81	60.72	0.08
25	33	37	62.75	62.79	-0.01
26	34	38	64.78	64.45	0.27
27	35	39	66.91	66.59	0.23
28	36	40	69.16	68.93	0.24
29	37	41	71.52	71.20	0.31
30	38	42	73.99	73.71	0.18
31	39	43	76.59	76.35	0.17
32	40	44	79.33	78.80	0.24
33	41	45	82.20	81.67	0.15
34	42	46	85.22	84.65	0.09
35	43	47	88.39	87.76	0.15
36	44	48	91.73	91.39	0.13
37	45	49	95.23	95.00	0.08
38	46	50	98.91	98.67	0.05
39	47	51	102.78	102.71	-0.11
40	48	52	106.84	106.80	

Node 42

Hydrophone Number			Planned Positions	Best Solution	
1-40	1-48	1-52	x(m/fmin)	x(m/fmin)	y(m/fmin)
1	1	1	0.00	0.00	0.00
2	2	2	1.67	1.73	0.12
3	7	7	3.40	3.19	0.07
4	11	15	5.28	5.03	0.10
5	13	17	7.19	6.68	0.05
6	14	18	9.22	8.64	0.06
7	15	19	11.36	10.60	-0.02
8	16	20	13.60	12.79	0.00
9	17	21	15.96	15.25	0.00
10	18	22	18.44	17.70	0.00
11	19	23	21.04	20.17	-0.02
12	20	24	23.77	23.21	0.01
13	21	25	26.65	25.93	-0.07
14	22	26	29.67	29.11	-0.05
15	23	27	32.84	32.28	-0.02
16	24	28	36.17	35.60	-0.06
17	25	29	39.67	--DEAD--	
18	26	30	43.35	42.86	-0.17
19	27	31	47.22	46.75	-0.21
20	28	32	51.29	51.00	-0.20
21	29	33	55.56	55.56	-0.19
22	30	34	57.22	--DEAD--	
23	31	35	58.97	59.06	-0.12
24	32	36	60.81	--DEAD--	
25	33	37	62.75	--DEAD--	
26	34	38	64.78	64.79	-0.11
27	35	39	66.91	67.05	-0.12
28	36	40	69.16	69.27	-0.05
29	37	41	71.52	--DEAD--	
30	38	42	73.99	--DEAD--	
31	39	43	76.59	76.37	-0.04
32	40	44	79.33	--DEAD--	
33	41	45	82.20	82.18	-0.06
34	42	46	85.22	--DEAD--	
35	43	47	88.39	--DEAD--	
36	44	48	91.73	--DEAD--	
37	45	49	95.23	95.20	0.00
38	46	50	98.91	--DEAD--	
39	47	51	102.78	--DEAD--	
40	48	52	106.84	--DEAD--	

Node 43

Hydrophone Number			Planned Positions	Best Solution	
1-40	1-48	1-52	x(m/fmin)	x(m/fmin)	y(m/fmin)
1	1	1	0.00	0.00	0.00
2	2	2	1.67	1.59	0.12
3	7	7	3.40	3.17	0.37
4	11	15	5.28	4.83	0.42
5	13	17	7.19	6.62	0.29
6	14	18	9.22	8.47	0.29
7	15	19	11.36	10.53	0.35
8	16	20	13.60	12.73	0.38
9	17	21	15.96	14.95	0.43
10	18	22	18.44	17.45	0.45
11	19	23	21.04	20.19	0.49
12	20	24	23.77	22.86	0.47
13	21	25	26.65	25.52	0.47
14	22	26	29.67	28.49	0.50
15	23	27	32.84	31.74	0.54
16	24	28	36.17	35.09	0.57
17	25	29	39.67	38.44	0.64
18	26	30	43.35	42.10	0.63
19	27	31	47.22	45.85	0.68
20	28	32	51.29	49.89	0.71
21	29	33	55.56	54.09	0.79
22	30	34	57.22	55.75	0.82
23	31	35	58.97	57.42	0.82
24	32	36	60.81	59.18	0.81
25	33	37	62.75	61.07	0.87
26	34	38	64.78	63.24	0.85
27	35	39	66.91	65.30	0.89
28	36	40	69.16	67.44	0.87
29	37	41	71.52	69.62	0.87
30	38	42	73.99	71.94	0.90
31	39	43	76.59	74.38	0.87
32	40	44	79.33	77.16	0.77
33	41	45	82.20	--DEAD--	
34	42	46	85.22	82.59	0.71
35	43	47	88.39	85.46	0.65
36	44	48	91.73	88.61	0.55
37	45	49	95.23	92.02	0.43
38	46	50	98.91	95.50	0.35
39	47	51	102.78	99.27	0.21
40	48	52	106.84	103.28	0.00

Node 44

Hydrophone Number			Planned Positions	Best Solution	
1-40	1-48	1-52	x(m/fmin)	x(m/fmin)	y(m/fmin)
1	1	1	0.00	0.00	0.00
2	2	2	1.67	1.64	0.17
3	7	7	3.40	--DEAD--	
4	11	15	5.28	--DEAD--	
5	13	17	7.19	6.92	0.29
6	14	18	9.22	8.91	0.23
7	15	19	11.36	11.00	0.17
8	16	20	13.60	13.18	0.10
9	17	21	15.96	15.46	0.09
10	18	22	18.44	17.72	0.06
11	19	23	21.04	20.19	-0.02
12	20	24	23.77	22.93	-0.06
13	21	25	26.65	25.73	-0.16
14	22	26	29.67	28.68	-0.17
15	23	27	32.84	31.86	-0.14
16	24	28	36.17	35.16	0.00
17	25	29	39.67	38.63	0.10
18	26	30	43.35	42.36	0.22
19	27	31	47.22	46.14	0.32
20	28	32	51.29	50.11	0.37
21	29	33	55.56	54.25	0.38
22	30	34	57.22	55.82	0.42
23	31	35	58.97	57.55	0.43
24	32	36	60.81	59.40	0.45
25	33	37	62.75	61.35	0.44
26	34	38	64.78	63.27	0.44
27	35	39	66.91	65.33	0.43
28	36	40	69.16	67.49	0.41
29	37	41	71.52	69.79	0.43
30	38	42	73.99	72.24	0.42
31	39	43	76.59	74.67	0.39
32	40	44	79.33	--DEAD--	
33	41	45	82.20	80.15	0.27
34	42	46	85.22	83.13	0.20
35	43	47	88.39	86.19	0.15
36	44	48	91.73	89.59	0.10
37	45	49	95.23	93.10	0.14
38	46	50	98.91	96.74	0.12
39	47	51	102.78	100.54	0.09
40	48	52	106.84	104.60	0.00

APPENDIX B

Displays of Source Tracks upon Convergence

This page intentionally left blank.

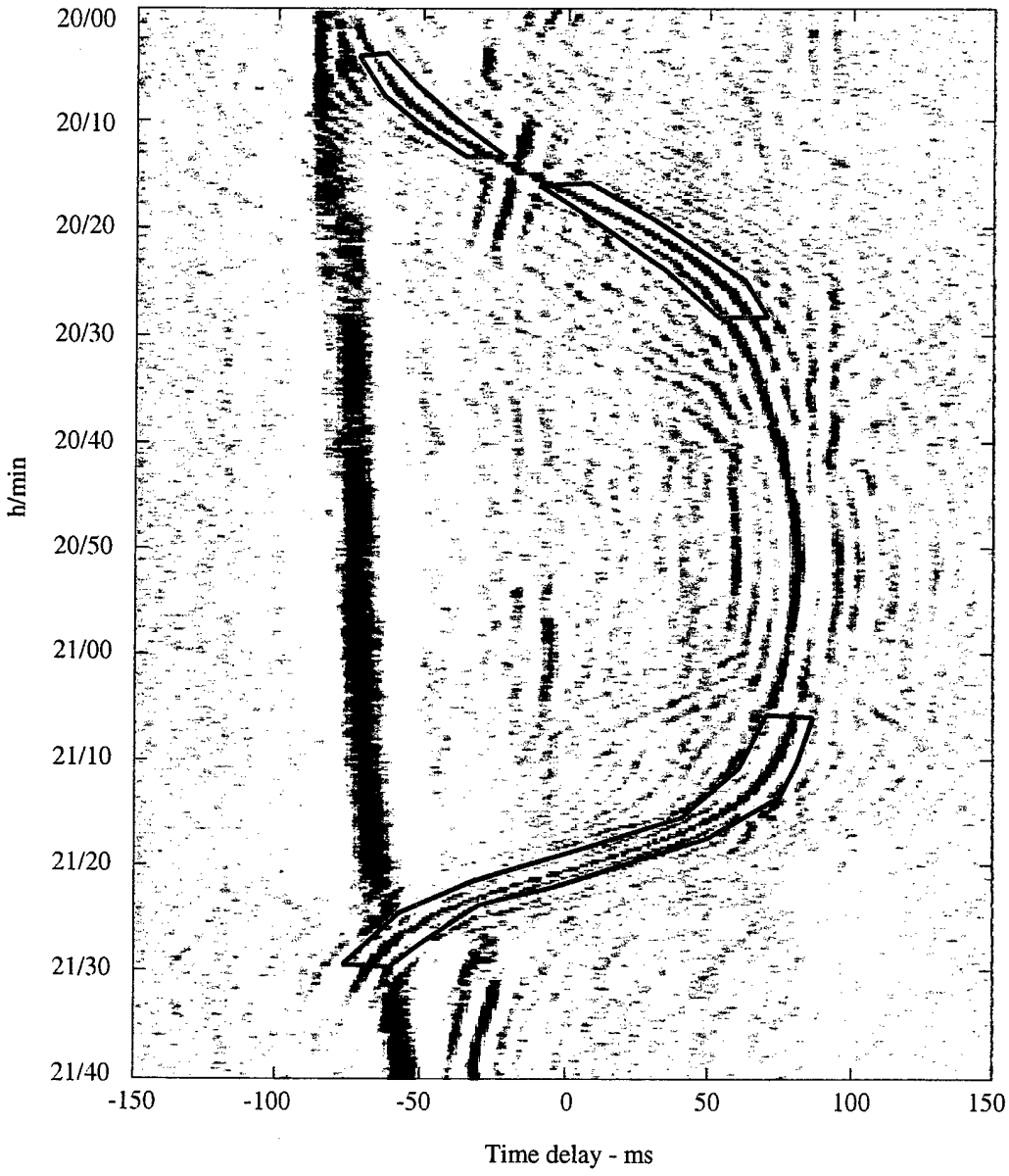

Figure B.1: Node 11. Omnixomni correlagram for near-field contact during AEL event, with processed track highlighted. Hydrophones 1 and 13, day/h/min: 084/20/00 to 084/21/40

AS-00-16

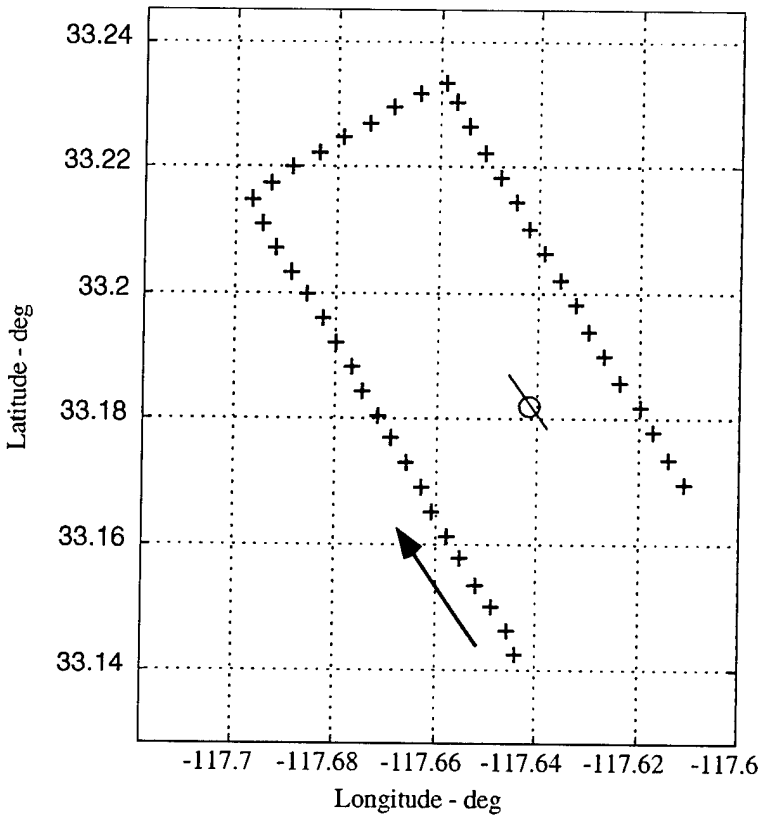

(a) Navigation geometry during AEL event, where a green "+" indicates time processed, a black "+" indicates time not processed, and a red "o" indicates receiver location.

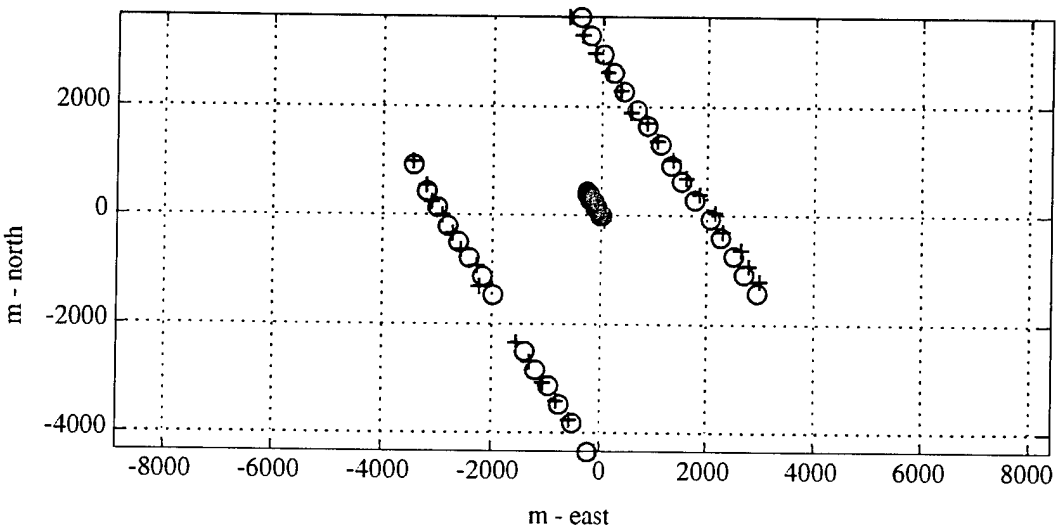

(b) Source and receiver positions upon convergence, where green indicates source location, red indicates receiver location, "+" indicates estimated location, and "o" indicates original location.

Figure B.2: Node 11. Navigation geometry during AEL event, and source track upon convergence. Day/h/min: 084/20/00

AS-00-17

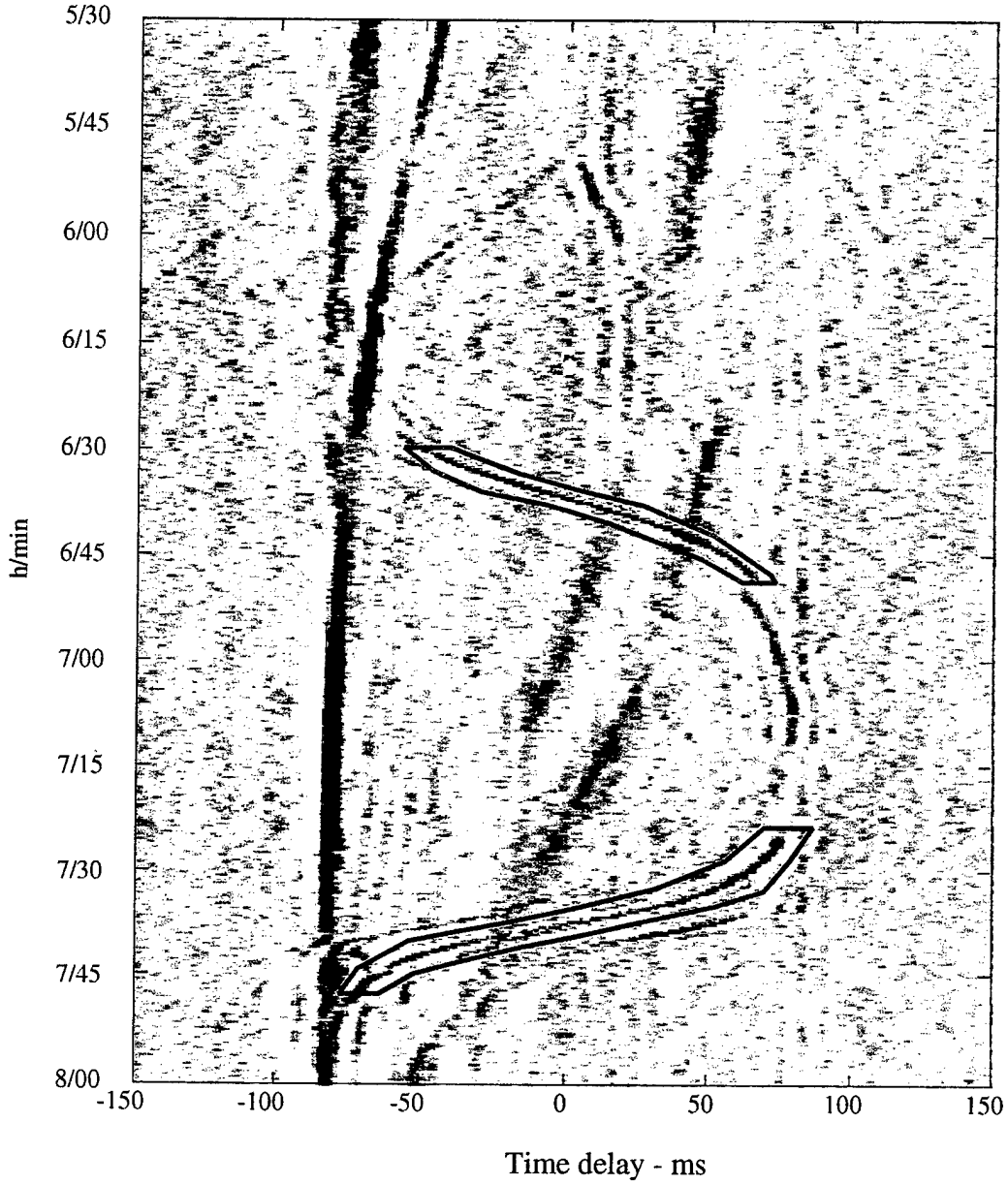

Figure B.3: Node 12. Omni×omni correlagram for near-field contact during AEL event, with processed track highlighted. Hydrophones 1 and 13, day/h/min: 085/05/30 to 085/08/00

AS-00-18

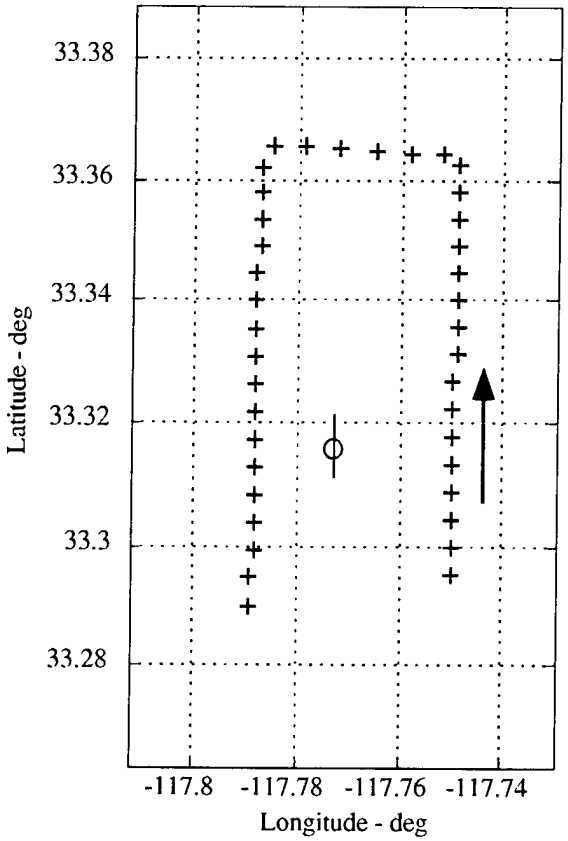

(a) Navigation geometry during AEL event, where a green "+" indicates time processed, a black "+" indicates time not processed, and a red "o" indicates receiver location.

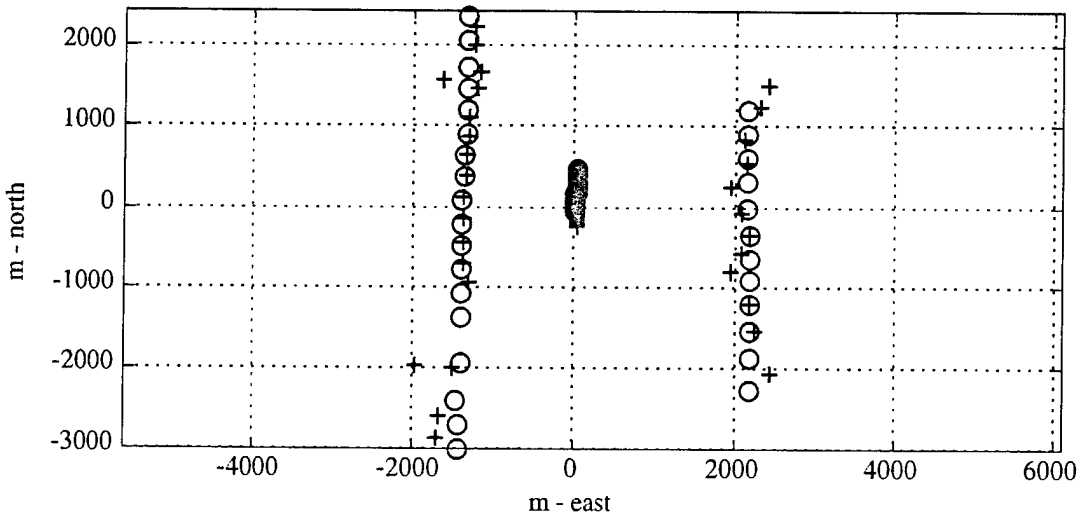

(b) Source and receiver positions upon convergence, where green indicates source location, red indicates receiver location, "+" indicates estimated location, and "o" indicates original location.

Figure B.4: Node 12. Geometry during AEL event (top) and source track upon convergence (bottom). Day/h/min: 085/05/30

AS-00-19

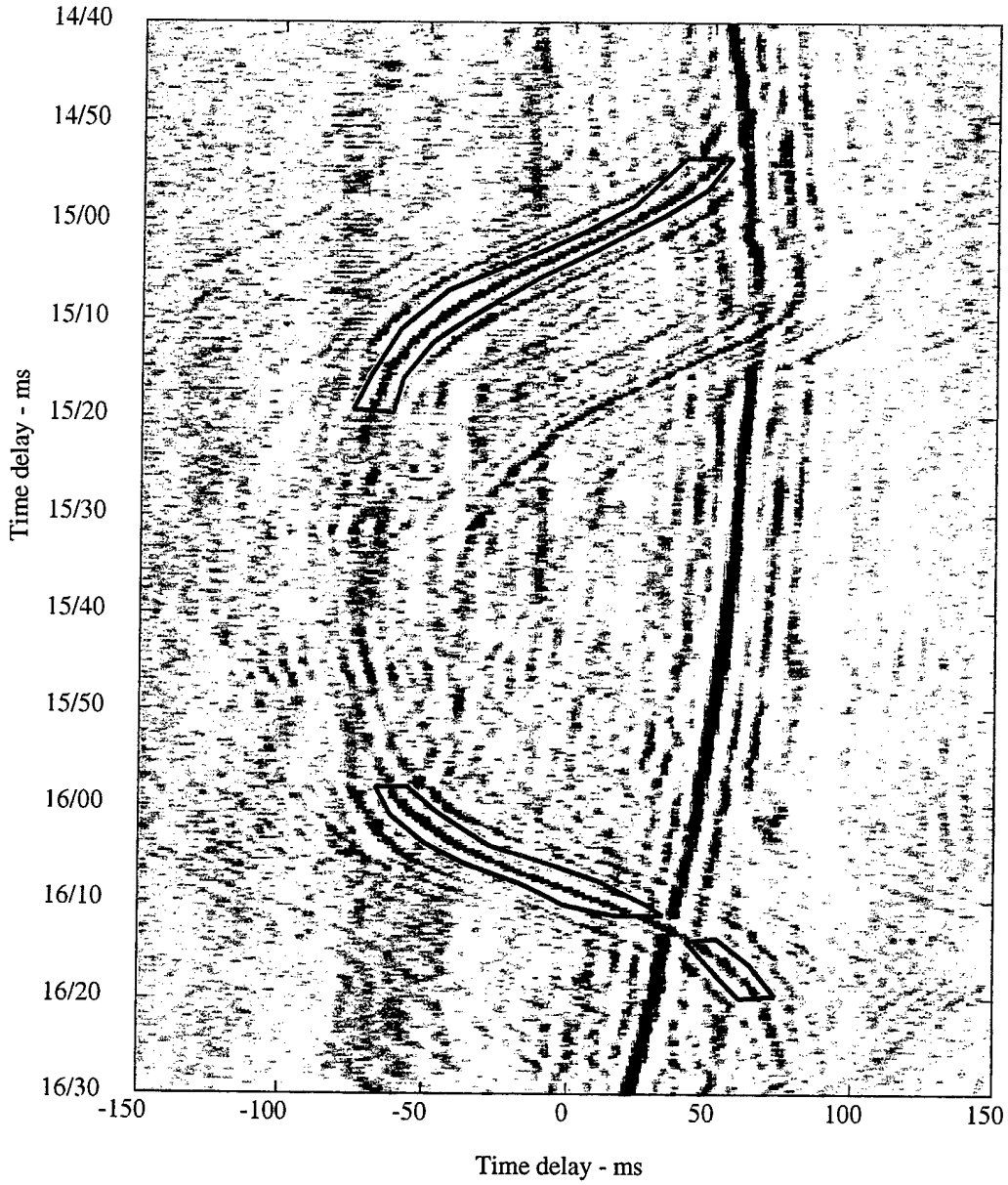

Figure B.5: Node 21. Omnixomni correlagram for near-field contact during AEL event, with processed track highlighted.
Hydrophones 13 and 20, day/h/min: 090/14/40 to 090/16/30

AS-00-20

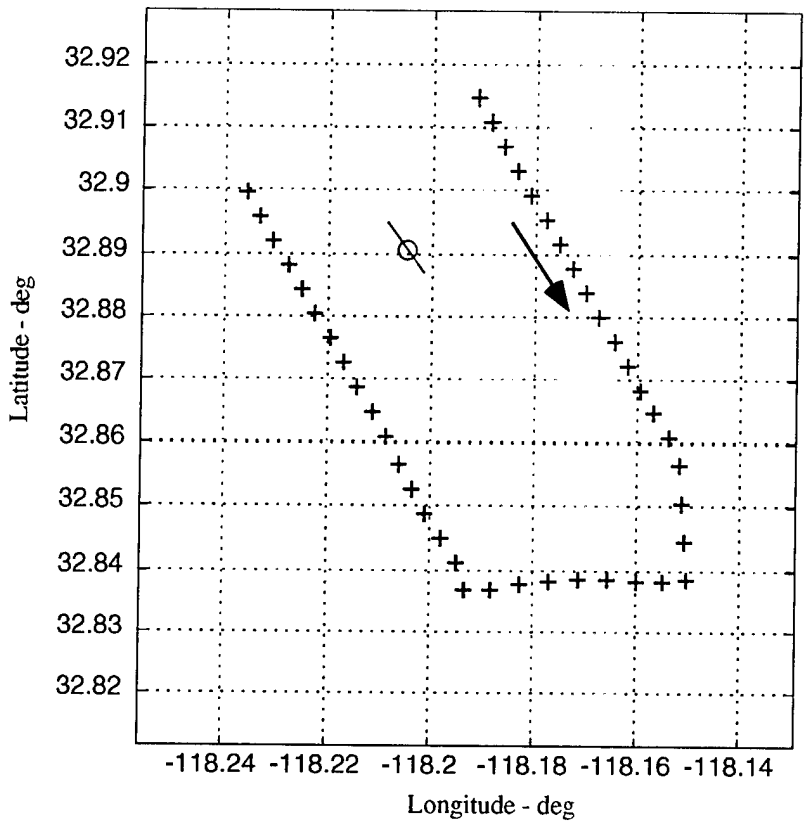

(a) Navigation geometry during AEL event, where a green "+" indicates time processed, a black "+" indicates time not processed, and a red "o" indicates receiver location.

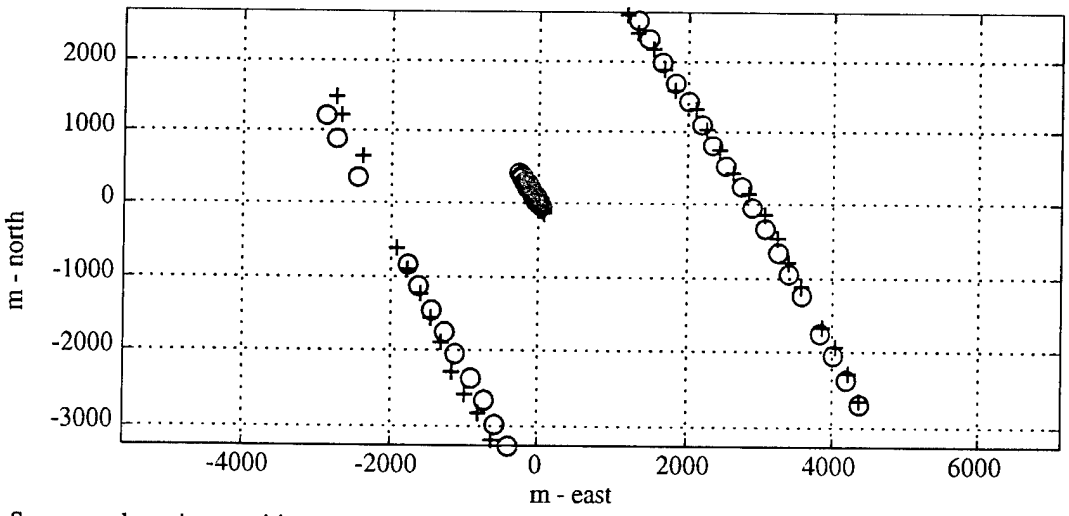

(b) Source and receiver positions upon convergence, where green indicates source location, red indicates receiver location, "+" indicates estimated location, and "o" indicates original location.

Figure B.6: Node 21. Geometry during AEL event (top) and source track upon convergence (bottom). day/h/min: 090/14/40

AS-00-21

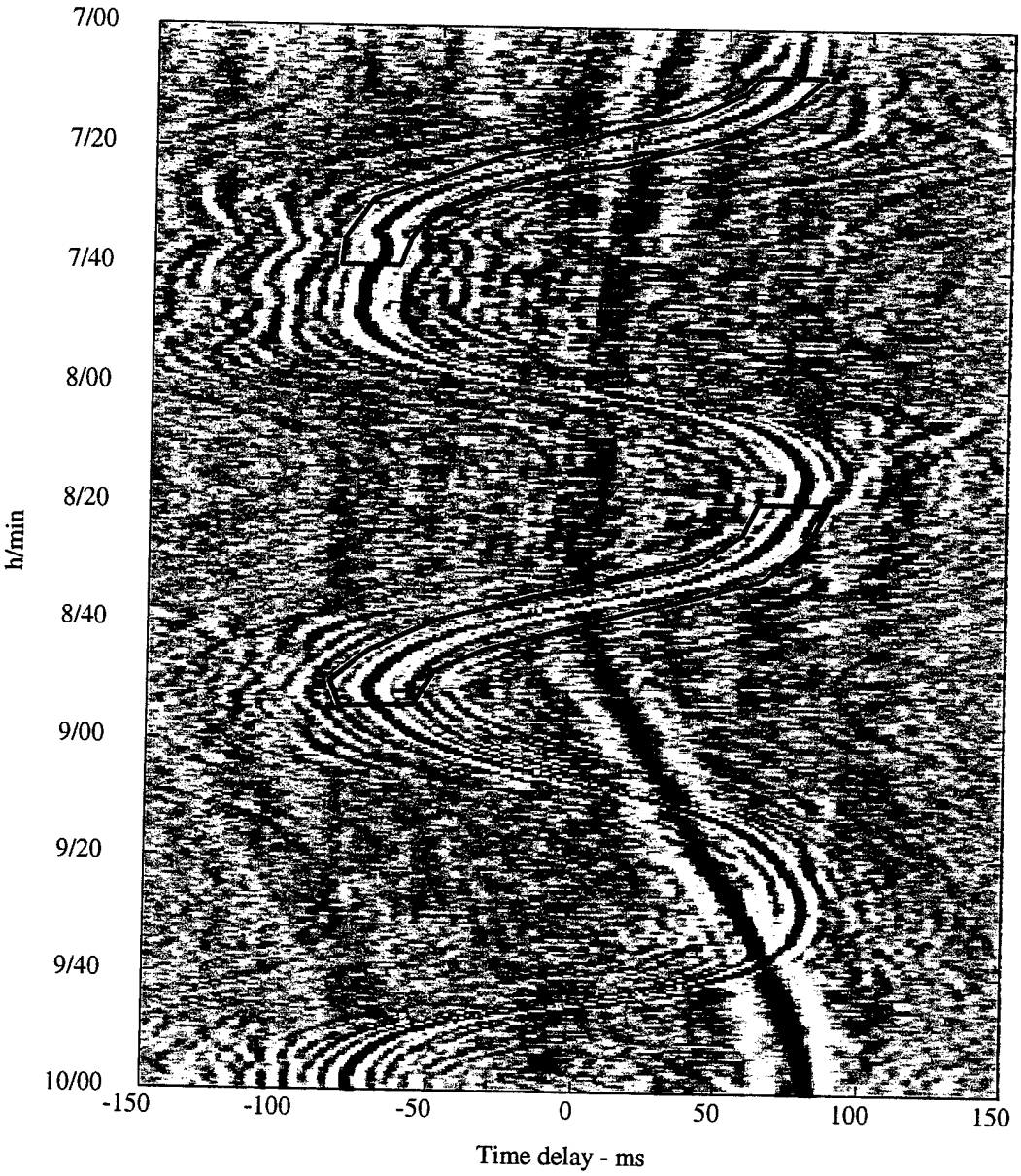

Figure B.7: Node 22. Omni×omni correlagram for near-field contact during AEL event, with processed track highlighted. Hydrophones 2 and 13, day/h/min: 107/07/00 to 107/10/00

AS-00-22

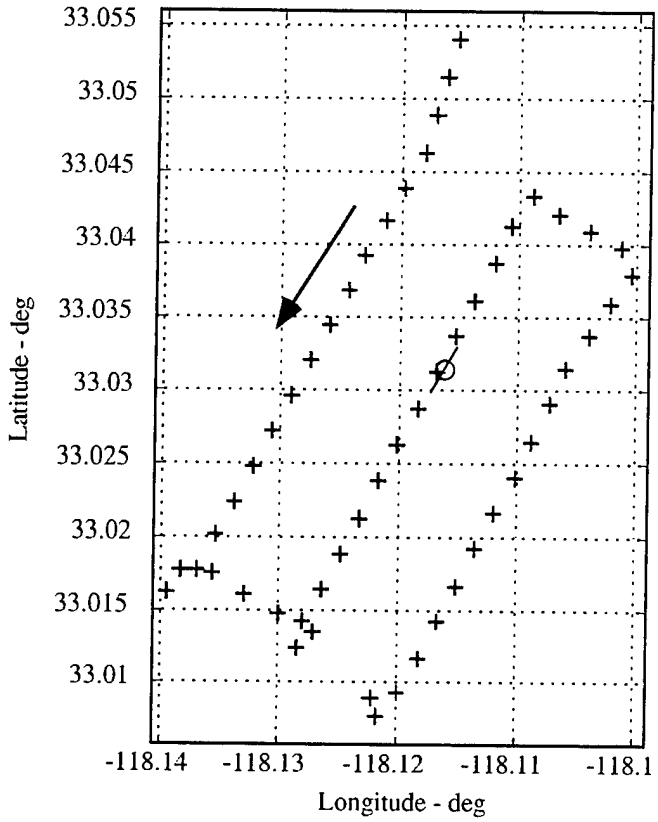

(a) Navigation geometry during AEL event, where a green "+" indicates time processed, a black "+" indicates time not processed, and a red "o" indicates receiver location.

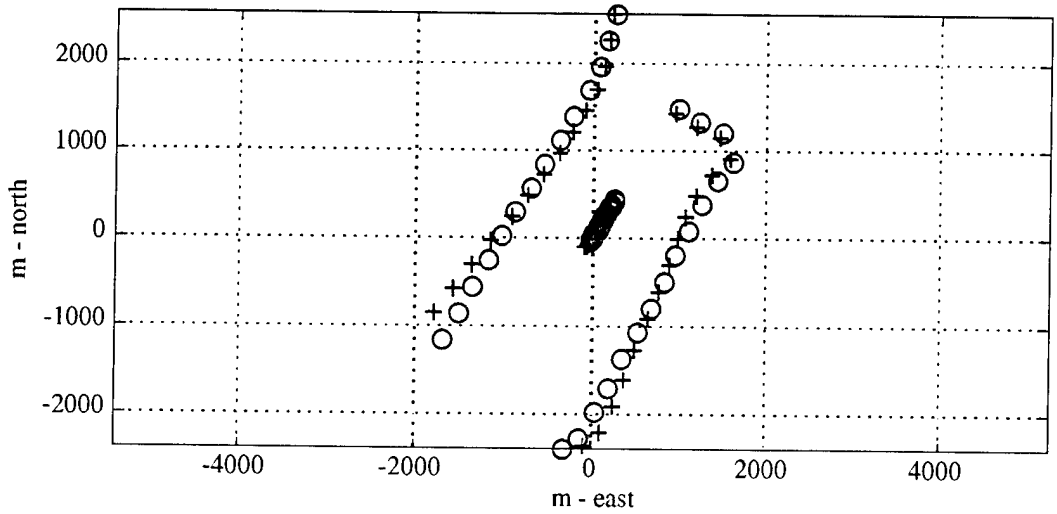

(b) Source and receiver positions upon convergence, where green indicates source location, red indicates receiver location, "+" indicates estimated location, and "o" indicates original location.

Figure B.8: Node 22. Geometry during AEL event (top) and source track upon convergence (bottom). Day/h/min: 107/07/00

AS-00-23

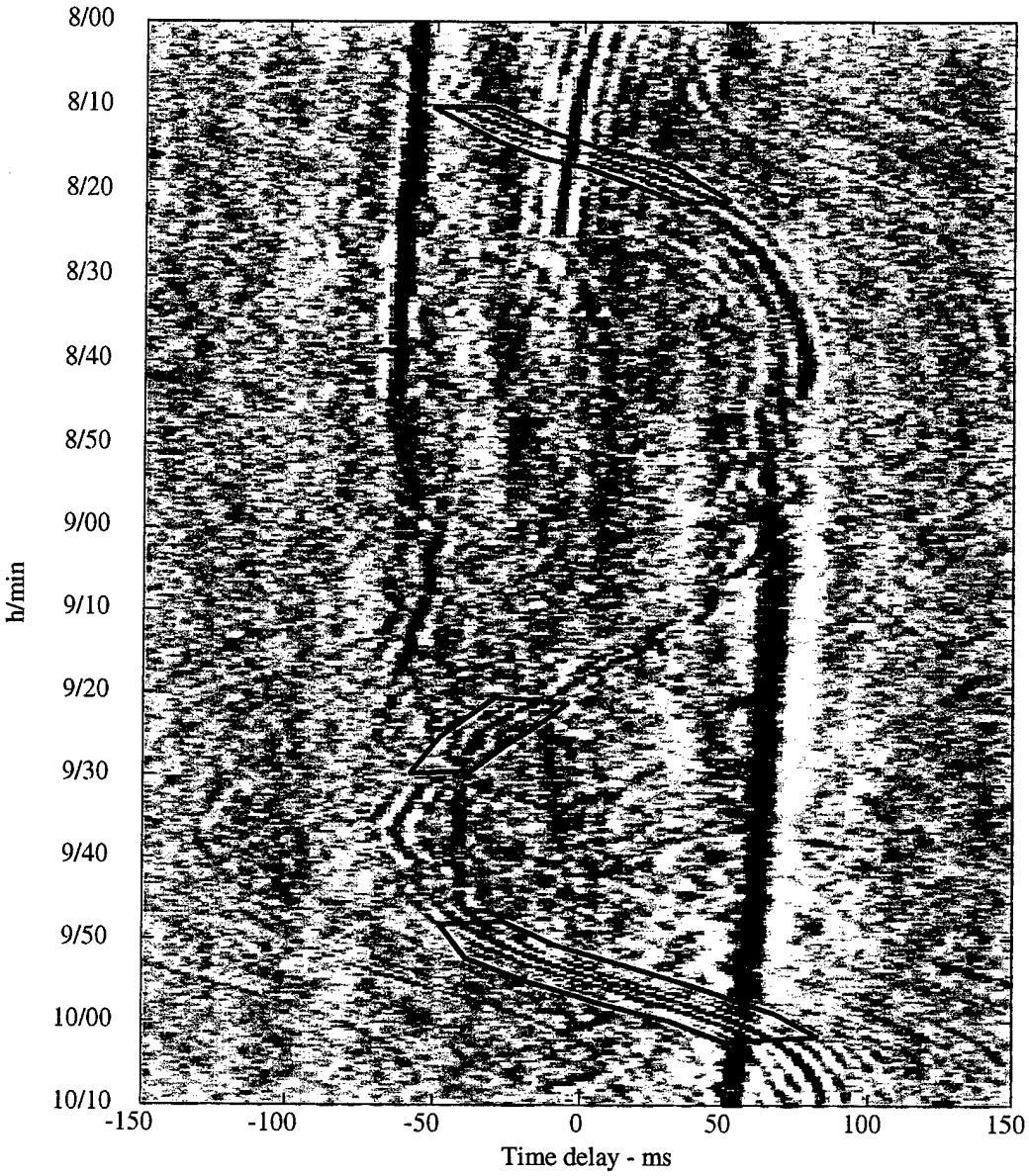

Figure B.9: Node 23. Omni×omni correlagram for near-field contact during AEL event, with processed track highlighted.
Hydrophones 1 and 13, day/h/min: 130/08/00 to 130/10/10

AS-00-24

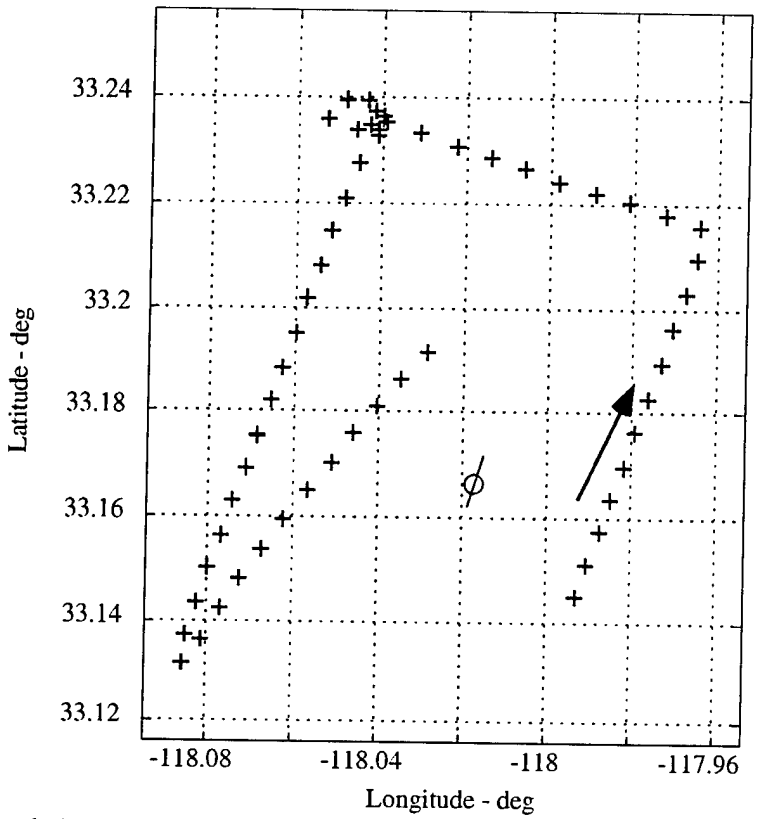

(a) Navigation geometry during AEL event, where a green "+" indicates time processed, a black "+" indicates time not processed, and a red "o" indicates receiver location.

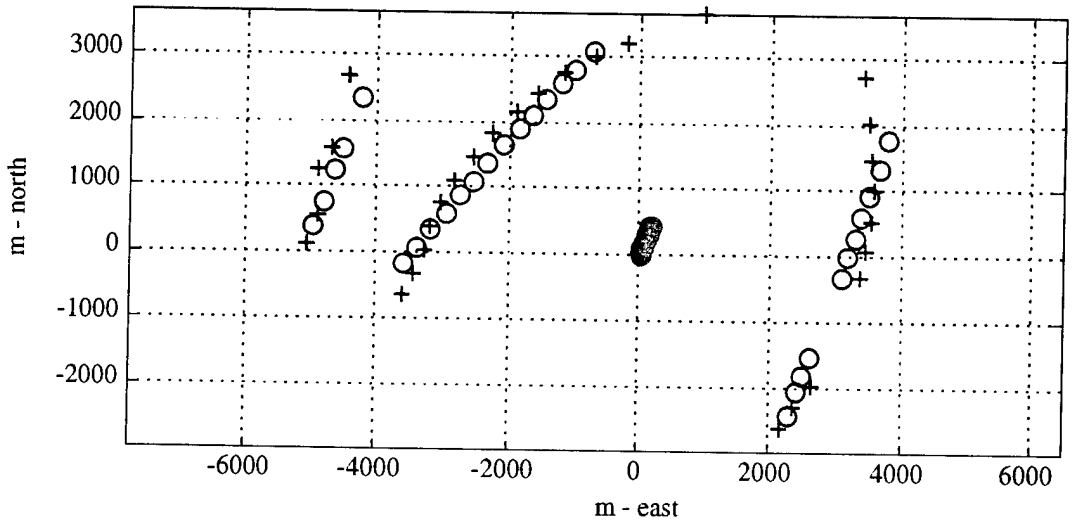

(b) Source and receiver positions upon convergence, where green indicates source location, red indicates receiver location, "+" indicates estimated location, and "o" indicates original location.

Figure B.10: Node 23. Geometry during AEL event (top) and source track upon convergence (bottom). Day/h/min: 130/08/00

AS-00-25

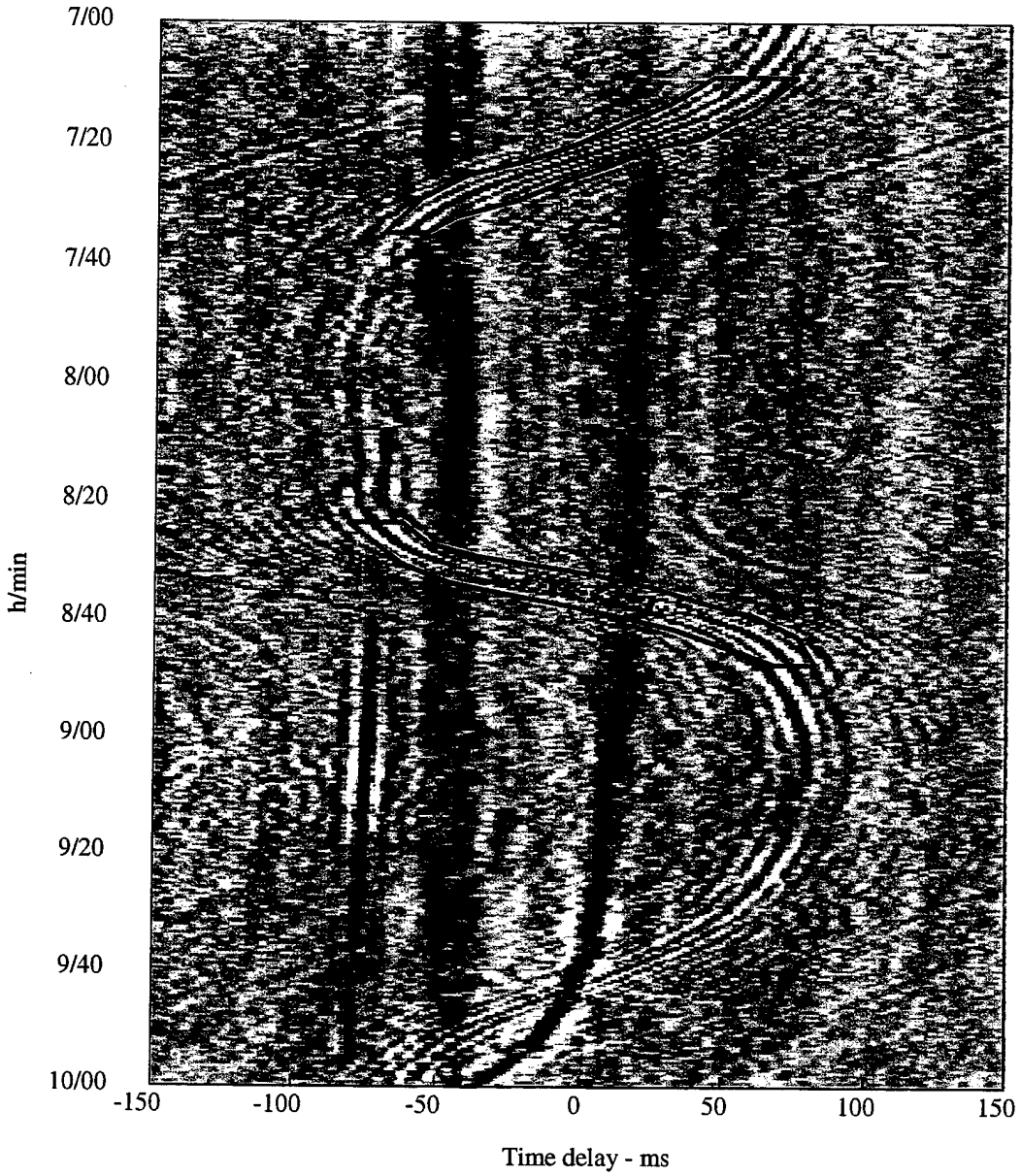

Figure B.11: Node 24. Omnixomni correlagram for near-field contact during AEL event, with processed track highlighted. Hydrophones 1 and 13, day/h/min: 090/07/00 to 090/10/00

AS-00-26

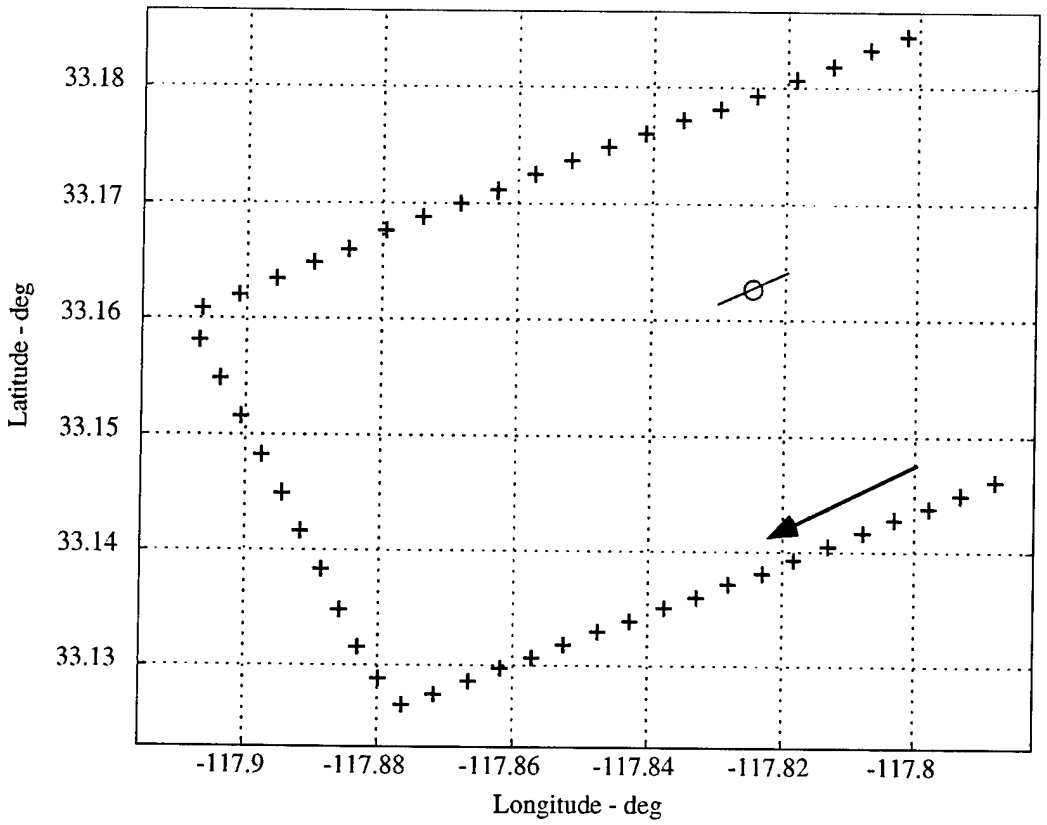

(a) Navigation geometry during AEL event, where a green "+" indicates time processed, a black "+" indicates time not processed, and a red "o" indicates receiver location.

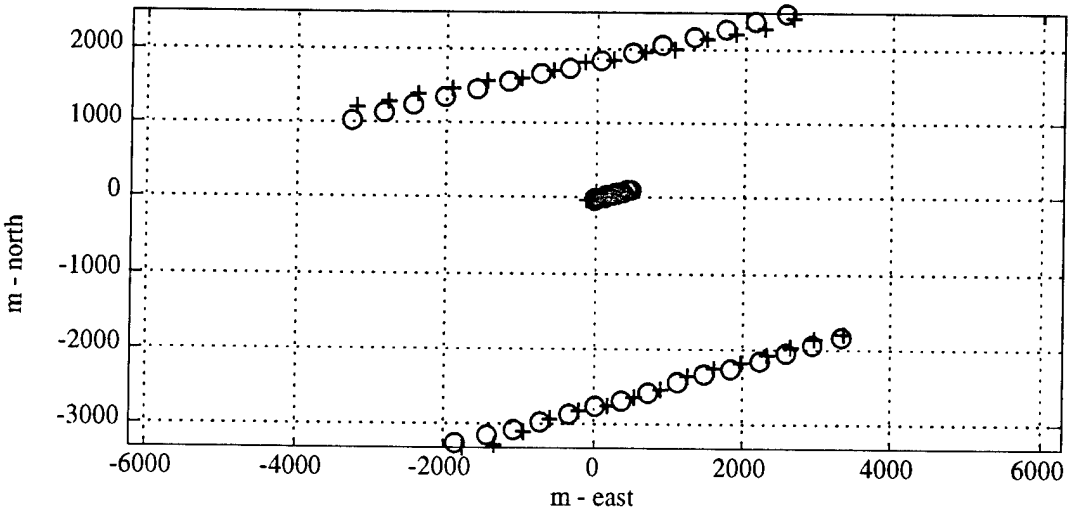

(b) Source and receiver positions upon convergence, where green indicates source location, red indicates receiver location, "+" indicates estimated location, and "o" indicates original location.

Figure B.12: Node 24. Geometry during AEL event (top) and source track upon convergence (bottom). Day/h/min: 190/07/00

AS-00-27

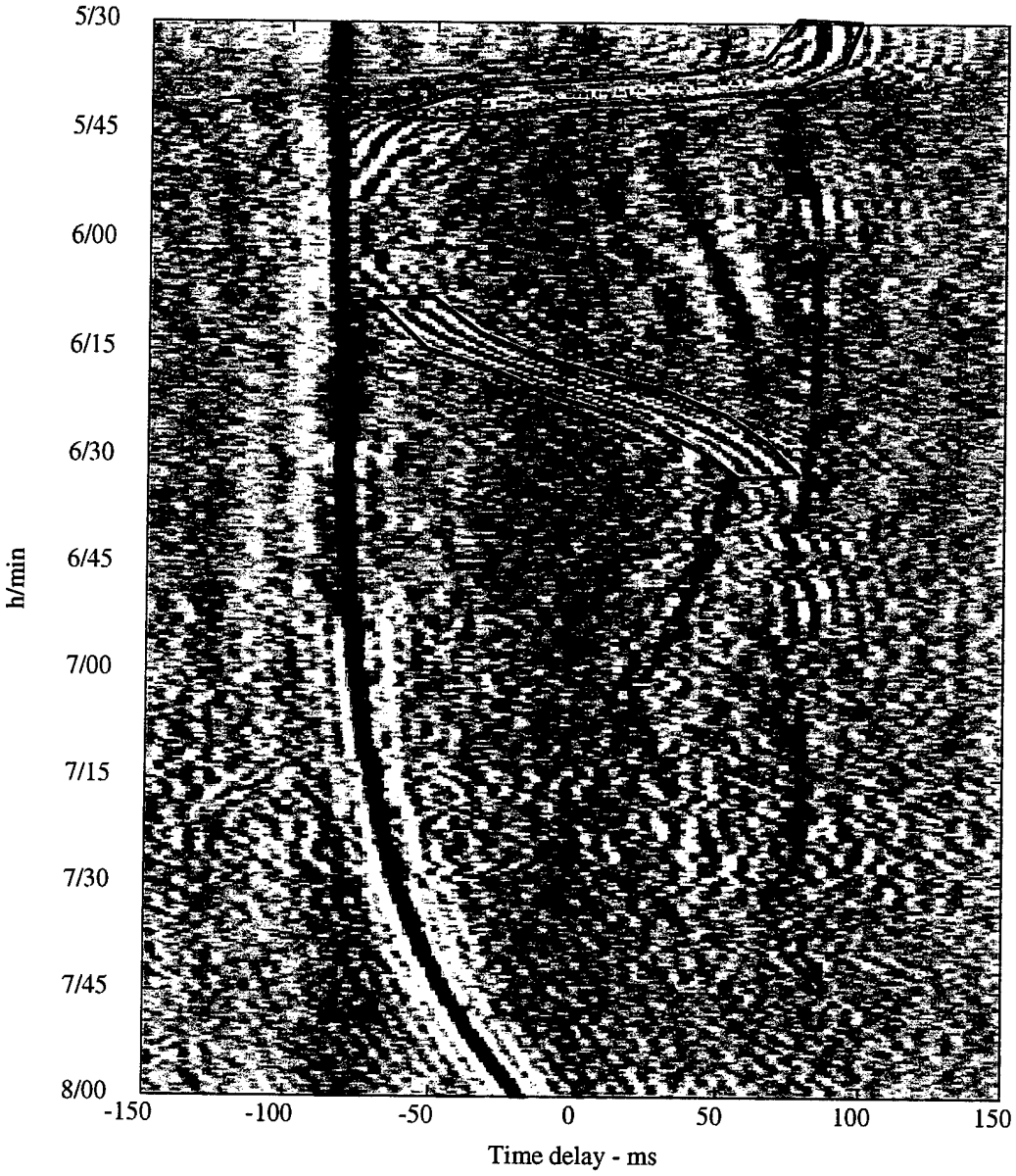

Figure B.13: Node 31. Omnixomni correlagram for near-field contact during AEL event, with processed track highlighted.
Hydrophones 1 and 13, day/h/min: 087/05/30 to 087/08/00

AS-00-28

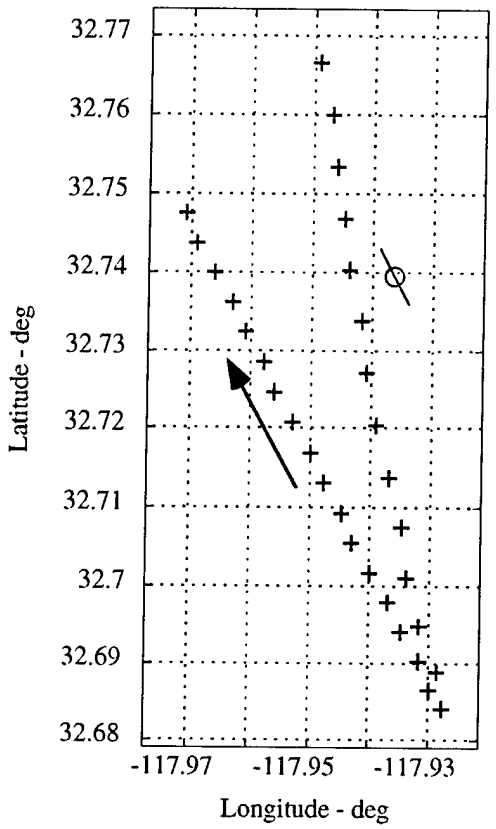

(a) Navigation geometry during AEL event, where a green "+" indicates time processed, a black "+" indicates time not processed, and a red "o" indicates receiver location.

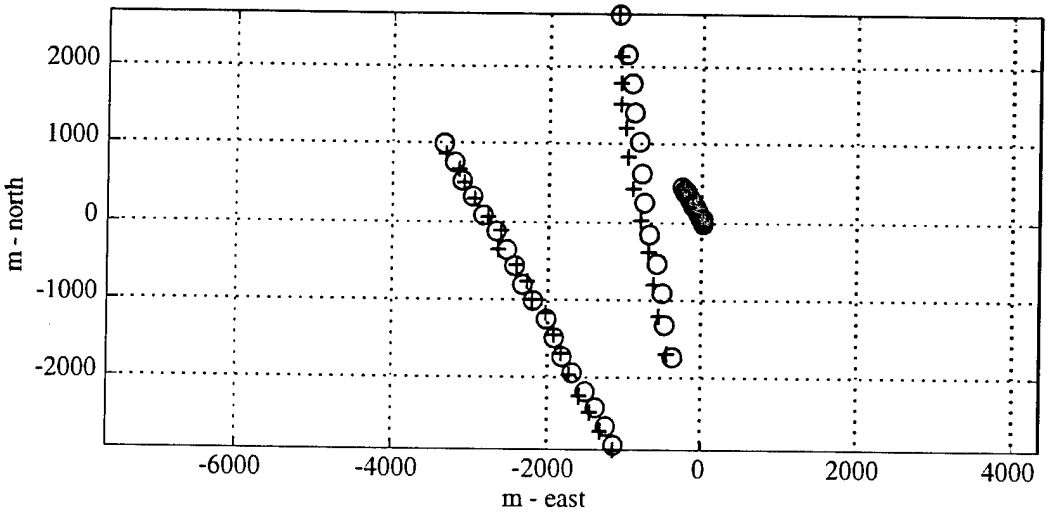

(b) Source and receiver positions upon convergence, where green indicates source location, red indicates receiver location, "+" indicates estimated location, and "o" indicates original location.

Figure B.14: Node 31. Geometry during AEL event (top) and source track upon convergence (bottom). Day/h/min: 087/05/30

AS-00-29

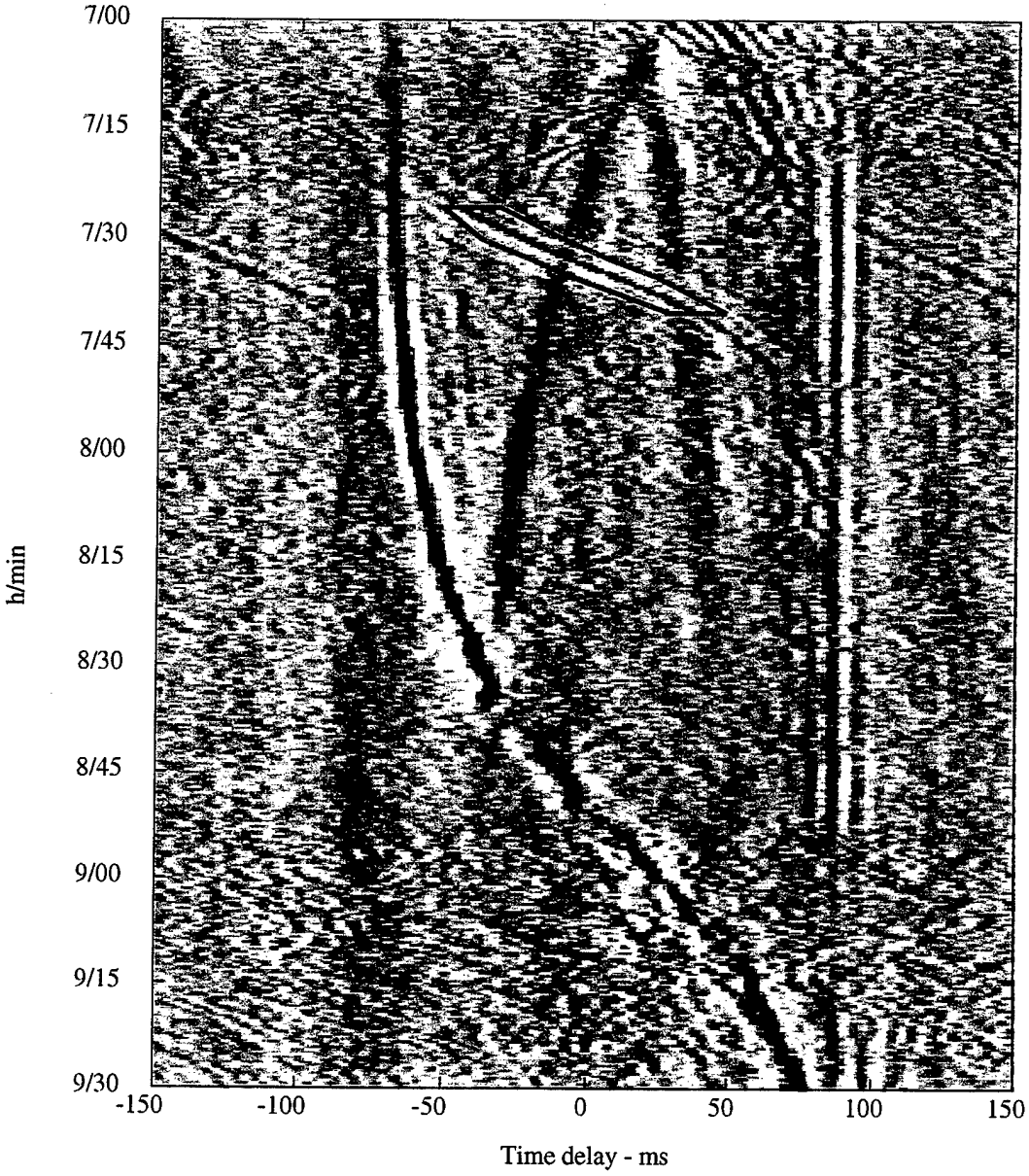

Figure B.15: Node 32. Omnixomni correlagram for near-field contact during AEL event, with processed track highlighted.
Hydrophones 1 and 13, day/h/min: 087/07/00 to 087/09/30

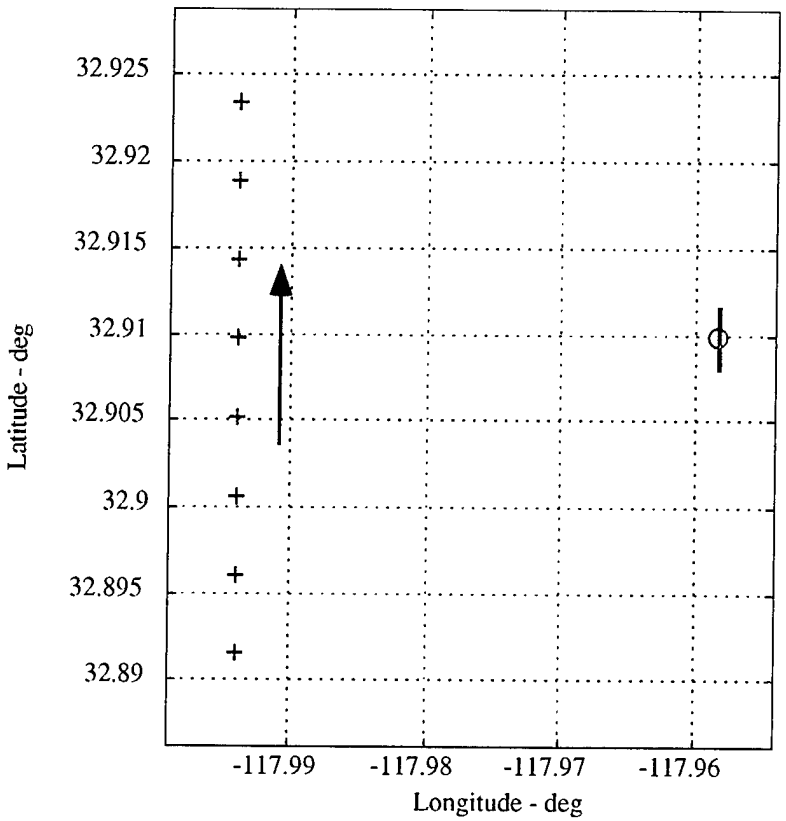

(a) Navigation geometry during AEL event, where a green "+" indicates time processed, and a red "o" indicates receiver location.

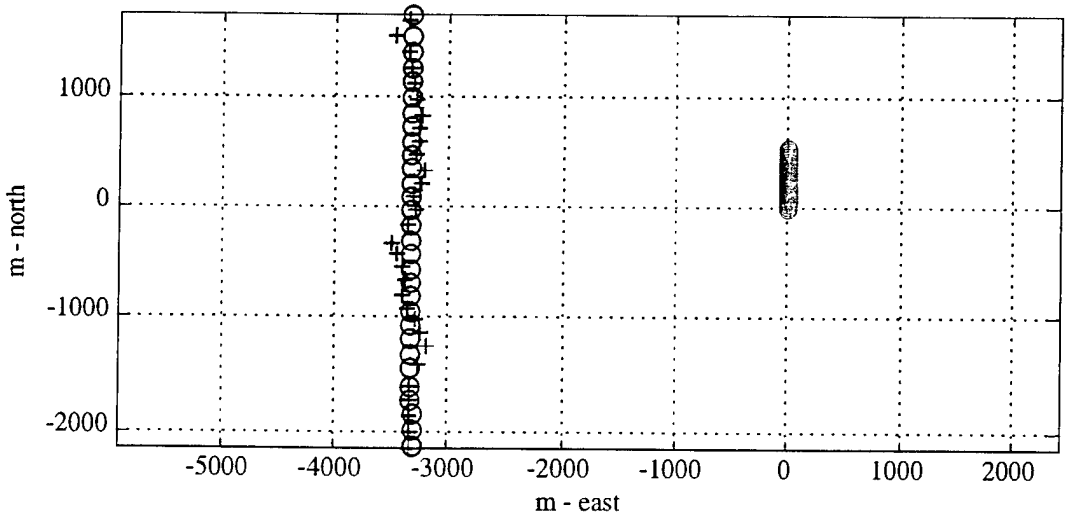

(b) Source and receiver positions upon convergence, where green indicates source location, red indicates receiver location, "+" indicates estimated location, and "o" indicates original location.

Figure B.16: Node 32. Geometry during AEL event (top) and source track upon convergence (bottom). Day/h/min: 087/07/00

AS-00-31

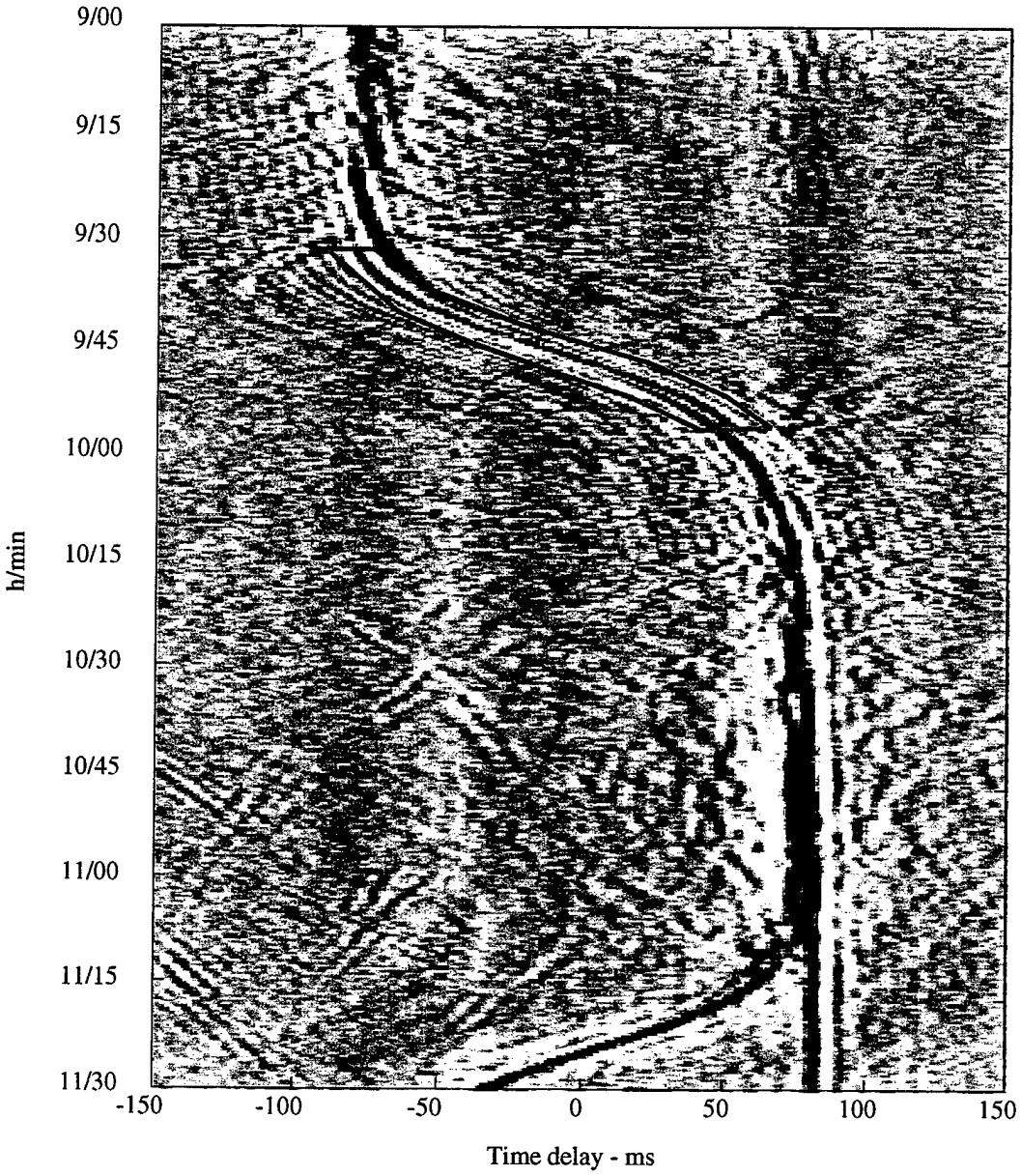

Figure B.17: Node 33. Omnixomni correlagram for near-field contact during AEL event, with processed track highlighted.
Hydrophones 1 and 13, day/h/min: 087/09/00 to 087/11/30

AS-00-32

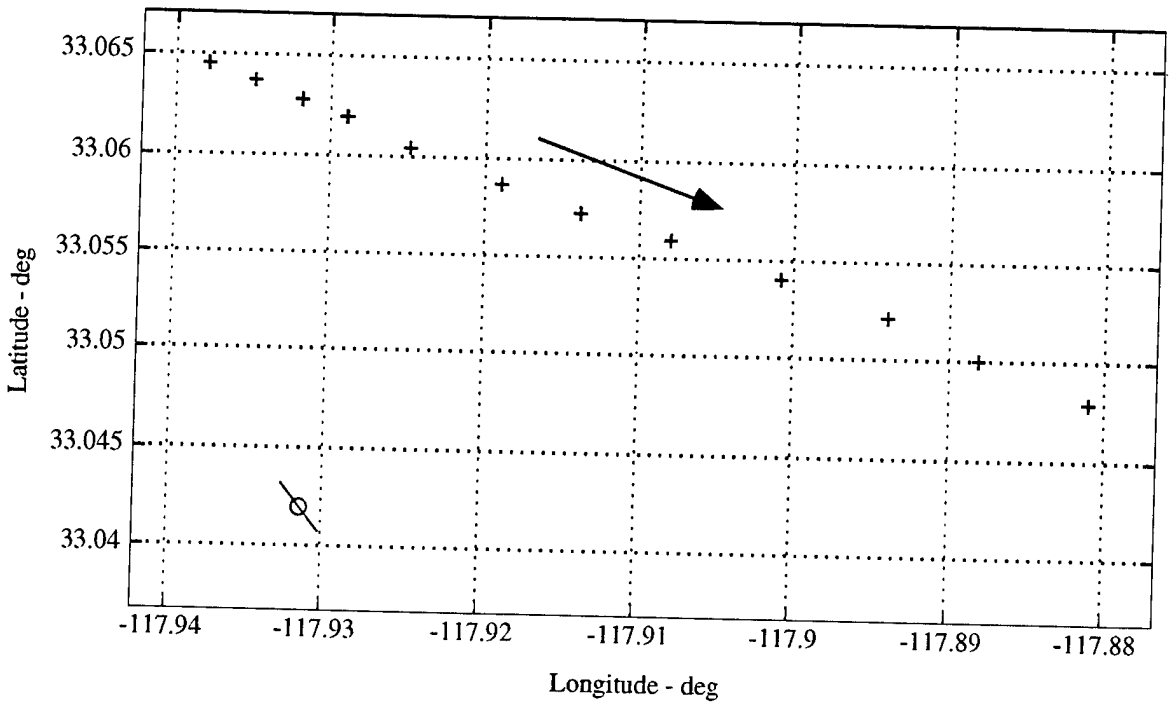

(a) Navigation geometry during AEL event, where a green "+" indicates time processed, and a red "o" indicates receiver location.

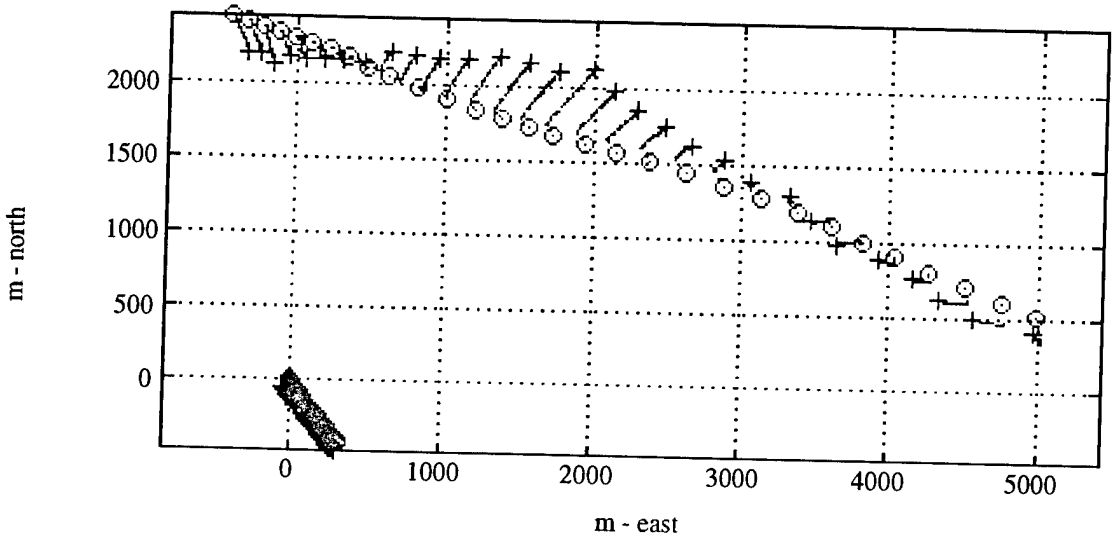

(b) Source and receiver positions upon convergence, where green indicates source location, red indicates receiver location, "+" indicates estimated location, and "o" indicates original location.

Figure B.18: Node 33. Geometry during AEL event (top) and source track upon convergence (bottom). Day/h/min: 087/09/00

AS-00-33

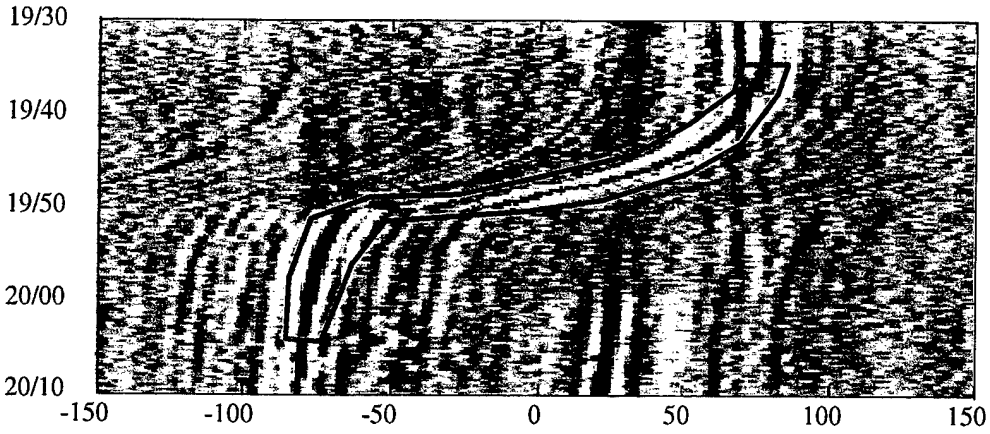

Figure B.19: Node 34. Omni correlagram during AEL event, with processed track highlighted. Only one pass is illustrated, but three passes were processed to provide the information for Fig. B.20. Hydrophones 1 and 13, day/h/min: 094/19/30 to 094/20/10

AS-00-34

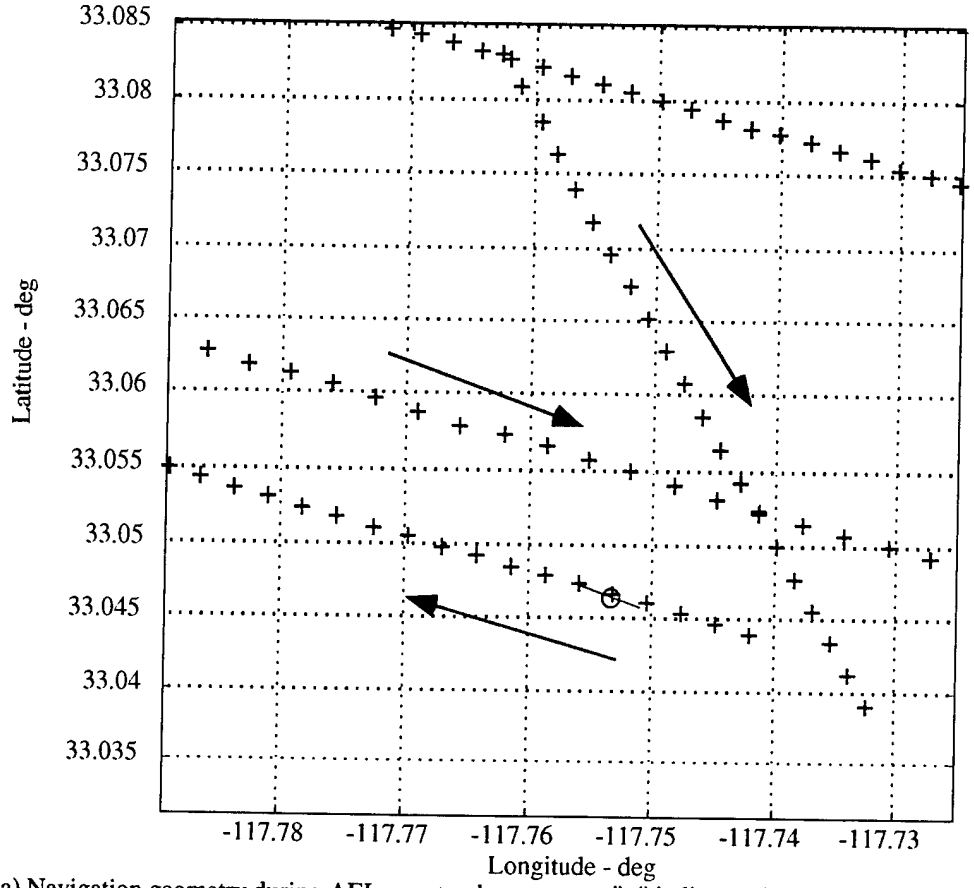

(a) Navigation geometry during AEL event, where a green "+" indicates time processed, a black "+" indicates time not processed, and a red "o" indicates receiver location.

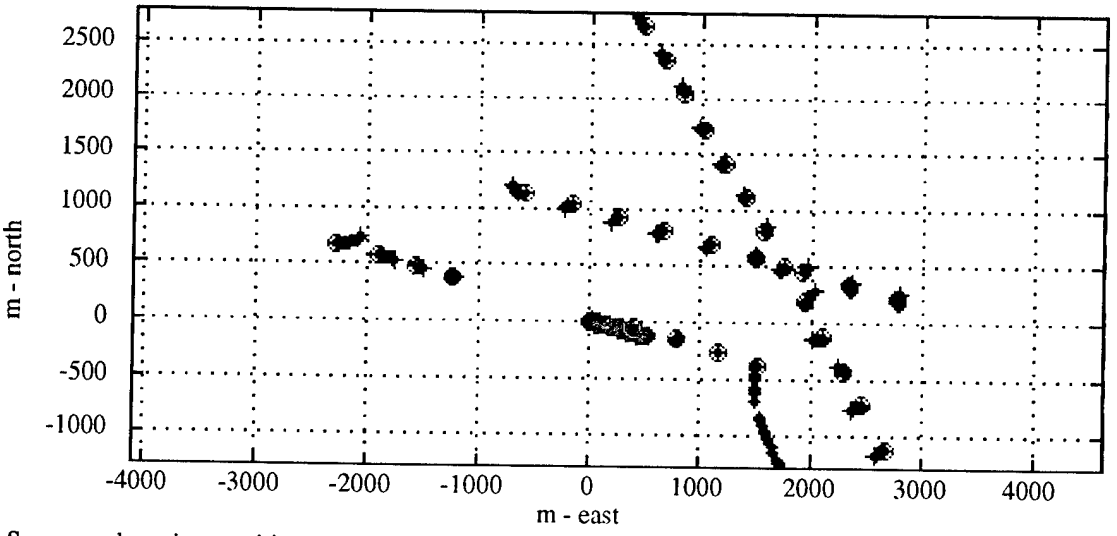

(b) Source and receiver positions upon convergence, where green indicates source location, red indicates receiver location, "+" indicates estimated location, and "o" indicates original location.

Figure B.20: Node 34. Geometry during AEL event (top) and source track upon convergence (bottom). Day/h/min: 094/18/20

AS-00-35

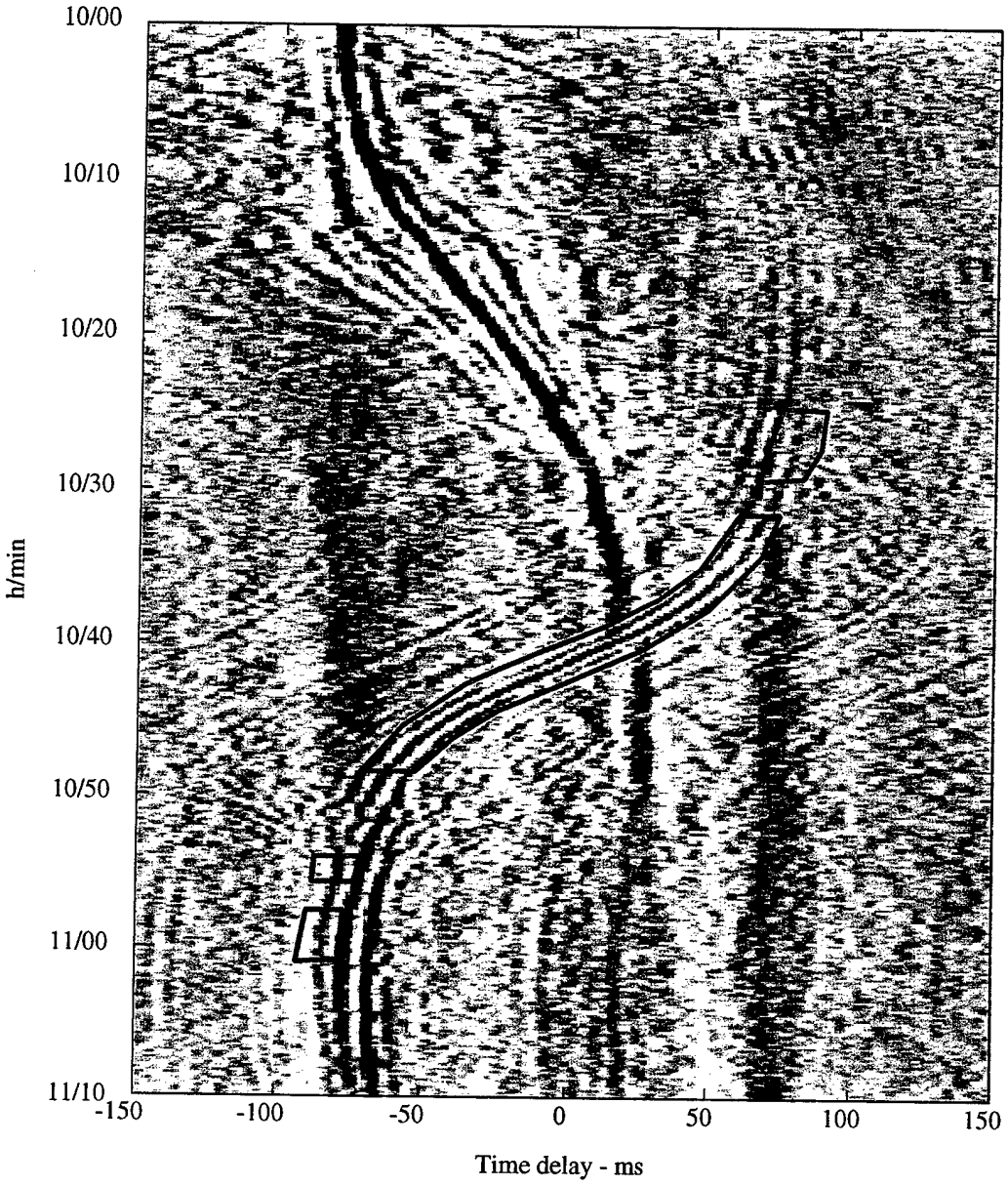

**Figure B.21: Node 41. Omnixomni correlagram for near-field contact during AEL event, with processed track highlighted.
Hydrophones 1 and 13, day/h/min: 130/10/00 to 130/11/10**

AS-00-36

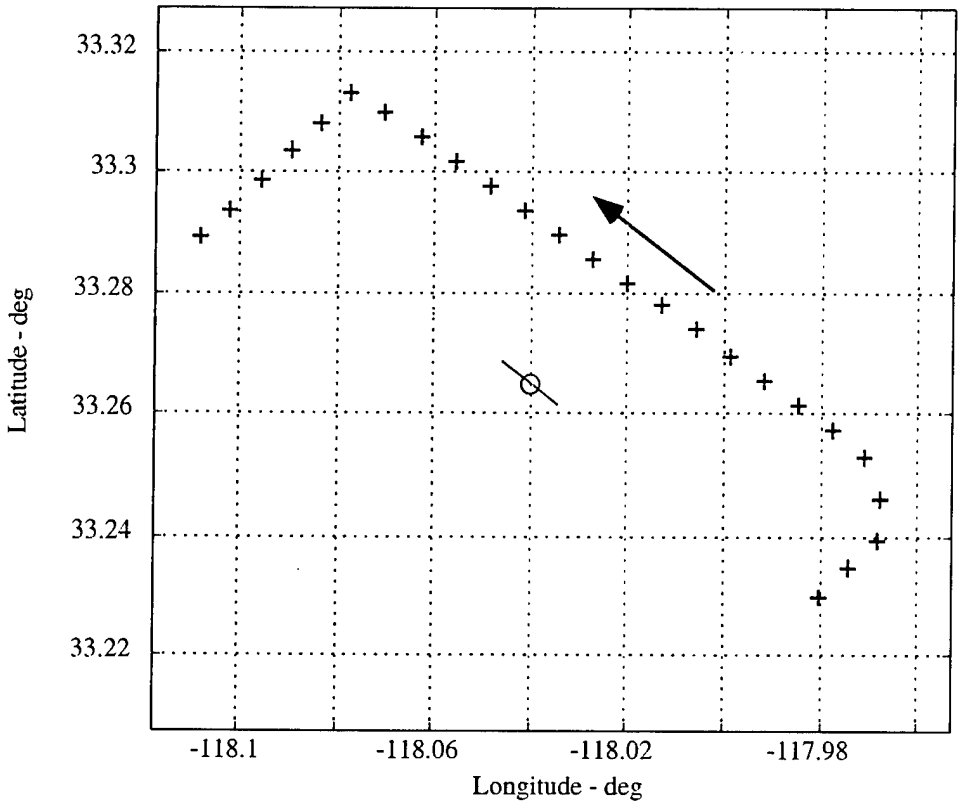

(a) Navigation geometry during AEL event, where a green "+" indicates time processed, a black "+" indicates time not processed, and a red "o" indicates receiver location.

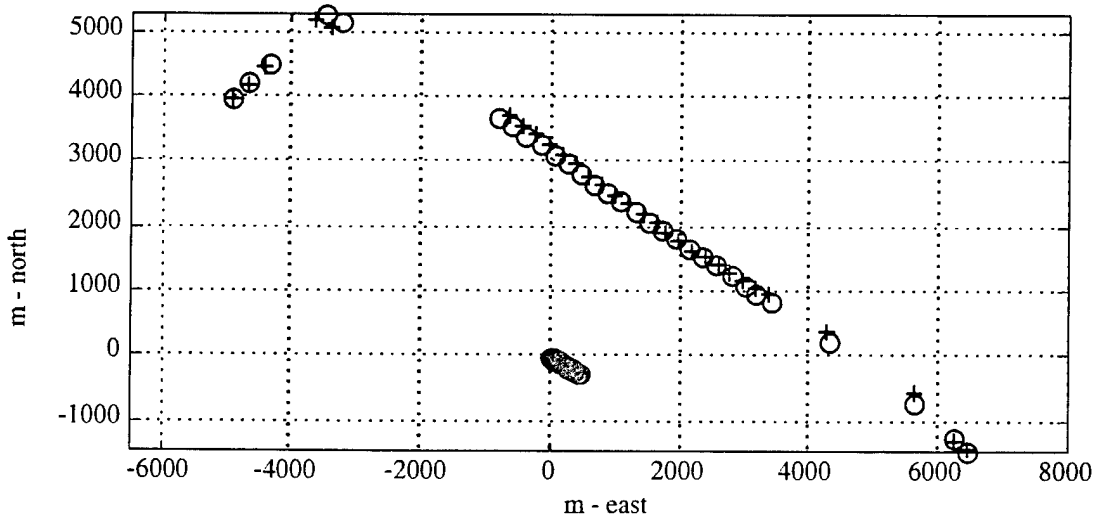

(b) Source and receiver positions upon convergence, where green indicates source location, red indicates receiver location, "+" indicates estimated location, and "o" indicates original location.

Figure B.22: Node 41. Geometry during AEL event (top) and source track upon convergence (bottom). Day/h/min: 130/10/00

AS-00-37

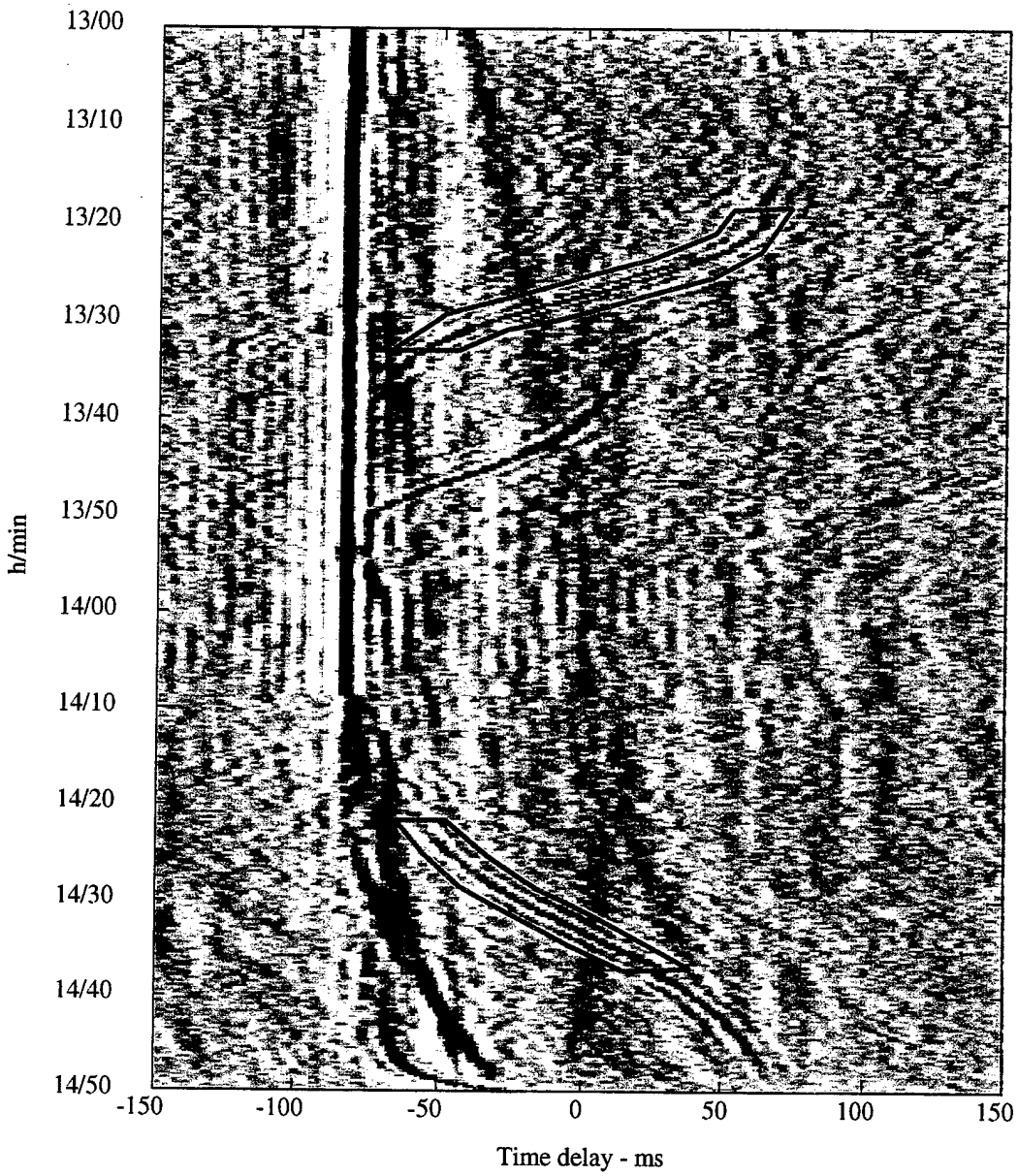

Figure B.23: Node 42. Omnixomni correlagram for near-field contact during AEL event, with processed track highlighted. Hydrophones 1 and 13, day/h/min: 130/13/00 to 130/14/50

AS-00-38

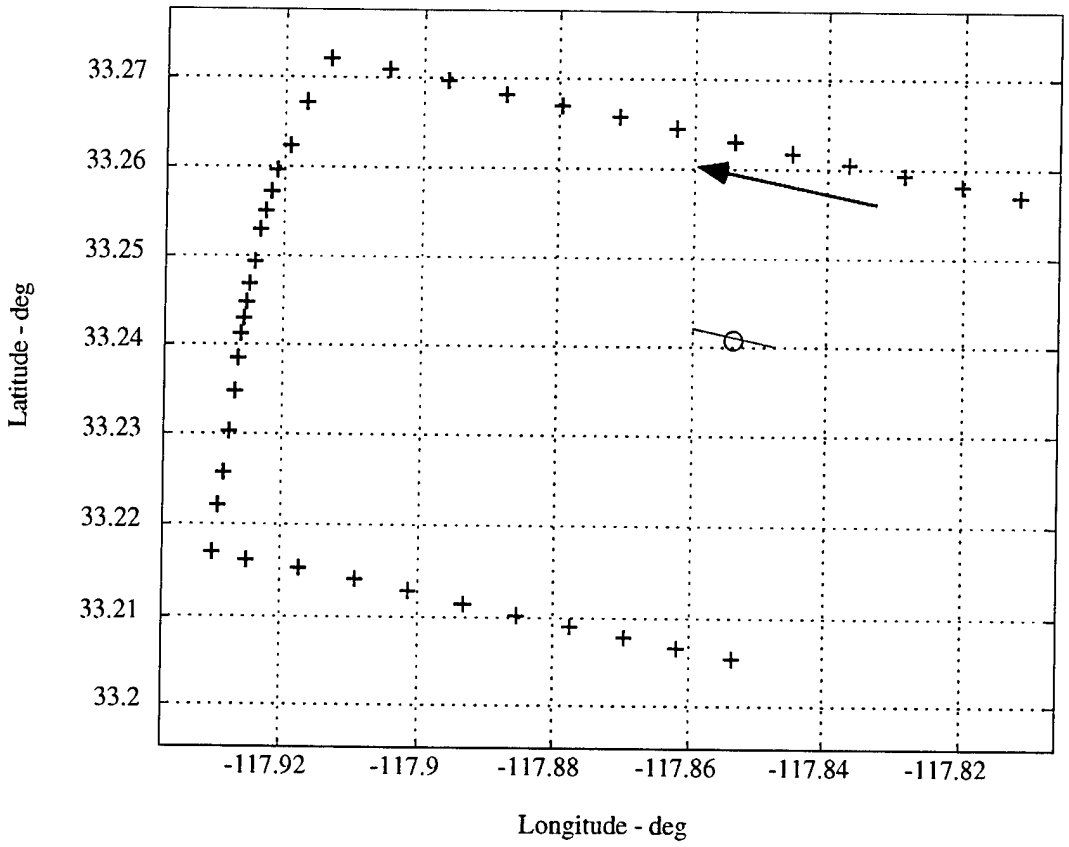

Figure B.24: Node 42. Navigation geometry during AEL event, where a green "+" indicates time processed, a black "+" indicates time not processed, and a red "o" indicates receiver location. Day/h/min: 130/13/00

AS-00-39

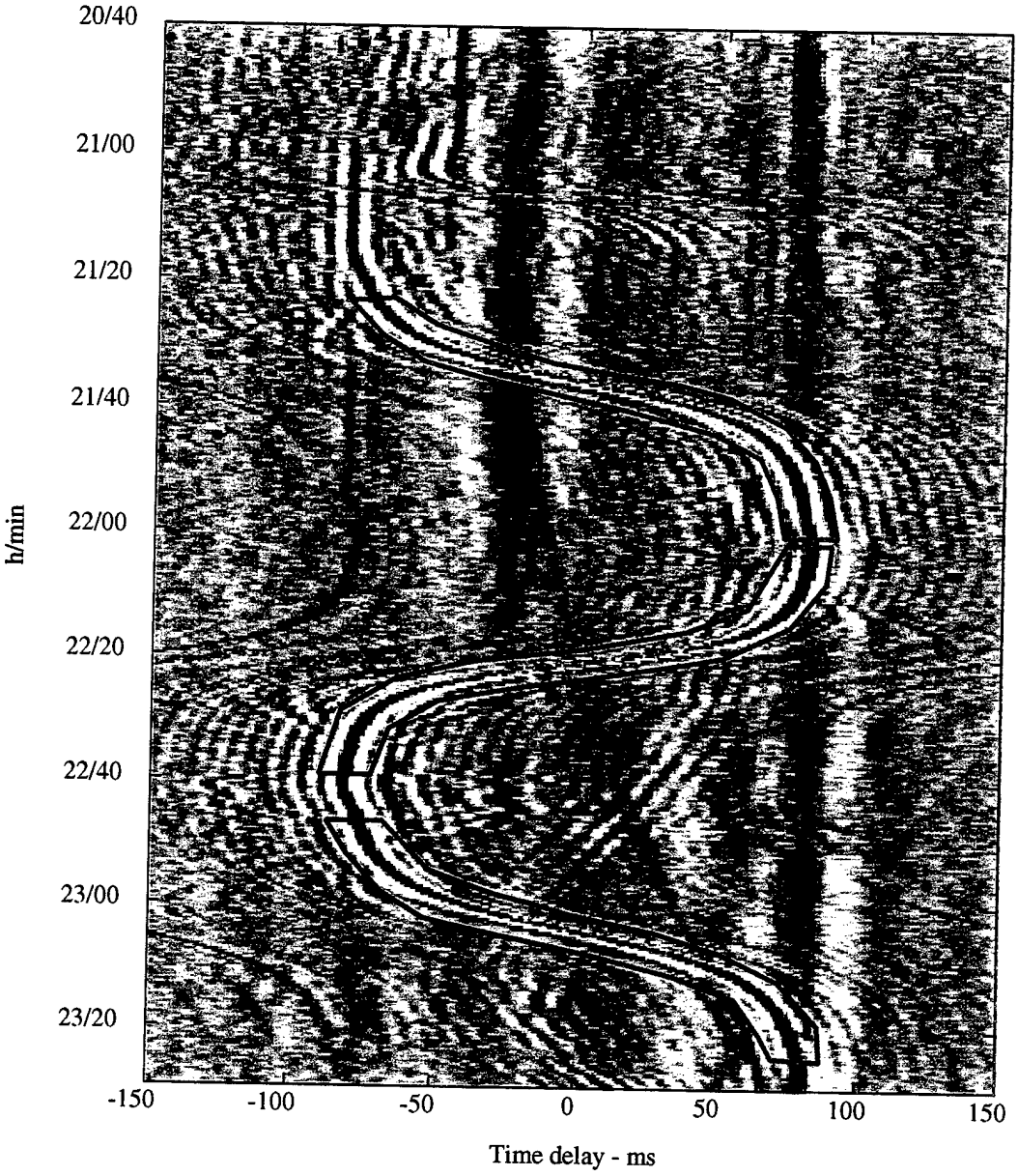

Figure B.25: Node 43. Omnixomni correlagram for near-field contact during AEL event, with processed track highlighted. Hydrophones 1 and 13, day/h/min: 101/20/40 to 101/23/30

AS-00-40

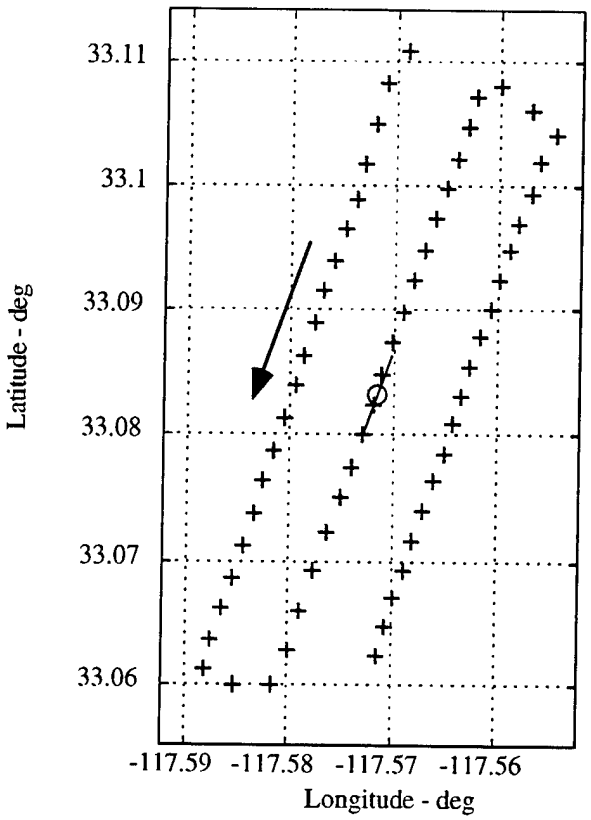

(a) Navigation geometry during AEL event, where a green "+" indicates time processed, a black "+" indicates time not processed, and a red "o" indicates receiver location.

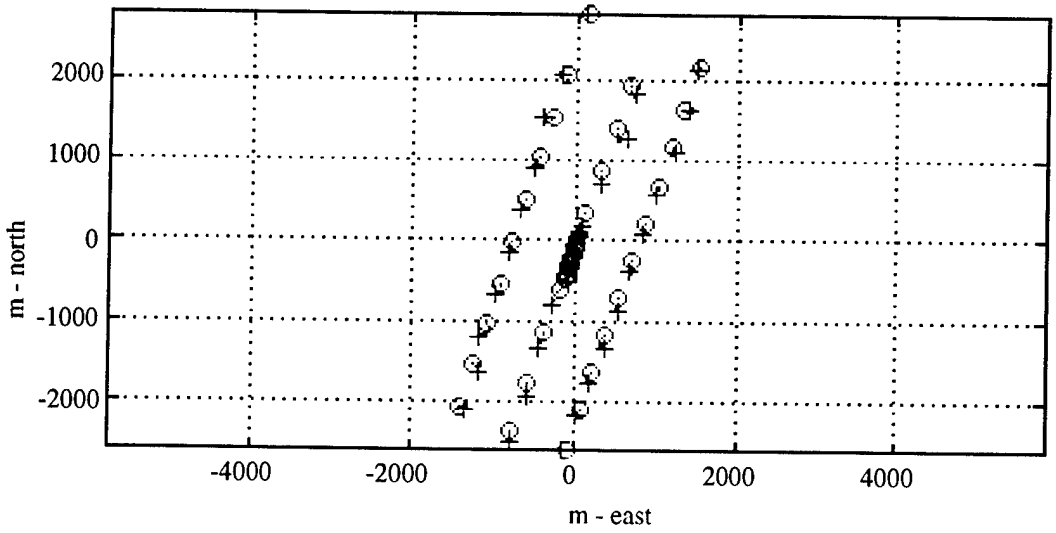

(b) Source and receiver positions upon convergence, where green indicates source location, red indicates receiver location, "+" indicates estimated location, and "o" indicates original location.

Figure B.26: Node 43. Geometry during AEL event (top) and source track upon convergence (bottom). Day/h/min: 101/20/40

AS-00-41

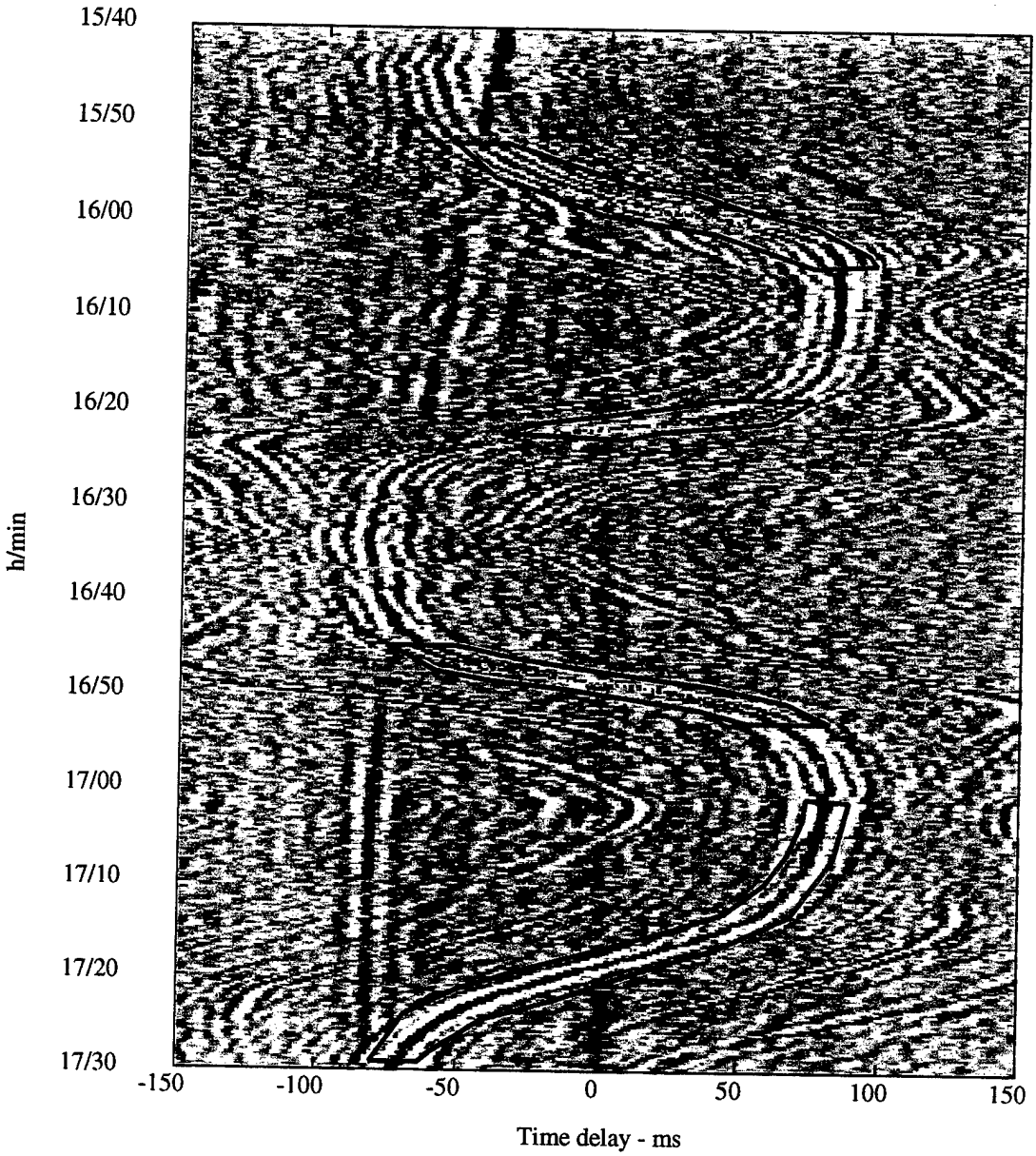

Figure B.27: Node 44. Omnixomni correlagram for near-field contact during AEL event, with processed track highlighted. Hydrophones 1 and 13, day/h/min: 084/15/40 to 084/17/30

AS-00-42

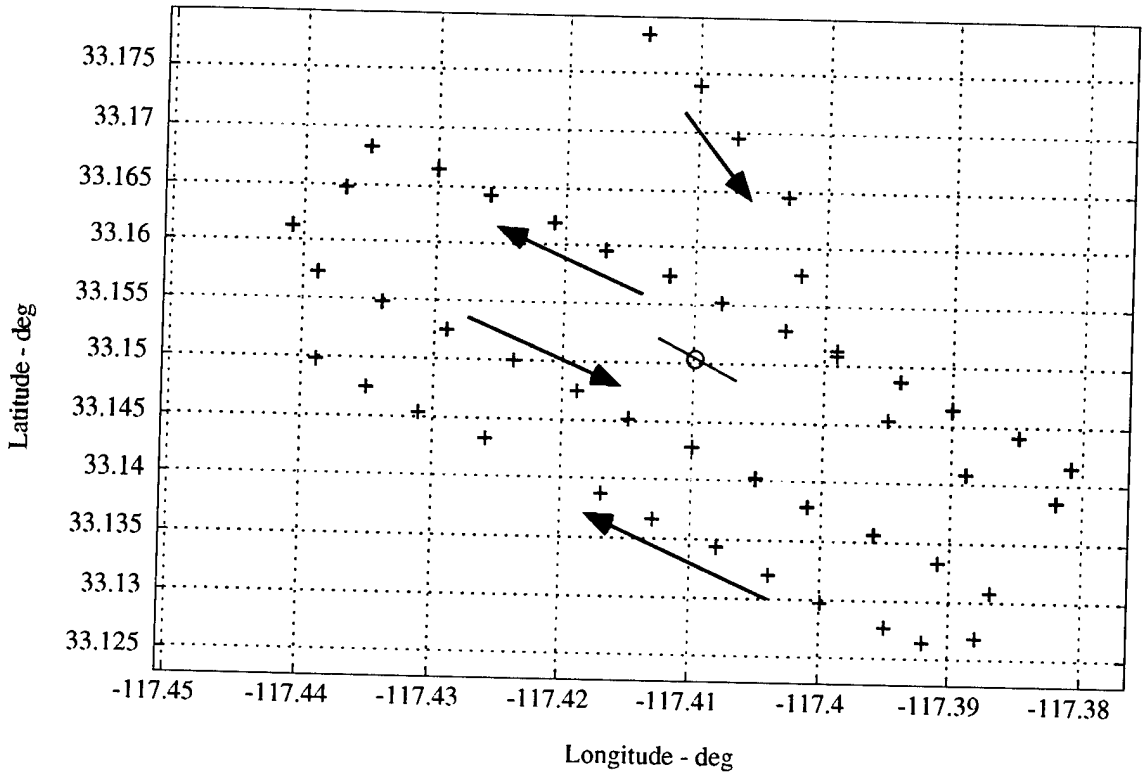

(a) Navigation geometry during AEL event, where a green "+" indicates time processed, a black "+" indicates time not processed, and a red "o" indicates receiver location.

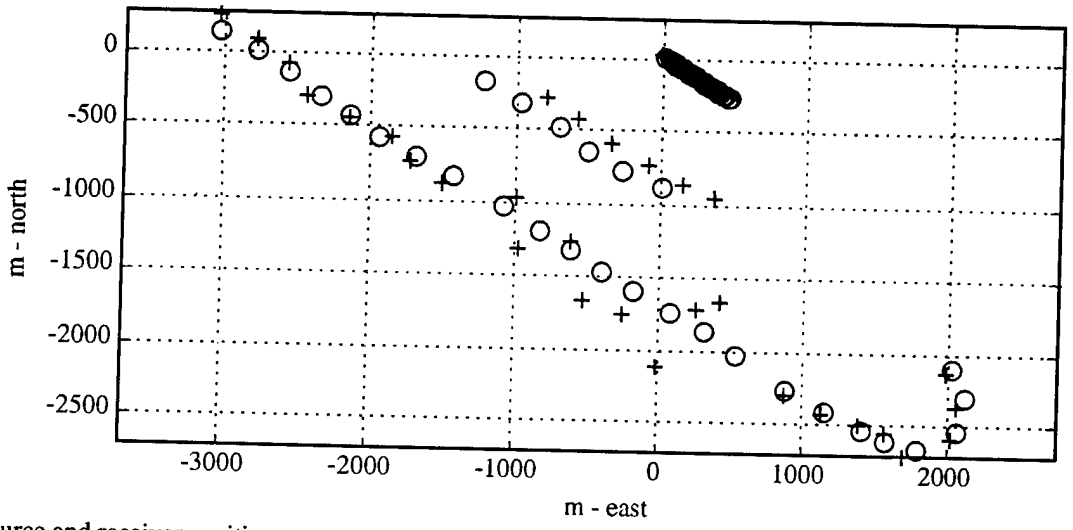

(b) Source and receiver positions upon convergence, where green indicates source location, red indicates receiver location, "+" indicates estimated location, and "o" indicates original location.

Figure B.28: Node 44. Geometry during AEL event (top) and source track upon convergence (bottom). Day/h/min: 084/15/40

AS-00-43

13 March 2000

DISTRIBUTION LIST FOR
ARL-TR-00-01
Technical Report under Contract N00039-94-D-0051
TO No. 0236, TD No. 1406046,
ADS Acoustic Test and Evaluation and System Engineering III

Copy No.

Commander
Space and Naval Warfare Systems
Command Headquarters
4301 Pacific Coast Highway (OT-1)
San Diego, CA 92110-3127

1 Attn: Mr. John Thornton, PMW 183A
2 Dr. Joe McCarthy, PMW 183
3 LCDR Rich Volkert, Code 18E

Commanding Officer
Space and Naval Warfare Systems Center, San Diego
53560 Hull Street
San Diego, CA 92152-5001

4 Attn: Mr. Pat Donahoe, PDE124-60
5 Mr. Roger W. Harris, Code 713

Commanding Officer
Operational Test and Evaluation Force
7970 Diven Street
Norfolk, VA 23505-1498

6 Attn: CDR Rory Calhoun, N43

Distribution List for ARL-TR-00-01 under Contract N00039-96-D-0051, TO No. 0236, TD No. 1406046
(cont'd)

Copy No.

7 DTIC-OCC
Defense Technical Information Center
8725 John J. Kingman Rd., Suite 0944
Fort Belvoir, VA 22060-6218

8 Mr. George Shepard
BBN Systems and Technologies
70 Fawcett Street
M/S 14-1C
Cambridge, MA 02138

9 Prof. Jim Wilson
Neptune Technology
3834 Vista Azul
San Clemente, CA 92672

10 Mr. Dan Goodfellow
Raytheon Systems Company
Submarine Signal Division
1847 W. Main Road
Portsmouth, RI 02871-1087

Applied Physics Laboratory
The Johns Hopkins University
11100 Johns Hopkins Road
Laurel, MD 20723-6099
11 Attn: Dr. Hugh South
12 Mr. Brad Bates

Distribution List for ARL-TR-00-01 under Contract N00039-96-D-0051, TO No. 0236, TD No. 1406046 (cont'd)

Copy No.

McKinney Engineering Library
ECJ 1.300
Austin, TX 78712
13 Attn: Librarian

14 Marton Garay, ARL:UT

15 David Grant, ARL:UT

16 Peter McCarty, ARL:UT

17 Mary Parse, ARL:UT

18 Carol Sheppard, ARL:UT

19 Evan Westwood, ARL:UT

20 Director's Office, Environmental Sciences Laboratory, ARL:UT

21 Library, ARL:UT